

**The tectonic evolution of the southeastern Terceira
Rift/São Miguel region (Azores) and associated
submarine volcanic & sedimentary processes**

Dissertation

with the aim of achieving a doctoral degree at the

Faculty of Mathematics, Informatics and Natural Science

Department of Earth Sciences

University of Hamburg

submitted by

Benedikt Johannes Weiß

Hamburg

2015

Day of oral defense: December 11th, 2015

The following evaluators recommend the admission of the dissertation:

Prof. Dr. Christian Hübscher

Dr. Thomas Lüdmann

Zusammenfassung

Das Terceira Rift erstreckt sich entlang des westlichsten Abschnitts der eurasisch-nubischen (afrikanischen) Plattengrenze. Schräg zur lokal vorherrschenden Extensionsrichtung verbindet es den Mittelatlantischen Rücken, kurz MAR, mit dem Bereich der Gloria Fault, in welchem die Plattengrenze durch eine Transformstörung gebildet wird. Das Rift, bestehend aus einer Abfolge tiefer Becken und vulkanischer Höhenlagen, liegt am nordöstlichen Rand eines für diesen Bereich mitten im Atlantischen Ozean ungewöhnlich flachen Plateaus, das durch starken submarinen Vulkanismus herausgebildet wurde und dessen Oberfläche mit einer Vielzahl vulkanischer Rücken überzogen ist. Diese Rücken bzw. Höhenlagen ragen zum Teil aus dem Atlantik heraus und bilden den mittleren und östlichen Azoren-Archipel. Das Forschungsgebiet der vorliegenden These umfasst den südöstlichen Abschnitt des Terceira Rifts, bestehend aus der Insel São Miguel, weiteren vulkanischen Rücken und benachbarter sedimentärer Becken. São Miguel ist einerseits das Verwaltungszentrum der Azoren und gleichzeitig ihre größte und mit 140.000 Einwohnern am stärksten besiedelte Insel. Regelmäßige Erdbeben und über die Insel verstreute hydrothermale Quellen erinnern die Bewohner dabei stets an die Gefahren, die das Leben auf einer vulkanisch aktiven Insel entlang einer geologischen Plattengrenze mit sich bringt. Trotz dieser Gefahren ist weder der geodynamische Ursprung der Insel im Speziellen, noch das ungewöhnliche tektonische und vulkanische Regime der Azoren im Allgemeinen hinreichend verstanden. Ebenso führten insbesondere die lediglich spärlichen bathymetrischen Informationen und das komplette Fehlen mehrkanal-reflexionsseismischer Daten dazu, dass weder die Verbreitung, noch die genaue Ausprägung des zu erwartenden submarinen Vulkanismus bekannt waren – genau so wenig, wie die submarinen Sedimentationsprozesse insgesamt.

Seit den frühen siebziger Jahren des letzten Jahrhunderts gilt das Terceira Rift als Ergebnis einer sukzessiven, von der *East Azores Fracture Zone (EAFZ)* ausgehenden Nordwärtsbewegung der eurasisch-nubischen Plattengrenze. Der auslösende Prozess sowie der genaue Verlauf der Plattengrenzenbewegung in Raum und Zeit sind jedoch nach wie vor nicht geklärt. Zu dieser Diskussion können die Ergebnisse der vorliegenden Arbeit signifikant beitragen. So war es auf Basis der hochauflösenden Bathymetrie und der reflexionsseismischen Daten einerseits möglich, dass komplexe submarine Störungssystem im Arbeitsgebiet zu kartieren und zu analysieren. Andererseits erlaubten die Daten erstmalig die Einführung einer seismischen Stratigraphie innerhalb der Sedimentbecken, aus der sich eine relative chronologische Abfolge vulkanischer und sedimentärer Prozesse ableiten ließ. Dieser Chronologie zur Folge entwickelte

sich das Rift ursprünglich orthogonal zu einer damals vorherrschenden SW-NE gerichteten Extension. Als diese vor circa 10 Ma eine WSW-ONO Richtung einnahm, begann sich das Spannungsregime innerhalb seines ursprünglichen Rahmens neu auszurichten, was letztendlich zu der Entstehung neuer NNW-SSO streichender Störungen und vulkanischer Rücken wie der Monaco Bank südlich von São Miguel führte. Dies zeigt deutlich, dass das Terceira Rift einem in sich neu-justiertem Rift-System entspricht, dessen Entwicklung stark an die Kinematik der eurasischen und der nubischen Platten geknüpft ist. Das Fehlen von rezent aktiven Störungen südlich von São Miguel zeigt zudem, dass sich die krustale Dehnung im Arbeitsgebiet, die sich aus der relativen Bewegung der beiden tektonischen Platten zueinander ergeben, allein auf den Bereich des südöstlichen Terceira Rifts konzentriert. Daraus kann auch abgeleitet werden, dass sich die Insel über einer ehemaligen Transformstörung entwickelt haben muss, die heute schräg zur Dehnungsrichtung liegt und die beiden an São Miguel angrenzenden Riftbecken untereinander verbindet.

Tektonische Bewegungen, die mit der Riftbildung einhergehen, beeinflussen zudem die submarinen Sedimentationsprozesse. So werden einerseits Bodenströmungen und Trübestrome durch Bruchflächen und vulkanische Lineamente abgelenkt; andererseits werden lokal mächtige Ablagerungen, wie z.B. Turbiditabfolgen oder Driftkörper, durch seismische Schocks destabilisiert. Die Seismizität führt zudem zu einem retrograden lokalen Einbrechen der Schelfkante und zur Bildung sich in den submarinen Hang einschneidender Schluchten. Demzufolge sind Massenumlagerungen ein weitverbreitetes Phänomen im Arbeitsgebiet und bilden das gesamte Spektrum vom Kollabieren einer Rückenflanke, dem plötzlichen Abrutschen von Sedimenten bis hin zu einem sukzessiven Kriechen ab. Die entsprechenden Sedimente sind dabei das Ergebnis von subaerischer und küstennaher Erosion São Miguels oder, in weit geringerem Ausmaß, Ablagerungen von äolisch verfrachtetem vulkanischem Auswurfmaterial. Der durch die Wellenerosion erzeugte Schelf der Insel weist eine durchschnittliche Breite von ca. 4.500 m auf und wurde vermutlich in seiner heutigen Form während des letzten Meeresspiegeltiefstandes angelegt. Demnach deutet die durchschnittliche Tiefenlage der Schelfkante (140 m) auf eine Langzeit-Subsidenz der Insel von ca. 0,6 mm/a hin. Die Küsten- bzw. Schelferosion und die Remobilisierung von Schelfsedimenten ging/geht dabei einher mit flächenhaften Trübestromen, die entlang des Hangs unterhalb der Schelfkante zur Ablagerung ausgedehnter Sedimentloben führten/führen. Da diese Loben nur im Norden der Insel zu beobachten sind, werden die flächigen Trübestrome mit den Stürmen des Nordatlantiks und deren Dünung, der insbesondere die Nordküste ausgesetzt ist, in Verbindung gebracht. Die Sedimentloben werden wiederum von Kanalsystemen durchschnitten. Diese haben ihren Ursprung an den Einschnitten der nördlichen Schelfkante und führen die kontinuierlich anfallenden terrestrischen und fluviolen Sedimente in Form von punktueller Trübestrome in Richtung Tiefsee ab. Im Gegensatz dazu führen die Trübestrome, die den südlichen Inselhang hinabfließen, zur Ablagerung von kleinskaligeren Turbiditloben und Sedimentwellen – wobei

sich die letzteren dort herausbilden, wo sich die Hangneigung und damit die Fließgeschwindigkeit stark verringert (sogenannte *cyclic steps* und *chutes-and-pools*).

Diesen destruktiven Erosionsprozessen steht Vulkanismus als konstruktiver Prozess gegenüber. Dass dieser auch explosive vulkanische Phasen umfasst, wird schon anhand der Tatsache deutlich, dass São Miguel aus drei als aktiv geltenden Stratovulkanen aufgebaut ist. Allerdings ist wenig darüber bekannt, in wie weit explosiver Vulkanismus im submarinen Bereich des südöstlichen Terceira Rifts eine Rolle spielt, wie er sich verteilt und in wie fern er ein Gefahrenpotential darstellt. In diesem Zusammenhang ermöglichte die hochauflösende Bathymetrie dieses Datensatzes die Identifizierung und Kartierung von 252 submarinen vulkanischen Kegeln, deren morphologische Charakteristiken und seismischen Abbilder eine explosive Natur belegen. Die Kegel weisen im Durchschnitt einen Durchmesser von (743 ± 405) m, eine Höhe von (139 ± 77) m bzw. einen Böschungswinkel von $(20 \pm 4)^\circ$ auf. Da das morphologische Erscheinungsbild einerseits nicht von der Wassertiefe abzuhängen scheint und andererseits denen von Schlackenkegeln auf São Miguel ähnelt, lassen sich folgende Schlussfolgerungen ziehen: die Eruptionsgeschichten sind 1) für alle Wassertiefen ähnlich, und 2) vergleichbar mit denen der Landstrukturen. Die submarinen Kegel liegen dabei entweder auf tektonischen Störungen, repräsentieren parasitäre Strukturen im submarinen Bereich der drei großen Stratovulkane oder bilden zusammen ein eigenständiges submarines Vulkansystem. Da die Kegel in Wassertiefen von weniger als 300 bis 400 m geringfügig niedrigere Höhen-zu-Durchmesser-Verhältnisse zeigen, wird angenommen, dass die Eruptionen diese Vulkane mit der Meeresoberfläche interagieren und damit eine Gefahr für Mensch, Tier und Technik oberhalb des Meeresspiegels darstellen können.

Diese Arbeit bietet demnach eine umfassende Studie der Prozesse, die die Entstehung der Azoren Inseln und deren submariner Umgebung prägen. Diese Prozesse umfassen die Geodynamik im Bereich des Archipels und die Plattenkinematik der angrenzenden tektonischen Platten, lokale Tektonik, Vulkanismus, ozeanische Strömungen, Trübeströme sowie destruktive Vorgänge, wie z.B. Schelferosion, Subsidenz und Massenumlagerungen.

Abstract

The Terceira Rift is located at the westernmost tip of the Eurasian-Nubian (African) plate boundary where it links a major transform fault (Gloria Fault) with the Mid-Atlantic ridge (MAR) oblique to the regional extension induced by plate kinematics. The rift is defined by a succession of deep basins and bathymetric highs or islands, all of them of volcanic origin. Southwest of the rift system, strong volcanism caused the generation of an unusual shallow plateau which is overprinted by several volcanic complexes, ridges and further volcanic islands altogether representing the central and eastern group of the Azores Archipelago. This thesis focuses on the southeastern basins of the Terceira Rift, adjacent volcanic ridges and the submarine slope of São Miguel, the largest island of the Azores and its administrative center. Both, the volcanic origin of the island and its location at the Eurasian-Nubian plate boundary are very present facts for the about 140,000 inhabitants, since seismicity and hydrothermal activity highly influence their workaday life and remind them of the significant risk potential. However, the geodynamic processes which cause the anomalous tectonic and volcanic setting, the occurrence of submarine volcanism and the resulting sedimentation processes are still not completely understood or even unknown, particularly due to missing high-resolution bathymetry as well as a total lack of multichannel seismic data.

Since the early seventies it is, in fact, known that the present-day Terceira Rift is the result of a northward movement of the plate boundary starting from its former location at the East Azores Fracture Zone (EAFZ), but both the trigger mechanism and the evolution in time are under debate. This thesis significantly contributes on this discussion, since the presented comprehensive high-resolution bathymetric and multichannel seismic data set allowed mapping the submarine fault system and the identification of a seismic stratigraphy in the sedimentary basins of the São Miguel region for the first time. According to these results, the Terceira Rift has developed orthogonally to previous SW-NE directed extensional stress, before a clockwise rotation in extension to WSW-ENE led to a rearrangement of the tectonic regime within the inherited setting and the creation of NNW-SSE trending faults and volcanic lineaments (e.g. the Monaco Bank south of São Miguel Island). This highlights the Terceira Rift to be a re-organized rift system predominantly controlled by plate kinematics. The absence of active faults south of the Terceira Rift additionally indicates that differential movement of the Eurasian and Nubian plates in the working area accumulates along the southeastern Terceira Rift only and that São Miguel Island presumably evolved above a leaky transform linking both adjacent rift basins.

Rift tectonics additionally control submarine sedimentation since, on the one hand, fault scarps and volcanic lineaments deflect turbidity and bottom currents. On the other hand, associated seismicity destabilizes high local accumulations of sediments, such as turbidites or drift deposits, and causes retrograde erosion of the shelf break forming downslope channel systems. Hence, mass wasting is a common phenomenon at the southeastern Terceira Rift involving sliding, slumping and flank collapsing. Sediments particularly results from São Miguel's onshore and coastal erosion and, in a minor degree, from onshore explosive volcanism. The present-day island shelf is characterized by an average width of approximately 4,500 m and is assumed to be formed during the last sea level minimum. An average water depth of the shelf break of ~140 m therefore indicates a long-term island subsidence rate of ~0.6 mm/a. Shelf erosion and remobilization of shelf deposits along the northern coast resulted/result in unconfined turbidity currents forming large sediment lobes at the island slope - most likely due to the exposure to North-Atlantic storm swell. These sediment lobes are incised by channel systems discharging the constant terrestrial and fluvial sediment supply of the island by confined turbidity currents. In contrast, turbidity currents at the southern slope generate cyclic steps, chutes-and-pools and turbidite lobes.

Although the explosive nature of the stratovolcanoes onshore São Miguel Island is obvious, little is known about explosive volcanism and its associated risk potential in the submarine domain of the southeastern Terceira rift. In this context, high-resolution bathymetry allowed mapping of 252 submarine volcanic cones, which are - based on a combined morphological and seismic interpretation – associated with explosive eruptions. These cones are characterized by a width of (743 ± 405) m, a height of (139 ± 77) m and slope angles of $(20\pm 4)^\circ$. Since the morphological characteristics do not vary with water depth (ranging from 120 m to 3200 m) and resemble those of monogenetic alkali-basaltic cinder cones onshore São Miguel, their eruption histories are assumed to be 1) independent of the water depth, and 2) comparable to onshore cinder cones. Submarine cones in the southeastern Terceira Rift are either controlled by faults, are secondary parasitic features of the onshore stratovolcanoes or superimpose an independent submarine volcanic system. Since the cones show a slightly decrease in their height to width ratio in water depths of less than 300-400 m, cone volcanism in those water depths apparently interacts with the water-air boundary and poses a hazard potential to the environment above the sea surface.

Summarizing, this thesis presents a comprehensive study of the processes controlling the evolution of the Azorean oceanic islands and their submarine environment, as being the geodynamic and plate kinematic setting of the Archipelago, local tectonics, volcanism, bottom and density currents as well as destructive processes, like shelf erosion, subsidence and mass wasting.

Table of Content

1.	Introduction.....	1
1.1.	The Eurasian-Nubian plate boundary & the Azores Archipelago.....	4
1.2.	Data set and study area.....	6
1.3.	Structure of the thesis and resulting publications.....	8
1.4.	Contributions of other persons.....	9
2.	The tectonic evolution of the southeastern Terceira Rift.....	11
	Abstract.....	11
2.1.	Introduction.....	11
2.2.	Geological context.....	13
2.2.1.	Terceira Rift & Azores Triple Junction	13
2.2.2.	Upper mantle anomaly	15
2.3.	Data and methods.....	16
2.4.	Results and interpretation.....	17
2.4.1.	South-Hirondelle Basin	17
2.4.1.1.	Observations bathymetry	17
2.4.1.2.	Observations seismic	19
2.4.1.3.	Combined interpretation of bathymetric and seismic data	20
2.4.2.	Monaco Graben & Monaco Bank	20
2.4.2.1.	Observations bathymetry	20
2.4.2.2.	Observations seismic	22
2.4.2.3.	Combined interpretation of bathymetric and seismic data	22
2.4.3.	Southwest Basin	23
2.4.3.1.	Observations bathymetry	23
2.4.3.2.	Observations seismic	23
2.4.3.3.	Combined interpretation of bathymetric and seismic data	26
2.4.4.	Lower southern slope of São Miguel & South Basin	26
2.4.4.1.	Observations bathymetry	26
2.4.4.2.	Observations seismic	26
2.4.4.3.	Combined interpretation of bathymetric and seismic data	30

2.4.5.	Povoação Basin & Big North High	31
2.4.5.1.	Observations bathymetry	31
2.4.5.2.	Observations seismic	31
2.4.5.3.	Combined interpretation of bathymetric and seismic data	34
2.4.6.	Summary of observations	35
2.5.	Discussion.....	36
2.5.1.	Relative chronostratigraphy	36
2.5.2.	Evolution of the southeastern Terceira Rift	37
2.5.3.	Age constrains	40
2.5.4.	Implications for the Azores Plateau evolution	41
2.6.	Conclusion.....	41
3.	Submarine explosive volcanism in the southeastern Terceira Rift.....	47
	Abstract.....	47
3.1.	Introduction.....	48
3.2.	Regional setting.....	50
3.3.	Data and methods.....	51
3.4.	Observations and interpretation.....	52
3.4.1.	Volcanism along structural lineaments	55
3.4.2.	Parasitic volcanism	57
3.4.3.	Volcanism at East-Formigas High	61
3.4.4.	Morphometrical characteristics and depths of volcanic cone	61
3.5.	Discussion.....	64
3.5.1.	Explosive or effusive evolution of volcanic cones?	64
3.5.2.	Backscatter facies of young and old cones	66
3.5.3.	Submarine volcanic domains	67
3.5.4.	Pyroclastic deep sea volcanism	68
3.6.	Conclusion.....	69

4.	Submarine sedimentation processes in the southeastern Terceira Rift.....	71
	Abstract.....	71
4.1.	Introduction.....	72
4.2.	Geological context.....	74
4.2.1.	Azores Plateau & Terceira Rift	
4.2.2.	Southeastern Terceira Rift & São Miguel region	
4.3.	Data and methods.....	76
4.4.	Submarine sedimentation processes: results and implications.....	77
4.4.1.	Shelf and slope morphology of São Miguel Island and associated sedimentation processes	
4.4.1.1.	Observations	
4.4.1.2.	Shelf erosion and subsidence at São Miguel Island	
4.4.1.3.	Evolution of the upper slope	
4.4.1.4.	Downslope sedimentation processes off the São Miguel Island shelf	
4.4.2.	Mass failures	
4.4.2.1.	Observations	
4.4.2.2.	Submarine slides	
4.4.2.3.	Flank collapses	
4.4.2.4.	Interaction of sedimentation, sediment remobilization and downslope density currents	
4.4.3.	Current controlled sedimentation	
4.4.3.1.	Observations	
4.4.3.2.	Conturites in the basin southwest of São Miguel Island	
4.4.3.3.	Drifts along fault scarps	
4.5.	Conclusion.....	96
5.	Conclusion and outlook.....	99
5.1.	Conclusion.....	99
5.2.	Outlook.....	101
	Bibliography.....	105
	Acknowledgements.....	123

1. Introduction

The thesis is based on a unique high-resolution bathymetric, backscatter and 2D multichannel reflection seismic data set, which covers the submarine slope of São Miguel Island, the adjacent basins and bathymetric highs. No bathymetric data with a comparable resolution is accessible for the São Miguel region and the multichannel reflection seismic data is the first one recorded in the Azores at all.

São Miguel is the largest island of the Portuguese Azores Archipelago (*Ilhas dos Açores*) and the administrative center of the Autonomous Region of the Azores (*Região Autónoma dos Açores*). It is located in the North Atlantic approximately 1500 km west of continental Portugal and 4500 km east of the North American Coast. The archipelago is distributed around the Azores Triple Junction, where the Eurasian, North-American and Nubian (African) plates meet, and consists of nine inhabited islands and several islets all of them of volcanic origin (Fig. 1.1).

Five of nine islands were struck by volcanic eruptions since they were settled in the mid-fifteenth century (Booth et al., 1978; Moore 1990). At São Miguel Island 57 trachytic and basaltic eruptions are documented during the past 5000 years including plinian and sub-plinian type eruptions. The island consists of three major stratovolcanoes and each of them has erupted during the past 500 years. All these facts show the high volcanic risk to the large population of São Miguel (140,000 inhabitants) and particularly Furnas Volcano (one of three stratovolcanoes at São Miguel) represents a significant risk, since it has erupted five times during the last 1,100 years (most recently 1630 AD) and is still showing high hydrothermal activity (Guest et al., 1999; Moore, 1991). In contrast to subaerial volcanism, little is known about the occurrence of submarine volcanism. Indeed, in 1957/1958 the Capelinhos tuff cone was formed expanding the Faial Island (Cole et al., 2001) – initiated by submarine volcanism – and submarine volcanic activity northwest of Terceira Island became obvious between 1998 and 2001, since hot lava “balloons” were observed at the sea surface (Kueppers et al., 2012). In the São Miguel region, low resolution bathymetric data (1 x 1 km) shows several bathymetric highs and volcanic ridges (Lourenço et al., 1998) generally indicating the presence of submarine volcanism but giving no clue on the eruption styles, the controlling mechanisms and the associated subaerial risk potential. Additionally, this region generally poses unique study conditions for submarine volcanism, since the deep basins and volcanic ridges/islands encompass a wide range of water depths. Since decreasing water depth involves a decreasing ambient pressure, submarine volcanism is expected to be more explosive the shallower it gets.

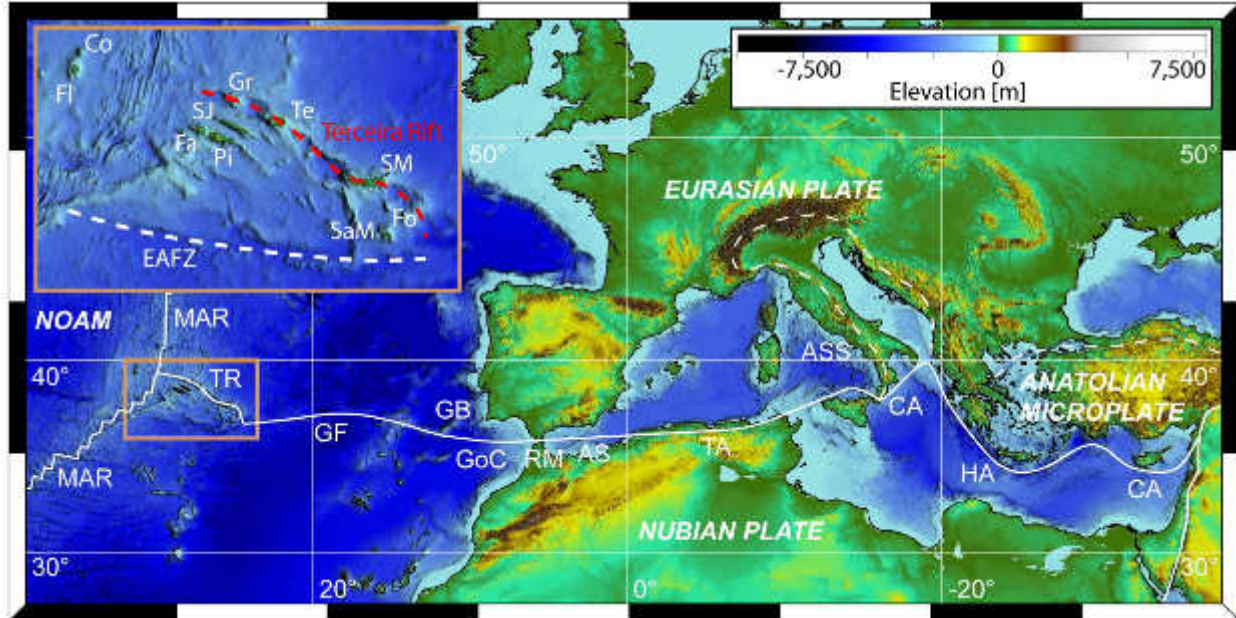


Fig. 1.1. Eurasian-Nubian plate boundary. Location of Mid-Atlantic Ridge (MAR) and the Eurasian-Nubian plate boundary simplified after Gente et al. (2003) and McClusty et al. (2003). NOAM: North American Plate; TR: Terceira Rift; GF: Gloria Fault; GB: Goringe Bank; GoC: Gulf of Cadiz; RM: Rif Mountains; AS: Alboran Sea; TA: Tell Atlas; ASS: Apennine Subduction System; CA: Calabrian Arc; HA: Hellenic Arc; CA: Cyprean Arc. Inset shows the Azores Archipelago and the Terceira Rift. EAFZ: East Azores Fracture Zone; Fl: Flores; Co: Corvo; Fa: Faial; Pi: Pico; SJ: São Jorge; Gr: Graciosa; Te: Terceira; SM: São Miguel; Fo: Formigas Islets; SaM: Santa Maria. Elevation data from ETOPO1.

At volcanic islands, hazard potential is posed by the constructional process, which is volcanism, but also by destructional processes like mass wasting and catastrophic flank collapses. Such slope instabilities are common at oceanic islands and significantly contribute to their erosion, together with e.g. subaerial and wave erosion, tectonics or subsidence (Ramalho et al., 2013). Prominent examples of giant landslides are described within the Canary Archipelago, where flank collapses substantially shape the on- and offshore morphology (e.g. Boulesteix et al. 2013). Collapses can be triggered by earthquakes and occur when the gravitational shear stress exceeds the sediment's mechanical shear strength (Løseth 1999). Gravitational shear can be increased by a high sedimentation rate resulting in an increasing sediment mass and/or depositional angle. Shear strength, on the other hand, is reduced e.g. by an increasing (relative) pore pressure in the sediment due to circulations of volcanic gases and hydrothermal fluids, high sedimentary load or sea level fall. Several large landslides are discussed for the Azores based on analyses of the onshore morphology of the islands, but most of them lack corresponding offshore observations (e.g. Hildenbrand et al., 2012a/b; Sibrant et al, 2014, 2015a). Hence, slope failures are proven with certainty at Pico Island only (Costa et al., 2014,

2015; Mitchell et al., 2012a). Indeed, a very recent study of Sibrant et al. (2015b) describe a further giant landslide at the eastern part of São Miguel Island based on, inter alia, the data set presented in this thesis, but apart from this the region totally lacks information concerning the occurrence of landslides at the slopes of São Miguel Island and the adjacent submarine volcanic edifices.

The geo-hazard potential of submarine volcanism and slope failures as well as information concerning submarine fault systems and their present-day activity, sedimentation pathways down the island slope, turbidity currents and the local stability or instability of sediment accumulations is of major interest to the local authorities with respect to risk management and industrial usage of the region. This thesis, therefore, will significantly contribute to 1) the knowledge of the occurrence of these processes, and 2) their understanding.

Beside these aspects, the São Miguel region as a segment of the so-called Terceira Rift is the result of a complex geodynamic setting. The Terceira Rift is defined by the islands of Graciosa, Terceira and São Miguel, the Formigas Islets and intercalated basins (Fig. 1.1 inset). It links the Mid-Atlantic Ridge (MAR) and a major transform fault known as Gloria Fault (Fig. 1.1). The evolution of the rift initiated after the Eurasian-Nubian plate boundary had moved northwards from its former position at the East Azores Fracture Zone (e.g. McKenzie, 1972; Krause and Watkin, 1970; Searle, 1980). However, the specific cause of this triple point movement is still unclear. The ongoing debate includes the hypotheses of a hot-spot interacting with the MAR (e.g. Gente et al., 2003), lithospheric stress induced by mantle convection (Adam et al., 2013) or changes in the Eurasian-Nubian plate kinematics (e.g. Luis and Miranda, 2008) and stress applied at the edge of the Eurasian Plate due to its geometry (Neves et al., 2013). A further unsolved question addresses the explicit nature of the Eurasian-Nubian plate boundary in the Azores domain. GPS data shows that Santa Maria and Graciosa resemble the relative plate movements of Nubia and Eurasia, respectively, whereas the islands of Faial, Pico, São Jorge, Terceira and São Miguel show intermediate behavior (Fernandes et al., 2006). Hence, it remained unclear for a long time if extension concentrates along the Terceira Rift only or if it is or was distributed. For the westernmost segment, recent studies proved a present-day diffuse plate boundary east of Graciosa and Faial forming a triple “area” with the MAR instead of a triple “point” (Marques et al., 2013, 2014a; Miranda et al., 2014), but suitable conclusions for the southeastern Terceira Rift cannot be drawn due to missing high-resolution bathymetric and seismic data. Contributing to these discussions is, therefore, a further major goal of this thesis.

1.1. *The Eurasian-Nubian plate boundary & the Azores Archipelago*

The geodynamic pattern of the Eurasian-Nubian plate boundary (Fig. 1.1) is characterized by an anti-clockwise rotation of the Nubian Plate relative to the Eurasian Plate around an Euler pole located offshore west of Africa (Nocquet, 2012; McClusky et al., 2003). This rotation causes a high variability of tectonic settings comprising converging segments in the eastern Mediterranean region becoming more and more oblique to the west, right lateral transpression (western Mediterranean) and transtension as well as oblique extension (Atlantic).

The eastern Mediterranean is dominated by the subduction of ancient oceanic Thethyan crust below the Anatolian Microplate (which is the deformed front part of the Eurasian plate) and the collision of stretched Eurasian and Nubian continental crust along the Cyprean Arc (Ben-Avraham et al., 1988; Netzeband et al., 2006; Robertson and Mountrakis, 2006) and the Hellenic Arc (Le Pichon and Angelier, 1979; McKenzie, 1972; Meulenkamp et al., 1987) (Fig. 1.1). The plate convergence causes the uplift of e.g. Cyprus and Crete (Meulenkamp et al., 1994) as well as the subaerial (e.g. Druitt, 1985) and associated submarine volcanism (Hübscher et al., 2015; Nomikou et al., 2013) in the Aegean volcanic arc.

To the west, the Hellenic Arc is linked to the Calabrian Arc (Polonia et al., 2011). The Calabrian Arc includes the volcanic arc of the Aeolian Islands and is part of the Apennine Subduction System, which is controlled by slab and trench retreat (Faccenna et al., 2004; Joliet et al., 2009; Wortel and Spakman, 2000).

Passing the Strait of Sicily, the plate boundary jumps to the southern coast of the Mediterranean and, hence, the western Mediterranean does not cover stretched Nubian but Eurasian crust. Further to the west, most of the Eurasian-Nubian convergence is accumulated along a 50-100 km wide E-W trending transpressive zone (Morel and Meghraoui, 1996), which involves the Tell Atlas mountains, the Alboran Sea and the Rif Mountains (Strait of Gibraltar). Associated deformation is characterized by active thrusting controlled by deep-rooted right-lateral transcurrent faults. West of the Strait of Gibraltar, within the Gulf of Cadiz, ocean-ocean convergence and associated subduction of Nubian crust led to the formation of an accretionary wedge (Gutscher et al., 2002), but present-day deformation is rather characterized by thrusting and right-lateral wrenching (Zitellini et al., 2009). This fault system southwest of the Iberian Peninsula was the source area of the 1755 Great Lisbon earthquake (Martinez Solares and López Arroyo, 2004). Most likely, it was the largest historical earthquake in Europe ever described (Baptista et al., 1998). It completely devastated the city of Lisbon by the combined effect of the earthquake itself, a conflagration and a subsequent tsunami (Zitellini et al., 2001).

West of the Goringe Bank deformation switches over to right-lateral transtension before the plate boundary is defined by a pure transform fault called Gloria Fault (Argus et al., 1989,

1.1. THE EURASIAN-NUBIAN PLATE BOUNDARY & THE AZORES ARCHIPELAGO

Laughton et al., 1972). Close to the Azorean island of Santa Maria, the Gloria Fault passes into the Terceira Rift, which merges with the Mid-Atlantic Ridge forming a diffuse triple junction (Marques et al., 2013, 2014a; Miranda et al., 2014).

The northward movement of this triple junction occurred synchronously to the final welding of Iberia to Eurasia between the Oligocene and lower Miocene (33-20 Ma, Luis and Miranda, 2008; Srivastava et al., 1990) and accompanied strong volcanism, intrusion of magma and the accretion of underplated material (Cannat et al., 1999; Luis et al., 1998). As a result, the Azores Plateau was molded resulting in an average crust thickness of 8-10 km (Luis and Neves, 2006; Silveira et al., 2010) and the formation of the Terceira Rift was initiated at around 20 Ma (Luis and Miranda, 2008). While extension of 4 mm/a is still occurring at the Terceira Rift domain (Fernandes et al., 2006), the formation phase of the plateau had ended at around 7 Ma and the constructed plateau was subsequently rifted from north to south by the Mid-Atlantic ridge (Gente et al., 2003). Submarine volcanism generated several linear volcanic ridges and complexes on top of the Azores Plateau, whose subaerial exposed parts represent the Azores Archipelago consisting of nine islands and several small uninhabited islets (Fig. 1.1 inset). The two westernmost islands, Flores and Corvo, lie on top of a NNE-SSW oriented ridge that is subparallel to the Mid-Atlantic Ridge. Both islands show no historic volcanic activity and oldest onshore lavas were dated to around 2 Ma years in case of Flores (Azevedo and Ferreira, 2006) and 1 Ma to 1.5 Ma in case of Corvo (França et al., 2006). Similar ages of 1 Ma to 1.3 Ma are reported for the central islands of Graciosa (Larrea et al., 2014; Sibrant et al., 2014), São Jorge (Hildenbrand et al., 2008; Silva et al., 2012) and Faial (Hildenbrand et al., 2012b). Age constraints at Terceira Island differ from 0.75 Ma to 3.5 Ma but a current study describes a maximum age of 0.4 Ma (Calvert et al., 2006 and references therein) similar to 0.3 Ma reported from the island of Pico (Cruz and Silva, 2000 and references therein). In contrast to the western islands, the central group lies on or form WNW-ESE oriented tectono-magmatic edifices (e.g. Hildenbrand et al., 2014; Lourenço et al., 1998). The region of the eastern islands lack such a clearly orientated setting but beside São Miguel Island the region is dominated by NW-SE to NNW-SSE trend (Lourenço et al., 1998). Reliable age constraints of onshore samples from the oldest, eastern part of São Miguel reveal maximum ages of 0.9 Ma (Johnson et al., 1998; Sibrant et al., 2015b). In this context, Santa Maria Island represents a special case since it is characterized by both, the oldest lavas with a maximum age of 5.7 Ma and the longest period of volcanic inactivity due to the fact that the latest eruption is dated to 2.8 Ma (Sibrant et al., 2015a).

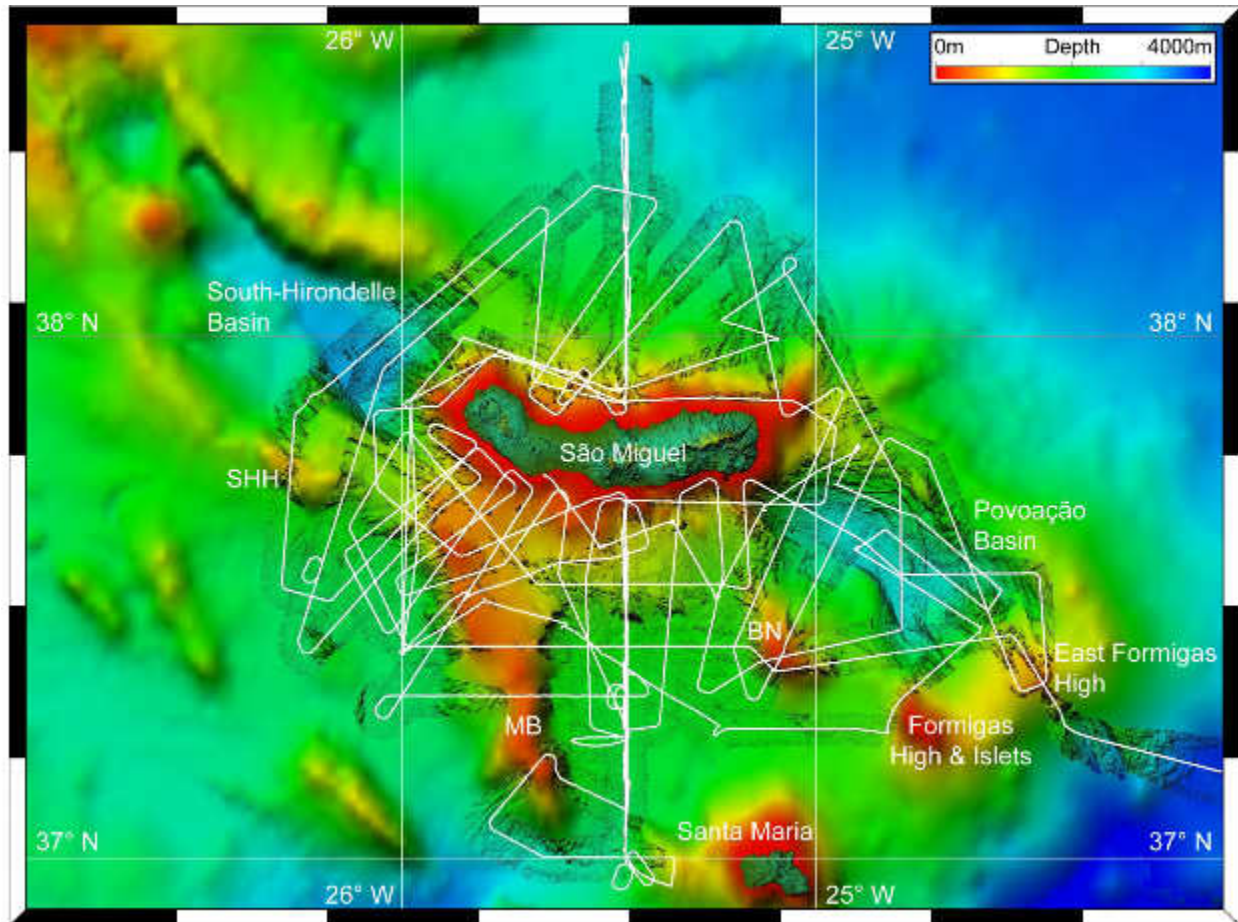


Fig. 1.2. Study area and data coverage of the M79/2 cruise. White line represents the ship track of the M79/2 cruise on board of RV METEOR. SHH: South-Hirondelle High; MB: Monaco Bank; BN: Big North High. Background bathymetric data from Lourenço et al. (1998). Onshore topographic data is from ASTER GDEM. Illumination from N320° with an altitude of 70°.

1.2. Data set and study area

The comprehensive data set presented in this thesis was recorded during the M79/2 cruise on board of RV METEOR in August/September 2009 (Hübscher, 2013). High-resolution bathymetric multibeam and backscatter data were acquired using the Kongsberg EM710 and EM120 echosounders stationary installed on board of RV METEOR. To obtain a continuous bathymetric coverage the high-resolution bathymetric data set was completed by a 1x1 km grid presented by Lourenço et al. (1998), which can be downloaded from http://w3.ualg.pt/~jluis/acoress_plateau.htm, and ETOPO1 bathymetry (~1.9x1.9 km) published by Amante and Eakins (2009). Additionally, bathymetric information at the northern shelf break described in chapter 4 was able to be completed by Kongsberg EM122 high-resolution data collected during the M113 cruise in January 2015. Onshore topography of São Miguel and Santa

1.2. DATA AND STUDY AREA

Maria was retrieved from the ASTER GDEM (30x30 m), which is a product of METI and NASA. In addition to the bathymetric and topographic information, the data set consists of 50 multi-channel seismic profiles with a total length of more than 1000 km (Fig. 1.2). More detailed descriptions of the bathymetric and seismic data itself and its processing will be given within the “Data and methods” sections of chapter 2, 3 and 4.

The data spreads around the island of São Miguel and covers the basins of the southeastern Terceira Rift, which are the South-Hirondelle Basin and the Povoação Basin northwest and southeast of the island. Southwest of the Terceira Rift, several bathymetric highs are present. The South-Hirondelle High is the shallowest part of a NW-SE oriented lineament, which forms the southwestern shoulder of the South-Hirondelle Basin. Between the islands of São Miguel and Santa Maria, Monaco Bank and Big North High represent dominant morphological features. Close to the intersection of the Terceira Rift and the Gloria Fault (which is not covered by our data), Formigas High and East Formigas High define the southeastern border of the Povoação Basin. The subaerially exposed part of the Formigas High is known as Formigas Islets. Since the vicinity of the islets is a protected area, no measurements were done there.

1.3. Structure of the thesis and resulting publications

The presented thesis is subdivided into five chapters consisting of the following content:

- Chapter 1: This chapter gives a first introduction and the general motivation of this study. Subsequently, an overview of the tectonic settings along the Eurasian-Nubian plate boundary is given focusing on the Terceira Rift region. It is followed by a short description of the working area (southeastern Terceira Rift) and the data the thesis is based upon.
- Chapter 2: Chapter 2 is based on a manuscript published in *Tectonophysics*: **Weiß, B.J., Hübscher, C., Lüdmann, T., 2015. The tectonic evolution of the southeastern Terceira Rift/São Miguel region (Azores). *Tectonophysics* 654, 75-95.** Within this publication, the complex submarine fault system is described and a seismic stratigraphy for the sedimentary basins in the working area is identified. Finally, a relative chronology of tectonic and volcanic processes is presented, which ultimately results in an evolutionary model for the southeastern Terceira Rift.
- Chapter 3: This chapter is based on a manuscript published in *Journal of Volcanology and Geothermal Research*: **Weiß, B.J., Hübscher, C., Wolf, D., Lüdmann, T., 2015. Submarine explosive volcanism in the southeastern Terceira Rift/São Miguel region (Azores). *Journal of Volcanology and Geothermal Research* 303, 79-91.** The submarine domain of the southeastern Terceira Rift reveals a large number of volcanic cones with a size of a few kilometers in width and a few hundred meters in height. These cones are mapped and analyzed in terms of their location and their morphological and surface characteristics. Seismic data highlights the internal structure and helps to distinguish between young and long-term volcanically inactive cones. Finally, the cones were classified and associated with explosive eruptions.
- Chapter 4: Chapter 4 is based on a manuscript submitted to *Marine Geology*: **Weiß, B.J., Hübscher, C., Lüdmann, T., Serra, N., 2015. Submarine sedimentation processes in the southeastern Terceira Rift/São Miguel region (Azores).** The characteristics and evolution of the shelf of São Miguel Island as well as downslope sedimentation processes are described. Bathymetric and seismic data at the lower slope and within the basin shows sliding, slumping, a flank collapse and current controlled deposition.

1.4. CONTRIBUTION OF OTHER PERSONS

Chapter 5: In the last chapter, the overall conclusions of the results obtained throughout the presented thesis are drawn. Finally, several further and/or unanswered scientific questions are stated and accompanied future or ongoing work is outlined.

1.4. Contributions of other persons

Chapters 2 and 3 are based upon manuscripts, which are published at *Tectonophysics* and *Journal of Volcanology and Geothermal Research*. Chapter 4 represents a manuscript, which has been submitted to an international scientific journal. Several persons have contributed to these manuscripts and their contributions are stated below:

Chapter 2: As my main doctoral adviser, Christian Hübscher (University of Hamburg) contributed to the ongoing discussion throughout the preparation phase of the manuscript. Comments of Thomas Lüdmann (University of Hamburg) as my second doctoral adviser and those of Fernando Ornales Marques (Universidade de Lisboa) and Neil Mitchell (University of Manchester) as the journal's reviewer helped to improve the manuscript.

Chapter 3: As my main doctoral adviser, Christian Hübscher (University of Hamburg) contributed to the ongoing discussion throughout the preparation phase of the manuscript. Daniela Wolf (University of Hamburg at that time) essentially contributed to mapping and statistical analysis of the volcanic cones. She provided the backscatter maps and reprocessed the seismic data for the detail study that is shown in chapter 3.4.2 and discussed in chapter 3.5.1. Comments of Thomas Lüdmann (University of Hamburg) as my second doctoral adviser and those of Paraskevi Nomikou (University of Athens) and Neil Mitchell (University of Manchester) as the journal's reviewer helped to improve the manuscript.

Chapter 4: Nuno Serra (University of Hamburg) conducted the modeling of the ocean currents within the working area. He also wrote the last paragraph of Chapter 4.3., describing the ocean circulation model. As my main doctoral adviser, Christian Hübscher (University of Hamburg) contributed to the ongoing discussion throughout the preparation phase of the manuscript. Comments of Thomas Lüdmann (University of Hamburg) as my second doctoral adviser helped to improve the manuscript.

2. The tectonic evolution of the southeastern Terceira Rift

Abstract

The eastern Azores Archipelago with São Miguel being the dominant subaerial structure is located at the intersection of an oceanic rift (Terceira Rift) with a major transform fault (Gloria Fault) representing the westernmost part of the Nubian-Eurasian plate boundary. The evolution of islands, bathymetric highs and basin margins involves strong volcanism, but the controlling geodynamic and tectonic processes are currently under debate. In order to study this evolution, multibeam bathymetry and marine seismic reflection data were collected to image faults and stratigraphy. The basins of the southeastern Terceira Rift are rift valleys whose southwestern and northeastern margins are defined by few major normal faults and several minor normal faults, respectively. Since São Miguel in between the rift valleys shows an unusual W-E orientation, it is supposed to be located on a leaky transform. South of the island and separated by a N120° trending graben system, the Monaco Bank represents a N160° oriented flat topped volcanic ridge dominated by tilted fault blocks. Up to six seismic units are interpreted for each basin. Although volcanic ridges hamper a direct linking of depositional strata between the rift and adjacent basins, the individual seismic stratigraphic units have distinct characteristics. Using these units to provide a consistent relative chrono-stratigraphic scheme for the entire study area, we suggest that the evolution of the southeastern Terceira Rift occurred in two stages. Considering age constrains from previous studies, we conclude that N140° structures developed orthogonal to the SW-NE direction of plate-tectonic extension before ~10 Ma. The N160° trending volcanic ridges and faults developed later as the plate tectonic spreading direction changed to WSW-ENE. Hence, the evolution of the southeastern Terceira Rift domain is predominantly controlled by plate kinematics and lithospheric stress forming a kind of a re-organized rift system.

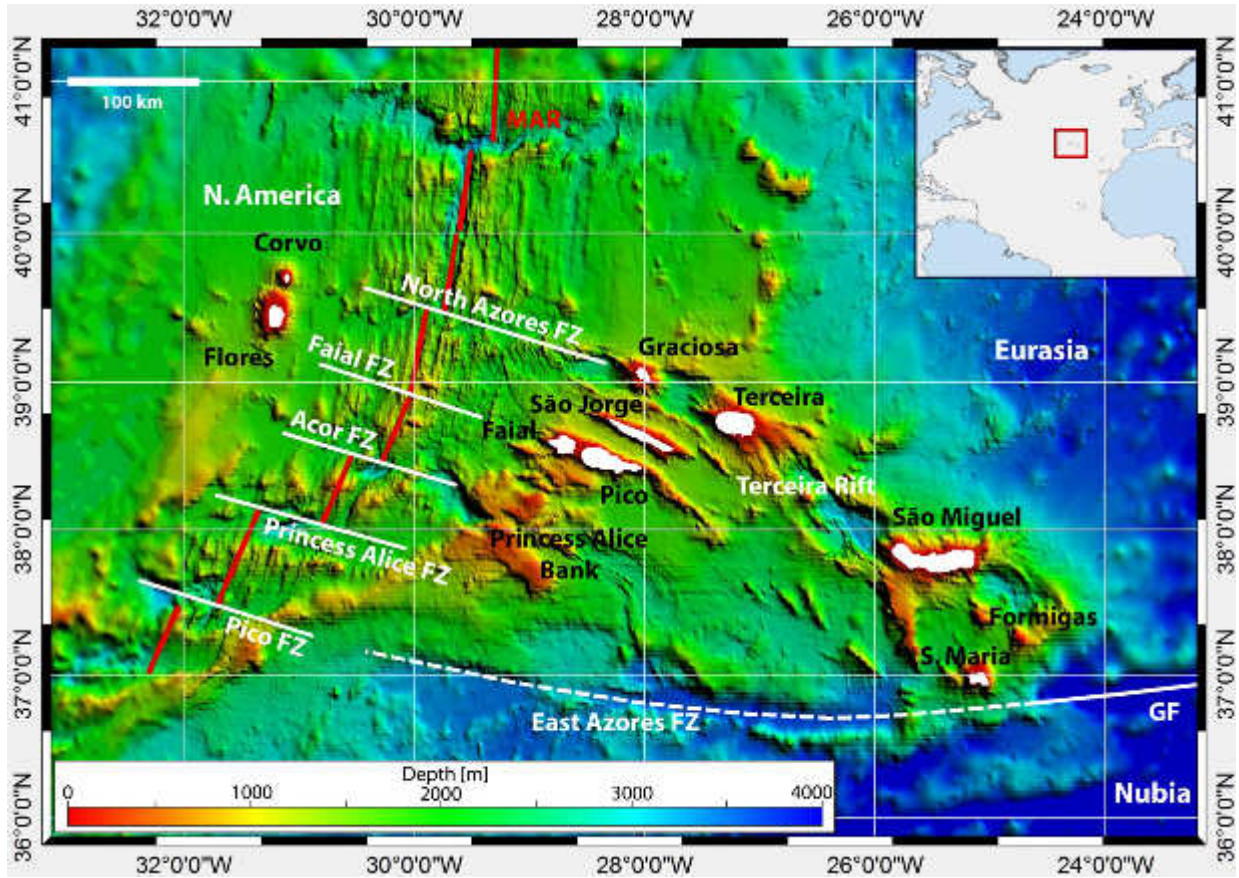


Fig. 2.1: Azores Plateau and corresponding structures. MAR: Mid-Atlantic Ridge; GF: Gloria Fault; FZ: Fracture Zone. Bathymetric data from Lourenço et al. (1998) and ETOPO1 (Amante & Eakins, 2009). Structural features after Luis et al. (1994).

2.1. Introduction

The Azores Archipelago is located at the Mid-Atlantic Ridge (MAR) where three major lithospheric plates converge (Fig. 2.1): the North American Plate in the west and the Eurasian and Nubian plates in the east, the last two separated from each other by a major transform fault (Gloria Fault). MAR and Gloria Fault are linked by an oblique oceanic rift system (Terceira Rift), which is accommodating dextral transtension in WSW-ENE direction caused by the relative movement of the Eurasian and Nubian plates (Fernandes et al., 2006; DeMets et al., 2010). Northward migration of the triple point and the evolution of the present-day Terceira Rift involved increased volcanism/magmatism causing the formation of the Azores Plateau (e.g. Luis et al., 1998; Georgen and Sankar, 2010), a prominent morphological high with an abnormal low water depth of ~2000 m. The volcanic islands at the northeastern rim of the Azores Plateau represent the present-day subaerial volcanism. Hence, the Terceira Rift resembles e.g. the

2.2. GEOLOGICAL CONTEXT

Spieß Ridge in the South Atlantic in terms of a volcanically active and oblique rift system linking a spreading axis with a major transform fault (Ligi et al., 1999; Mitchell et al., 2000).

Both, the jump of the triple junction and the strong volcanism are associated with the existence of a hot spot (e.g. Schilling, 1975; Cannat et al., 1999; Gente et al., 2003) or an anomalously volatile-enriched upper mantle (e.g. Schilling et al., 1980, Bonatti, 1990) which once interacted or is still interacting with the MAR. Yet, the initiation of the Azores Plateau evolution correlates with changes in the relative plate movements of Nubia and Eurasia (Luis and Miranda, 2008) and the increased volcanism is proposed to be caused by stretching of the lithosphere (e.g. Luis et al., 1994; Marques et al., 2013, 2014a; Métrich et al., 2014). Hence, it is still up for debate if the tectonic evolution of the elevated seafloor and the volcanic ridges is mainly controlled by upper mantle processes or induced by lithospheric stress due to tectonic plate kinematics.

In this context, the presented study aims for a deeper insight in the geological evolution of the southeastern Terceira Rift and its submarine basins and highs in time and space. Based on a unique high resolution bathymetric and seismic 2D multi-channel data set, we mapped the complex submarine fault systems and identified a seismic stratigraphy for the sedimentary basins in the São Miguel region. Therefore, the first objective is to describe the submarine faults and volcanic ridges before distinguishing between different sedimentation conditions and the corresponding tectonic and/or volcanic processes. The different stratigraphic sequences then have to be correlated between the basins. This will allow us to evaluate a relative chronology of tectonic and volcanic processes in the working area, which will ultimately result in an evolutionary model for the southeastern Terceira Rift. Finally, general implications will be drawn in terms of structural development and nature of the whole Azores Plate Boundary.

2.2. Geological Context

2.2.1. Terceira Rift & Azores Triple Junction

The Azores Archipelago consists of 9 islands (Fig. 2.1). The two westernmost islands (Corvo, Flores) are located on present-day stable North American Plate, whereas the central (Graciosa, Terceira, São Jorge, Faial, Pico) and eastern islands (São Miguel, Santa Maria, Formigas Islets) are distributed along the Nubian-Eurasian plate boundary. The northeastern islands and intercalated basins are known as Terceira Rift, which is defined by the South-Hirondelle Basin, São Miguel Island, the Povoação Basin and the Formigas ensemble in the working area (Fig. 2.2).

To the South, the East Azores Fracture Zone (EAFZ) forms the southern boundary of the Azores Plateau (Fig. 2.1) representing the fossil trace of the Gloria Fault on the Nubian Plate (Krause

2. THE TECTONIC EVOLUTION OF THE SOUTHEASTERN TERCEIRA RIFT

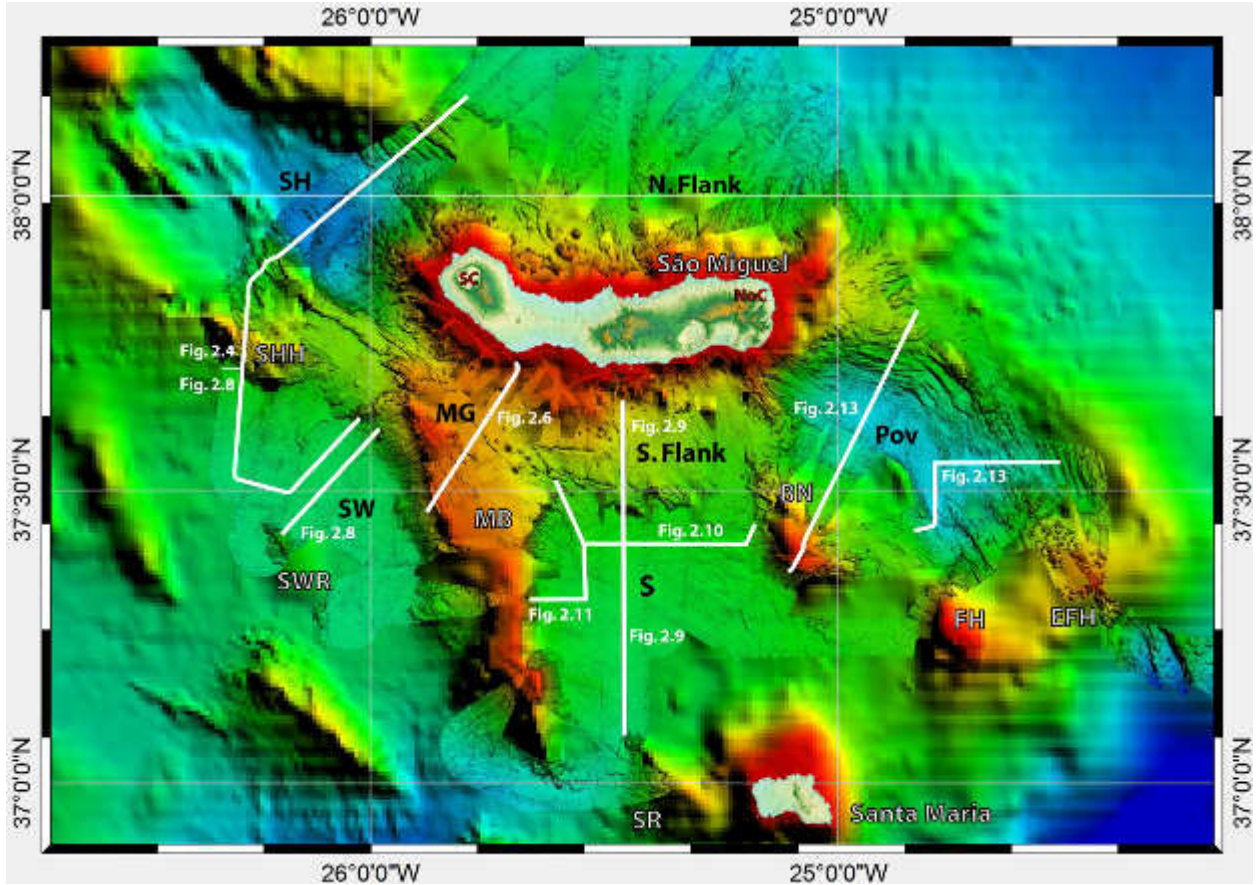


Fig. 2.2: Deposition centers and structures in the working area and location of seismic profiles shown in this chapter. Deposition centers (black): SH: South-Hirondelle Basin; MG: Monaco Graben; SW: Southwest Basin; S: South Basin; Pov: Povoação Basin. Submarine Highs (white): SHH: South-Hirondelle High; SWR: Southwest Ridge; SR: South Ridge; MB Monaco Bank; BN: Big North High; FH: Formigas High; EFH: East Formigas High. Onshore volcanos (red): SC: Sete Cidades Volcano; NoC: Nordeste Complex.

and Watkins, 1970; McKenzie, 1972; Searle, 1980; Luis and Miranda, 2008). At its transition to the Pico Fracture Zone, the EAFZ originally formed the triple point with the MAR in a ridge-fault-fault (RFF) setting. Synchronously to the final stage of the Iberia-Eurasia suture between Oligocene and lower Miocene (33 - 20 Ma; Srivastava et al., 1990; Luis and Miranda, 2008), the triple point moved northward either in one (Searle, 1980; Gente et al., 2003) or in several steps (Luis et al., 1994; Vogt and Jung, 2004) possibly forming an interim independent Azores Micro Plate (Luis et al., 1994). However, significant extension of 4 mm/a started to occur in the Azores domain at ~20 Ma initiating the evolution of the Terceira Rift in a N50° extensional setting (Luis and Miranda, 2008). While the extension rate is still 4 mm/a (Fernandes et al., 2006), extensional direction rotated from N50° to the present-day ~N70° direction (DeMets et al., 2010) ~10 Ma ago (Luis and Miranda, 2008). Until 7 Ma, the formation of the Terceira Rift involved the accretion of large volumes of extrusives and intrusives as well as underplated material (Luis et al., 1998; Cannat et al., 1999; Gente et al., 2003). This caused the creation of

2.2. GEOLOGICAL CONTEXT

thickened crust (Luis and Neves, 2006; Dias et al., 2007; Georgen and Sankar, 2010; Silveira et al., 2010) referencing to the abnormal elevated seafloor of the Azores Plateau.

Today, the triple junction is located 150 – 250 km north of its former position (Fig. 2.1) forming a diffuse triple junction area between the Acor and North Azores Fracture Zone (Marques et al., 2013, 2014a; Miranda et al., 2014), where the MAR spreading rate increases from 20 mm/a in the south to 22 mm/a in the north (DeMets et al., 2010). Further to the east and west of Terceira, extension is mainly accommodated along N110°-120° striking linear volcanic ridges (with São Jorge and Faial/Pico representing an extreme case) and N120°-160° trending faults (e.g. Lourenço et al., 1998; Miranda et al., 1998; Hildenbrand et al., 2014; Miranda et al., 2014), which overprint MAR related N15° fabrics. Southeast of Terceira, extension concentrates at the southeastern Terceira Rift, where N140° to N150° trending structures become abruptly prominent (Lourenço et al., 1998; Miranda et al., 1998; Fernandes et al., 2006). These different trends are assumed to be the result of plate boundary effects (Georgen and Sankar, 2010; Neves et al., 2013) and structural heritage (Navarro et al., 2009). They form a diffuse plate boundary consisting of several tectonic blocks (Miranda et al., 1998; Lourenço et al., 1998) and en échelon horst graben structures (Marques et al., 2013, 2014a; Miranda et al., 2014). Local seismicity is dominated by normal and strike-slip faulting (Udias et al., 1976; Grimison and Chen, 1986; Buforn et al., 1988; Borges et al., 2007) within a right lateral transtensional regime. However, sinistral strike-slip events have been recognized as well (Hirn et al., 1980).

2.2.2. Upper mantle anomaly

Ridge jump and strong volcanism in the Azores domain are attributed to an interaction of a hot-spot with the MAR by several authors. This coincides with the observation of geochemical anomalies (e.g. Schilling, 1975; White and Schilling, 1978; Bourdon et al., 2005) and an anomalous elevated ridge-axis (e.g. Schilling 1985; Detrick et al., 1995; Thibaud et al., 1998; Escartín et al., 2001). Based on tomographic studies (e.g. Montelli et al., 2006; Yang et al., 2006; Silveira et al., 2006, 2010), corresponding negative seismic velocity anomalies beneath the Azores are observed. Starting interaction between MAR and a moving hot-spot initiated the northward migration of the triple junction (Vogt and Jung, 2004) and caused enhanced volcanism forming the Azores Plateau. After the hot-spot had passed the ridge, the constructed plateau was rifted and normal seafloor spreading has reestablished (Cannat et al., 1999; Escartín et al., 2001; Gente et al., 2003). Involved mantle upwelling partly accounts for the depth anomaly associated with the Azores Plateau and traction of the mantle flow beneath the lithosphere controls rifting processes along the Terceira rift (Adam et al., 2013).

In contrast, other authors refer to the fact that the islands are young and do not reflect a hot-spot-track in terms of a clear age progression (Beier et al., 2008). As an alternative, they propose upper mantle domains with an enriched volatile content (Bonatti, 1990; Asimow et al.,

2004) or the decompression of a “wet” mantle caused by extensional tectonics (Métrich et al., 2014) to contribute to the enhanced volcanism.

2.3. Data and methods

This work is based on high resolution bathymetric data and a 2D multi-channel seismic data set collected by University of Hamburg scientists on board of *RV METEOR* during cruise M79/2 in 2009 (Hübscher, 2013). The seismic data set consists of profile lines with a total length of 1000 km spread around São Miguel Island. The seismic signals were generated by an array of two GI-Guns with a generator volume of 45 cubic inch and an injector volume of 105 cubic inch each. For data recording a 600 m long asymmetric digital streamer was used, containing 144 channels with an average increment of 4.2 m. Shots were released every 25 m at a speed of 5 kn. Data processing first encompassed trace editing and CMP sorting with a CMP increment of 5 m. Subsequently, several bandpasses with 10/20/300/400 Hz, spike and noise burst filter, FX-deconvolution and FK-filter were applied before NMO-correction and post stack time migration.

High resolution bathymetric data were synchronously recorded using the Kongsberg EM710 and EM120 Multibeam echosounders installed on board of *RV METEOR*. During processing, navigation errors were interpolated and depths/positions were recomputed using sound velocity profiles. After beam editing was applied for every single swath to eliminate spikes and noisy data, the data was gridded with a spacing of 26 x 26 m. However, since the horizontal accuracy is limited to ~2% of the water depth, effective resolution in water depth higher than 1300 is less. The background bathymetric information is a superposition of a 1 x 1 km grid of data presented by Lourenço et al. (1998), which can be found under http://w3.ualg.pt/~jluis/acoress_plateau.htm, and ETOPO1 data (~1.9 x 1.9 km) published by Amante and Eakins (2009). The topographic data shown is originated from ASTER GDEM, which is a product of METI and NASA.

For this study, faults were picked based on the high resolution bathymetry only. Presented rose diagrams summarize the strike of fault segments weighted by fault lengths. Counts of picked fault segments are given in the upper left corner of the diagram inset (Figs. 2.3, 2.5 and 2.12). Dip angles of fault scarps were measured based on the EM120/EM710 data using the program *FLEDERMAUS* (© by QPS).

Intervening bathymetric highs and volcanic ridges hamper the direct stratigraphic correlation of the sedimentary basins. Nevertheless, characteristics and geometry of seismic units as well as onlap configurations between them allow us to identify a relative chronology encompassing three major phases in the evolution of the working area. An overview of these evolutionary

2.4. RESULTS AND INTERPRETATION

stages, a brief description of the associated geological processes and the equivalent seismic units are given in Tab. 2.1 presented in Sub-chapter 2.5. Colors of Tab. 2.1 match the colors of the corresponding seismic units presented in Figs. 2.4, 2.6, 2.8, 2.9, 2.10, 2.11 and 2.13 as well as the color-code of the sketches in Figs. 2.13 and 2.14. Units associated with two major phases are described by a gradual transition of the corresponding colors (e.g. SH2-5b in Fig. 2.4). The nomenclature of the seismic units is based on the abbreviation of the depositional center (e.g. MG for Monaco Graben). Units of different depositional centers with the same number are associated with the same geological phase of evolution and therefore trace the relative chronology in the working area (see Tab. 2.1). Sediment thicknesses are given in milliseconds [ms] throughout the text, since a velocity analysis was not performed during data processing. Assuming interval velocities of 2000 m/s within the sedimentary units, milliseconds are equivalent to meters.

2.4. Results and interpretation

The working area is dominated by a succession of bathymetric highs (strongly over-printed by tectonism) and basins. Combined descriptions of bathymetric expression, seismic profiles and the resulting stratigraphy are presented for 5 geographical sub-areas treated in an anticlockwise manner around São Miguel (Fig. 2.2): South-Hirondelle Basin (SH), Monaco Graben (MG) & Monaco Bank (MB), Southwest Basin (SW), South Basin (S) & southern island slope and Povoação Basin (Pov). Additional information are given in the appendix (App. 2.1 and App. 2.2).

2.4.1. South-Hirondelle Basin

2.4.1.1. *Observations bathymetry*

The bathymetry northwest of São Miguel Island is dominated by the South-Hirondelle Basin (SH) with a maximum water depth of 3250 m (Fig. 2.3). To the southwest, the basin is bordered by a volcanic ridge including the South-Hirondelle High and, to the northeast, by a further volcanic ridge, both dissected by numerous normal faults with typical vertical offsets of 200/300 m. Fault scarps of the northeastern ridge dip basinwards with 30-45°. Some of the faults apparently reach the submarine slope of Sete Cidades Volcano, where they offer/offered a pathway for magma to ascent resulting in chains of elongated volcanic structures or cones. In contrast, the southwestern ridge is more complex as it is offset by inward dipping faults. Corresponding fault scarps again reveal dip angles of 30-45°. The basin itself is asymmetric since the northeastern flank shows an average slope angle of 5°, whereas the southwestern flank is

2. THE TECTONIC EVOLUTION OF THE SOUTHEASTERN TERCEIRA RIFT

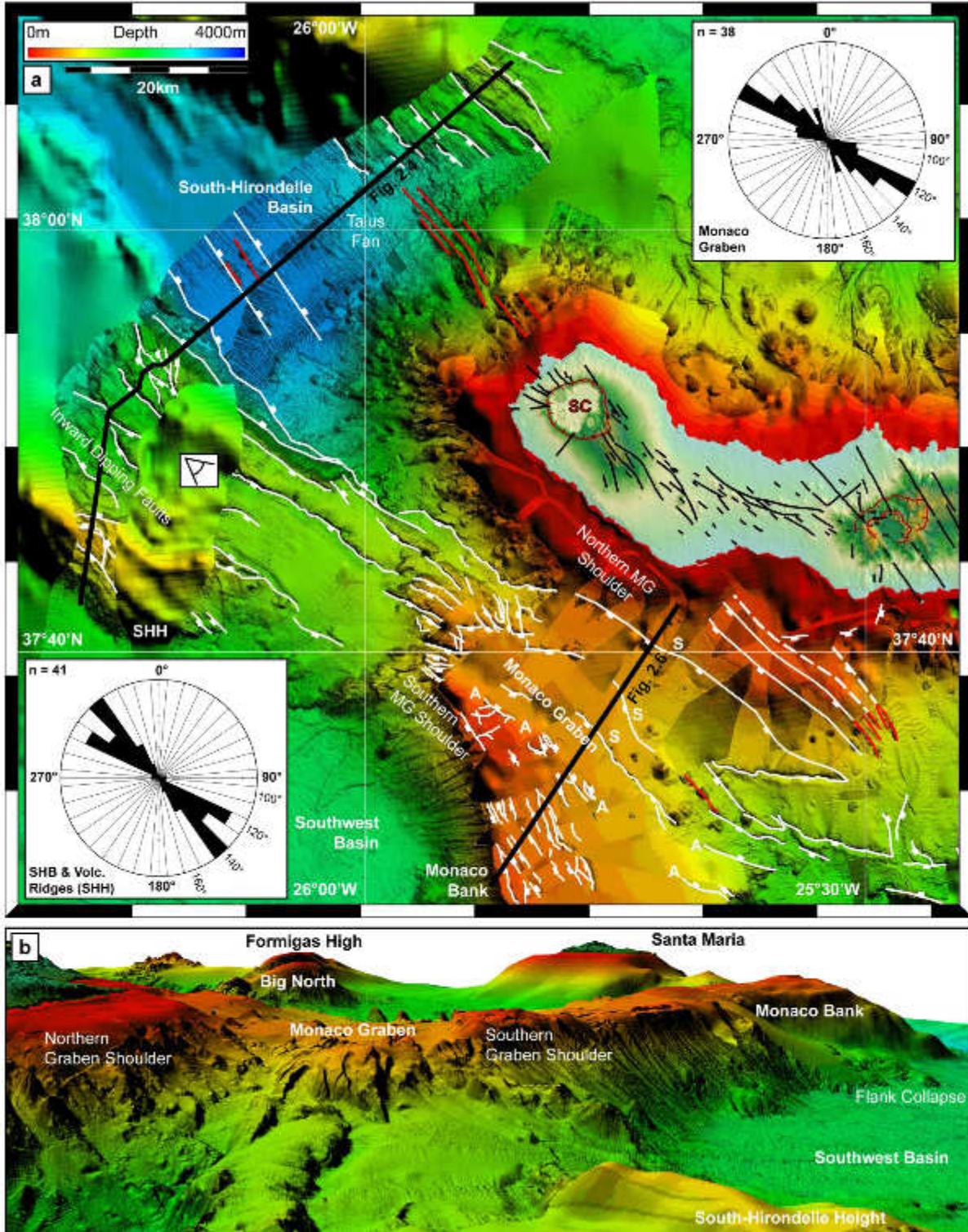


Fig. 2.3: Bathymetry and picked faults in the western working area (a) and 3D view (b). Monaco Graben is bounded to the south by an antithetic fault A, which also separates N120° and N160° setting. S marks the synthetic normal faults described in the text (a). White line: Fault. Dashed white line: Inferred fault. Red line: Volcanic lineament. Thick black lines indicate seismic profiles. Onshore faults based on Queiroz (1997), Ferreira (2000) and Carvalho et al. (2006). SHB: South-Hirondelle Basin; SHH: South-Hirondelle High. Eye symbol denotes viewing direction of bottom 3D sight. Illumination from N90° with an azimuth of 60°.

2.4. RESULTS AND INTERPRETATION

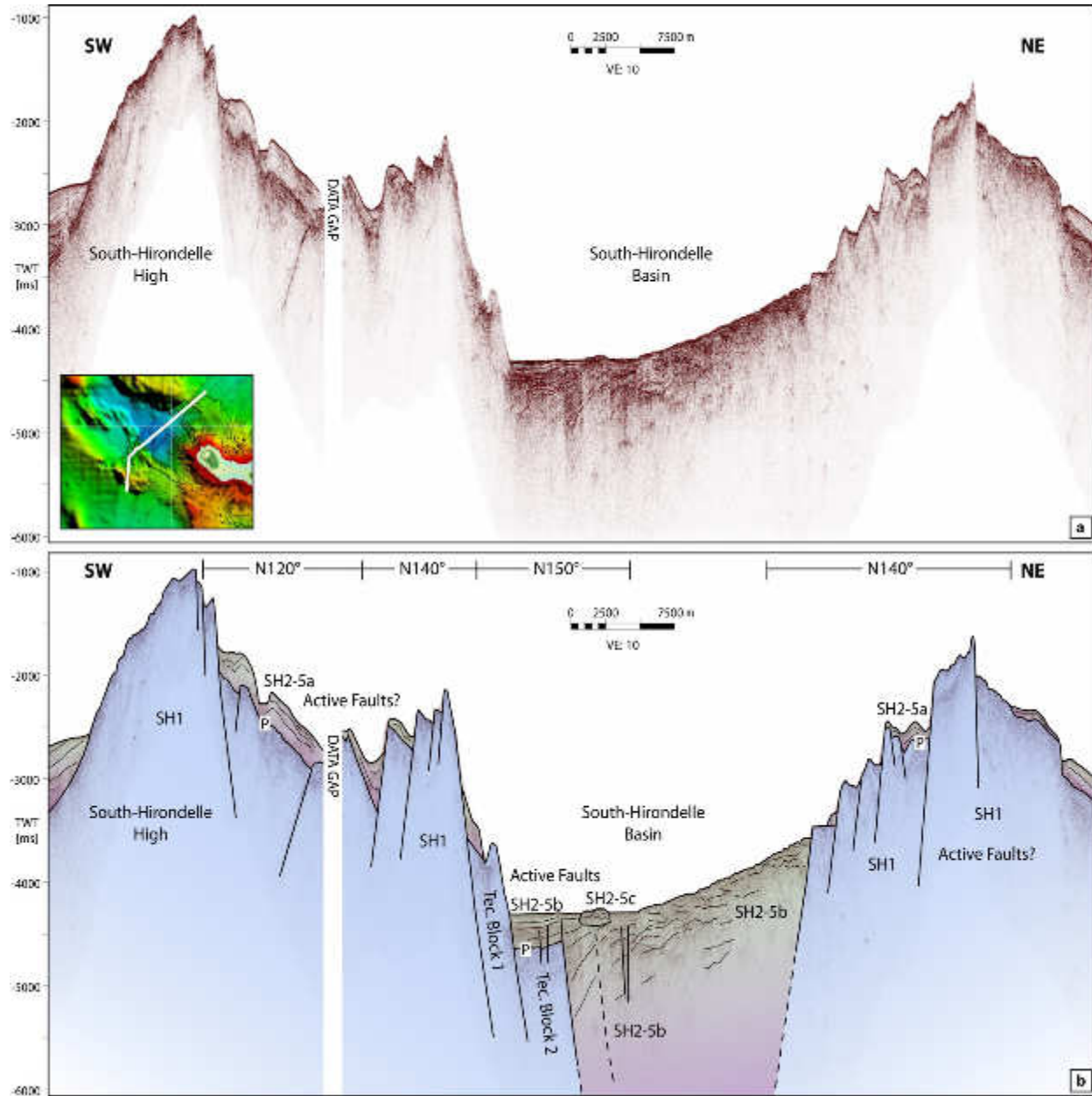


Fig. 2.4: Seismic section (a) and corresponding interpretation (b) covering the South-Hirondelle Basin and the adjacent volcanic ridges west of São Miguel Island in a SW-NE direction. Dashed line: Inferred fault. VE: Vertical Exaggeration. For the section's location see inset, Fig. 2.2 or 2.3.

formed by two major fault scarps each dipping with 25-30° and altogether revealing a vertical offset of 1600 m.

Three dominant strike directions were identified. Faults at the northeastern ridge strike ~N140°. Two faults piercing the seafloor in the basin and the major fault at the lower slope of the southwestern ridge trend ~N150°. On top of the southwestern ridge, again a comparable

N140° trend is observable, but interfering with a N120° oriented fault system. These faults continue to the southeast where they merge with the mainly N120° trending Monaco Graben.

2.4.1.2. *Observations seismic*

Four distinct seismic units are resolved within the basin (Fig. 2.4). SH1 represents the acoustic basement and is highly offset by normal faults. The volcanic ridges bordering the basin are both covered by a thin sedimentary unit (SH2-5a), which reveals sub-parallel reflections and masks basement faults south of the data gap. Inside the basin, unit SH2-5b shows distorted and irregular high amplitude reflections where the seafloor slightly dips basinward. Where the seafloor is flat, SH2-5b is characterized by divergent reflections dipping southwest. On top, the small unit SH2-5c is piercing the seafloor. It is characterized by strong chaotic and disrupted reflections.

2.4.1.3. *Combined interpretation of bathymetric and seismic data*

Due to the high reflection amplitude, we interpret reflection “P” as the magmatic/volcanic basement (Fig. 2.4). The lenticular geometry of SH2-5a and the presence of moats adjacent to escarpments in the basement suggest current controlled deposition (Rebesco et al. 2014 and references therein) on top of the rift flanks. The lateral variation of the internal stratification of SH2-5b implies a lateral variation of depositional processes. The northeastern part represents a talus fan. In contrast, the southwestern part is well stratified and shows strong internal reflections implying an obviously alternating acoustic impedance and a vertically alternating succession of turbidites and hemipelagic sediments, respectively. SH2-5c is the southeastern tip of a volcanic lineament (red line within the basin in Fig. 2.3a) and – consequently – of volcanic origin. The South-Hirondelle Basin represents a graben with dominant N140-150° oriented normal faults within the basin. The divergent reflection pattern of southwestern SH2-5b is a clear evidence for syn-sedimentary tectonics and indicates major vertical movements along the southwestern basin margin (Fig. 2.4). The recent activity of the N140° trending faults on top of the northeastern ridge and its southwestern counterpart is ambiguous. Depositional voids can be considered either as current induced moats or as the consequence of recent tectonics. These two processes do not exclude each other, both processes may act simultaneously. Mapped faults within Sete Cidades region (Queiroz, 1997; Ferreira, 2000) trend N140° and represent the onshore continuation of the faults shaping the southern flank of the northeastern ridge (Fig. 2.3a).

2.4. RESULTS AND INTERPRETATION

2.4.2. Monaco Graben & Monaco Bank

2.4.2.1. *Observations bathymetry*

The Monaco Graben (MG) separates the island shelf in the north and the Monaco Bank Plateau (Fig. 2.3a/b). Several predominantly circular cones are located within the graben, most of them in the very southeast where the graben pinches out. The graben flanks are defined by the smooth 10-15° dipping slope of the island's shelf in the north and a steep flank in the south showing slope angles of up to 70° (marked with A in Fig. 2.3a).

Monaco Bank (MB) represents a prominent 70 km long bathymetric feature with a maximum width of 25 km (Fig. 2.5a/b). Being elevated by 1700-2000 m above the surrounding basin floors, its top is characterized by a plateau slightly ascending to the northwest. This plateau forms the southern shoulder of the Monaco Graben (Fig. 2.3b). A set of normal faults disrupt the western bank from north to south usually characterized by vertical offsets of 50-100 m. The scarps mostly dip westwards with 30-45°. To the east, faulting becomes less obvious.

Faults show two orientations: Monaco Graben reveals a clear N120° main trend (see upper right rose diagram in Fig. 2.3a); faults on top of Monaco Bank strike N160° similar to Monaco Bank itself (see left rose diagram of Fig. 2.5a).

2.4.2.2. *Observations seismic*

On top of Monaco Bank, sediment cover is thin and seismically not resolvable (Fig. 2.6). Accordingly, the basal seismic unit MG2 is subcropping here. It is characterized by low penetration and strong reflection amplitudes. Inside Monaco Graben, two seismic units can be determined. Lower unit MG3 shows a variable reflection pattern from sub-parallel to divergent, contorted and tilted. It partly overlies the basement (horizon Q) unconformably with increasing thickness to the north-east. Horizon R marks the transition from (sub-) parallel to divergent and oblique reflection pattern of unit MG4/5 and also correlates with the root of two of the cones mentioned in Sub-chapter 2.4.2.1.

2.4.2.3. *Combined interpretation of bathymetric and seismic data*

The Monaco Graben forms a N120° trending and northeast tilting half-graben system with a basement sheared by four synthetic normal faults (marked with S in Fig. 2.3a). Its southern rim is a steep antithetic fault, which also acts as boundary between the N120° and N160° fault setting (marked with A in Fig. 2.3a). The faults clearly offset internal stratification, but vanish within unit MG3 indicating that major tectonics ceased during that time (Fig. 2.6). In the northeast, one synthetic fault transects the seafloor. However, sediments of unit MG4/5 southwest of the fault are neither tilted nor do they show any indications to be dragged

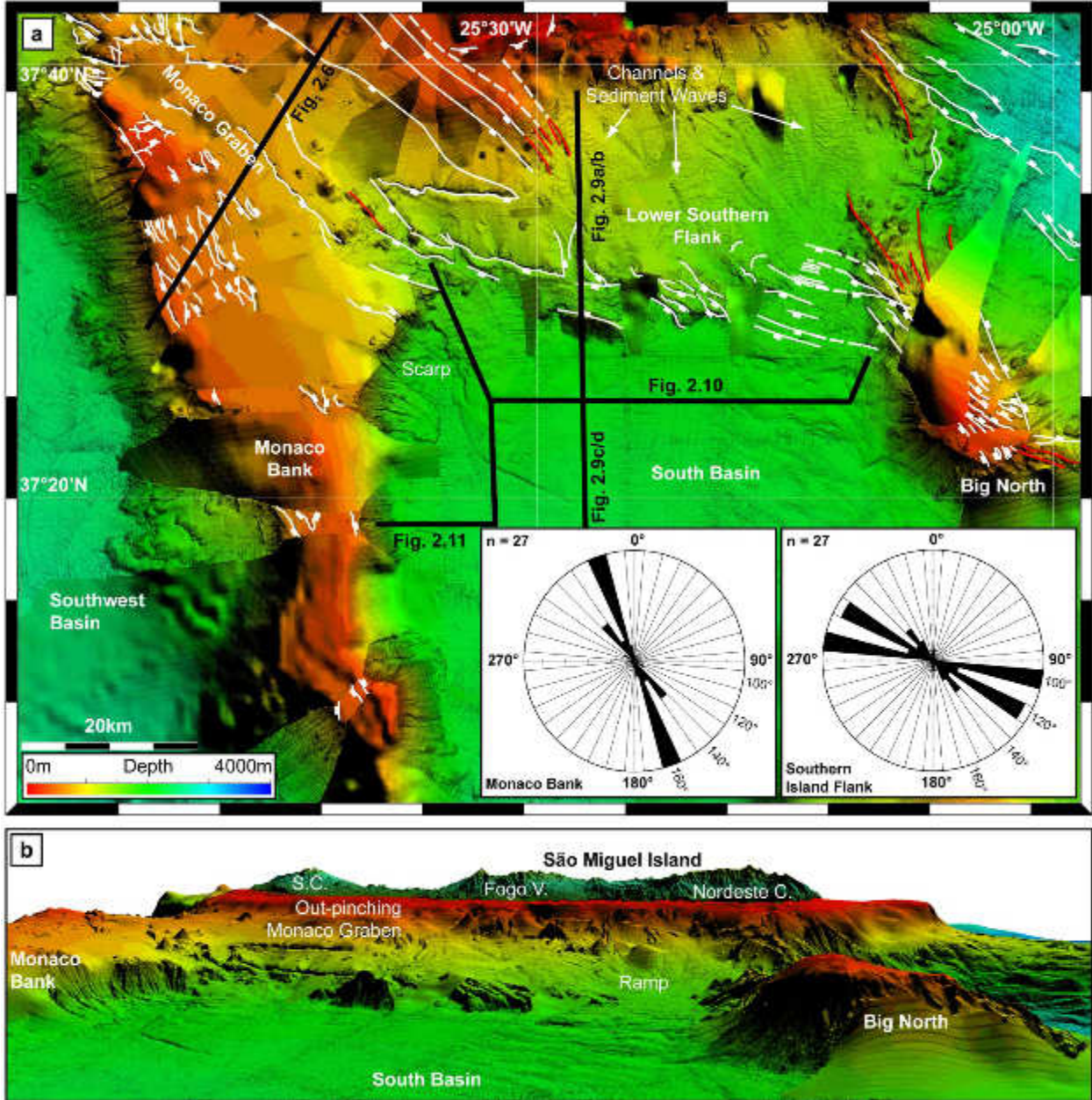


Fig. 2.5: Bathymetry and picked faults in the southern working area (a) and 3D view (b). White line: Fault. Dashed white line: Inferred fault. Red line: Volcanic lineament. Thick black lines indicate seismic profiles. S.C.: Sete Cidades Volcano. Viewing direction of 3D sight from Santa Maria Island to the north. Illumination from N90° with an azimuth of 60°.

(Fig. 2.6b, inset). Due to the convex shape of MG4/5 northeast of the fault, we rather assume bottom currents to be the reason for non-deposition along the fault plane instead of recent tectonic movements. This is also in accordance with the fact that Monaco Graben shows no recent seismicity (App. 2.1). Hence, we interpret MG4/5 as predominantly current controlled post-tectonic sediments. The tilted and divergent reflection pattern of MG3 reflects growth-

2.4. RESULTS AND INTERPRETATION

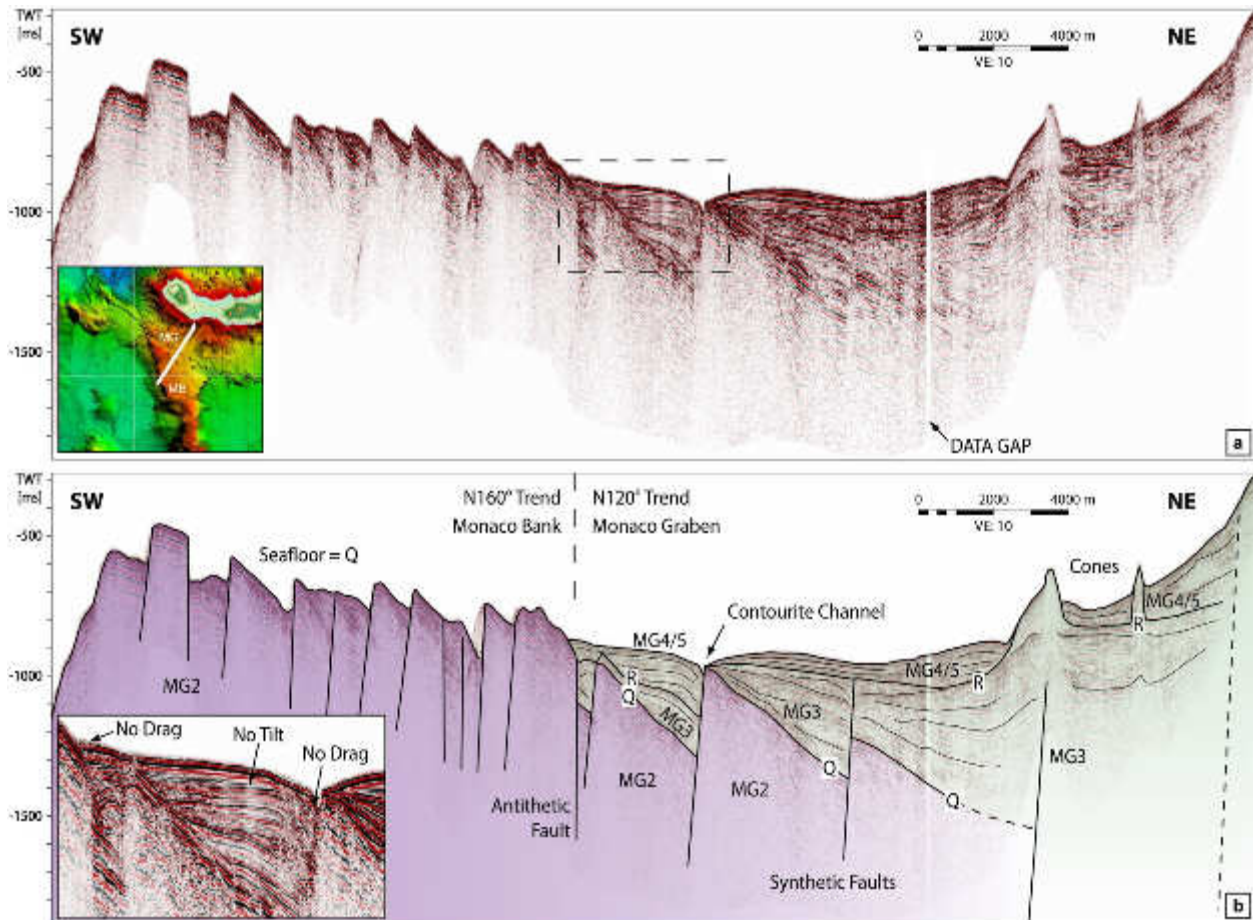


Fig. 2.6: Seismic section (a) and interpretation (b) covering the Monaco Graben southwest of São Miguel Island. Dashed line: Inferred fault. Dashed black box indicates location of zoomed seismic in (b). MG: Monaco Graben; MB: Monaco Bank. VE: Vertical Exaggeration. For the section's location see inset, Fig. 2.2, 2.3 or 2.5.

strata indicating syn-tectonic sedimentation conditions during graben formation. A northward increasing thickness of unit MG3 (Figs. 2.6 and 2.7) refers to a major sediment source north of the graben, probably indicating strong volcanism in the present-day Sete Cidades region. However, the cones interpreted as to be of volcanic origin (see Stretch et al. (2006) and Mitchell et al. (2012b) for comparable structures southeast of Pico Island) show that volcanism also occurred within the graben. Younger MG4/5-sediments onlap the cone flanks (Fig. 2.6), thus indicating that volcanism stopped at the end of graben formation (Chapter 3). Since MG2, interpreted as volcanic basement, is not covered by sediments on top of Monaco Bank, it is not possible to derive any kinematic conditions in time along the N160° trending faults system.

2. THE TECTONIC EVOLUTION OF THE SOUTHEASTERN TERCEIRA RIFT

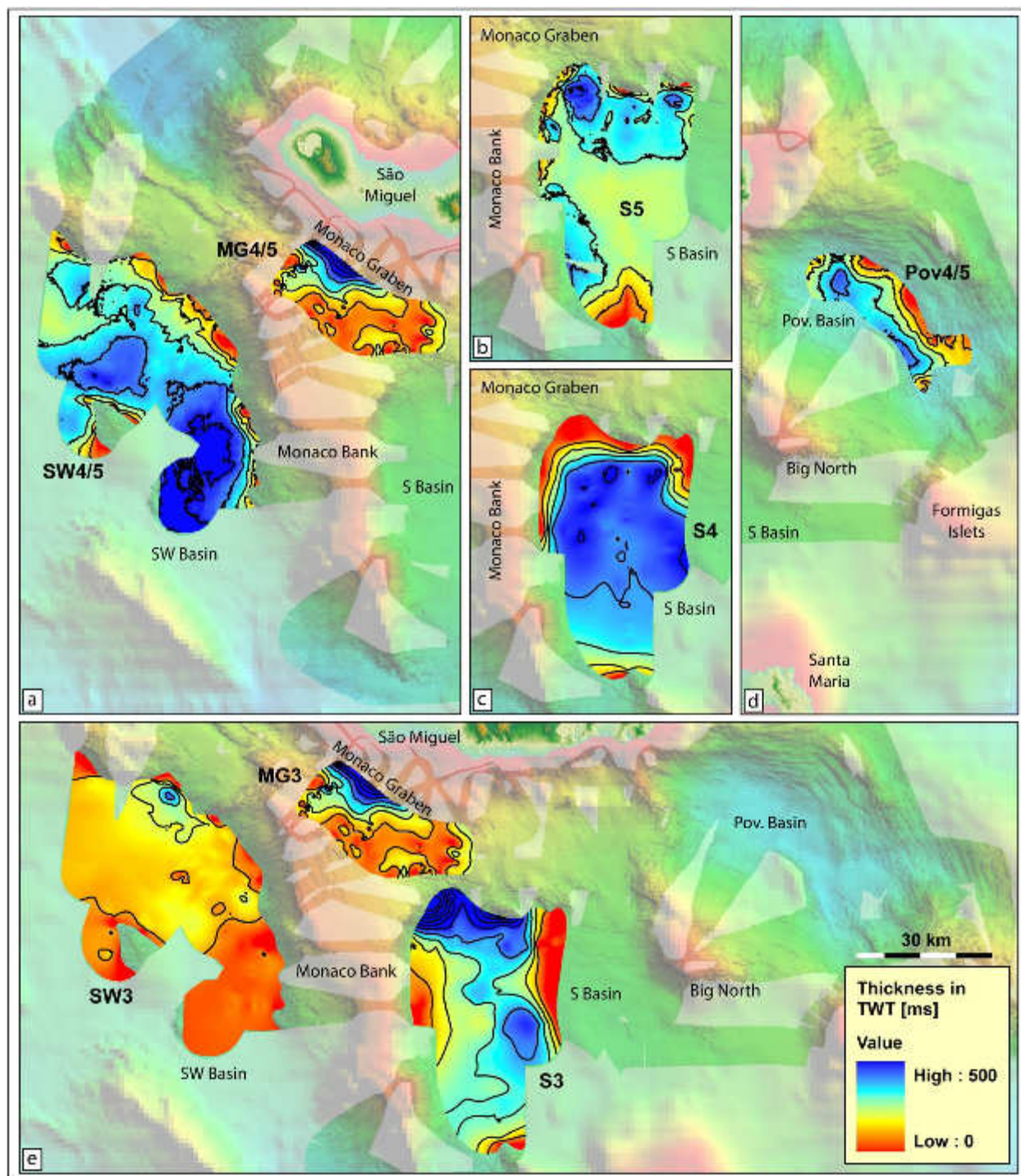


Fig. 2.7: Thickness of seismic units as defined in the text. (a) Units SW4/5 and MG4/5; (b) unit S5; (c) unit S4; (d) unit Pov4/5; (e) units SW3, MG3 and S3. Scale is in ms, isopachs every 100 ms (corresponds to m, if an interval velocity of 2000 m/s in the sediments is assumed). Upward alignment of sub-figures correspond to the chronology of their deposition. See also Tab. 2.1.

2.4. RESULTS AND INTERPRETATION

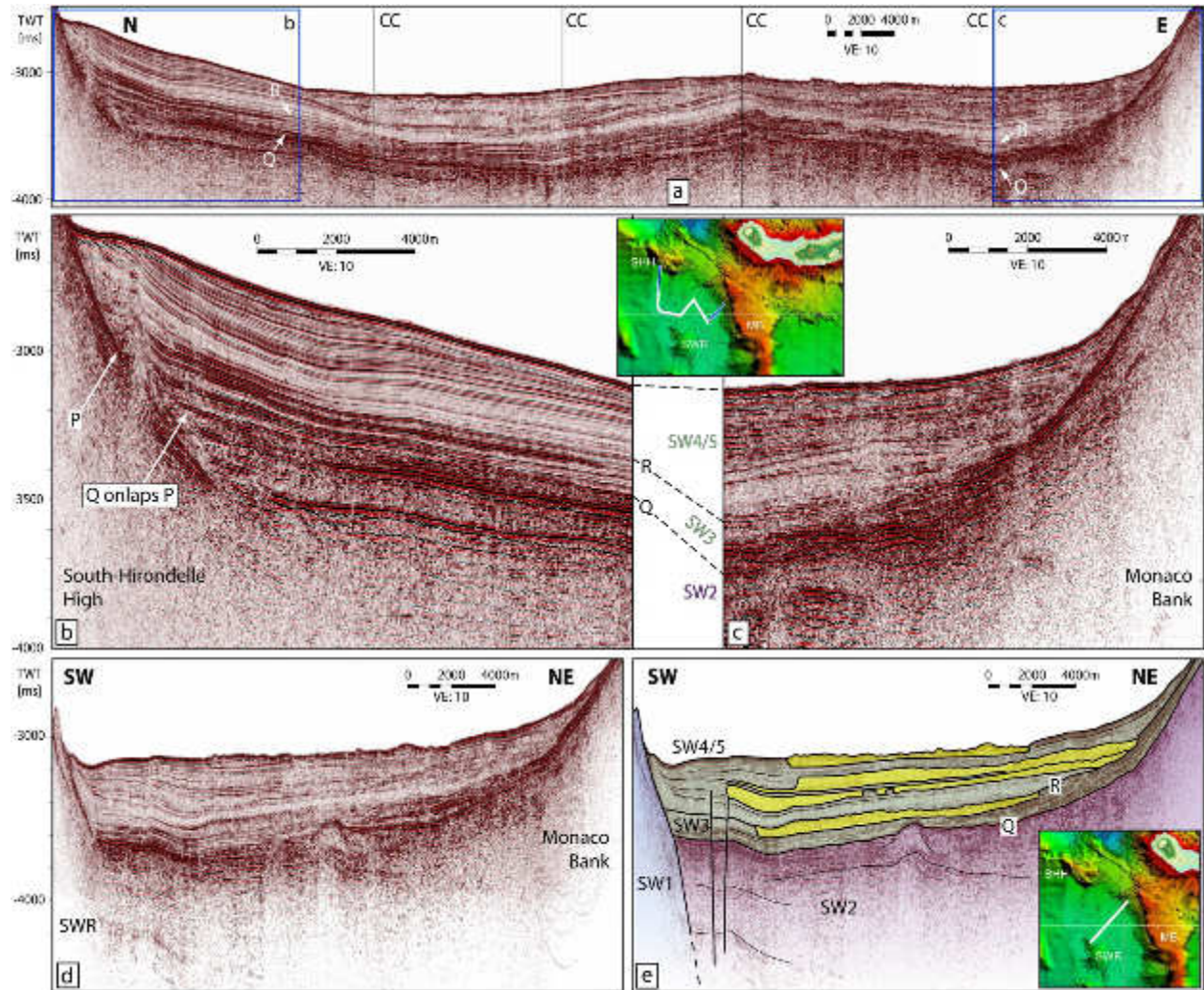


Fig. 2.8: Seismic sections in the basin southwest of São Miguel Island. (a) Composite plot connecting the South-Hirondelle High (SHH) and Monaco Bank (MB). It shows that the flank of MB in (c) and horizon Q, respectively, onlaps the SHH in (b). SW-NE oriented seismic line (d) and its interpretation (e). Note the onlap configuration of horizon Q at the Southwestern Ridge (SWR). Yellow color indicates mass transport deposits. VE: Vertical Exaggeration. For the section's location see inset or Fig. 2.2. Vertical black lines indicate course changes (CC).

2.4.3. Southwest Basin

2.4.3.1. Observations bathymetry

The Southwest Basin (SW) is located southwest of São Miguel Island and is bounded by the South-Hirondelle High in the north and the N160° trending Monaco Bank in the east (Fig. 2.2). In the southwestern part, a ~N130° oriented volcanic ridge (Southwest Ridge) is observable.

2.4.3.2. *Observations seismic*

The basin comprises four seismic units (Fig. 2.8a-e). Horizon Q traces the continuation of the flank of Monaco Bank and represents the top of unit SW2 (Fig. 2.8c/e). It shows a strong irregular reflection pattern with low penetration proximal of Monaco Bank and passes over to parallel reflections in the distal domain. Horizon Q and SW2, respectively, onlap the flanks of South-Hirondelle High (horizon P in Fig. 2.8b) and the Southwest Ridge (SW1 in Fig. 2.8e). Overlying unit SW3 shows a similar spatial reflection pattern, but reflections appear more regular. It converges towards the east where SW3 merges with the flank of Monaco Bank. Sediment thickness reaches a maximum of up to 420 ms in the northeastern part of the basin (Fig. 2.7e). Horizon R is the base of unit SW4/5 (Fig. 2.8b,c,e), which is characterized by a package of low reflection amplitudes at its bottom. Near the bathymetric highs in the north and southwest, SW4/5 reveals truncated and/or converging to parallel reflections (Fig. 2.8b/d). Further to the east, intercalated packages with mostly chaotic, hummocky or contorted reflections are observable (Fig. 2.8c, marked in yellow in Fig. 2.8e) and the overall reflection pattern becomes more irregular. Thickness increases to the south, where it reaches maximum values of more than 500ms (Fig. 2.7a).

2.4.3.3. *Combined interpretation of bathymetric and seismic data*

The high amplitudes and highly irregular reflections of SW2 terminating within the flank of Monaco Bank (no onlap) identify this unit as being generated and deposited during the volcanic development of Monaco Bank (Fig. 2.8c/e). This also applies to SW3, as the unit converges towards the flank of Monaco Bank as well, but due to the more regular reflections we suggest that this unit rather represents erosional products than in-situ generated volcanic material. Thickness distribution (Fig. 2.7e) and geometry (Fig. 2.8c) indicate the bathymetric high between the South-Hirondelle High and Monaco Bank as major sediment source. Distal of the Monaco Bank, sedimentation became more uniform, which is also reflected by the parallel reflection pattern in the western basin (Fig. 2.8a,b,d). SW2 and SW3 both onlap the flanks of the South-Hirondelle High (Fig. 2.8b) and the N130° trending Southwest Ridge (Fig. 2.8d/e) highlighting that the N160° trending Monaco Bank must be geologically younger. After the evolution of Monaco Bank, uniform sedimentation in the basin resulted in the parallel stratified reflection pattern of SW4/5 (Fig. 2.8a/e). In contrast, disrupted and irregular reflections at the northeastern basin margin indicate mass transports. The intercalated packages with chaotic and contorted reflection patterns (Fig. 2.8a, marked in yellow in Fig. 2.8e) reflect the associated rough and blocky deposits (Bull et al., 2009).

2.4. RESULTS AND INTERPRETATION

2.4.4. Lower southern slope of São Miguel & South Basin

2.4.4.1. *Observations bathymetry*

The submarine domain south of São Miguel consists of the island's slope and the South Basin (Fig. 2.5a). The slope is characterized by the out-pinching Monaco Graben in its western part and by a ramp of $\sim 500\text{km}^2$ dipping basinward with 2° to 3° in its eastern part (Fig. 2.5b). The South Basin shows water depths ranging from 1800 m in the northwest to 2300 m in the south. It is bordered by the Monaco Bank in the west, by the Big North High in the east and by the N140° trending South Ridge (SR) / Santa Maria Island in the south (Fig. 2.2). Both regions are separated by a set of faults and tilted blocks.

These faults reveal a strong Monaco Graben related N120° trending component in the west (Fig. 2.5a). In the east, faults trend N100°. They mainly dip to the south terminating at the northwestern flank of the Big North High.

2.4.4.2. *Observations seismics*

Seismic penetration at the lower slope of São Miguel is low and a sub-division in multiple stratigraphic units is not possible (Fig. 2.9a/b). The reflection pattern shows high amplitudes and distorted reflections. Downslope, northward dipping reflections are observable before the slope terminates at a bathymetric high, which reveals weak internal stratification parallel to its southern flank.

In contrast, the sedimentary infill of the South Basin can be separated into six seismic units. The lowermost units S1a (Fig. 2.9c/d) and S1b (Fig. 2.10) are both characterized by limited penetration, chaotic reflections and high amplitudes at the top. Unit S2 is poorly imaged, at least a weak internal stratification can be traced (Fig. 2.9c/d and Fig. 2.10). In the west, top of S2 (horizon Q) merges with the flank of Monaco Bank (Fig. 2.11). Overlying unit S3 shows a sub-parallel stratification, which terminates in an onlap configuration against S2 (Fig. 2.11), S1a (Fig. 2.9) and S1b (Fig. 2.10) in the west, south and east, respectively. Top of S3 (horizon R) is defined by the northwestern basin flank where Monaco Graben pinches out (Fig. 2.10/2.11). Here, S3 shows its maximum thickness (Fig. 2.7e) and internal reflections downlap on horizon Q (Fig. 2.10). In the basin, S3 is concordantly overlain by the well stratified seismic unit S4 showing a constant thickness of approximately 450 ms (Fig. 2.7c). S4 onlaps S1a in the south (Fig. 2.9c/d) and terminates vertically against a package of disrupted, contorted and tilted reflections onlapping S3 in the northwest (e.g. Fig 2.11). In the east, S4 terminates vertically against or onlaps a package of chaotic/distorted reflections covering unit S1b (see large yellow areas on top of horizon R in Fig. 2.10). However, the western base of this package is hardly detectable, but is possibly coinciding with horizon R. In the basin center, uppermost seismic

2. THE TECTONIC EVOLUTION OF THE SOUTHEASTERN TERCEIRA RIFT

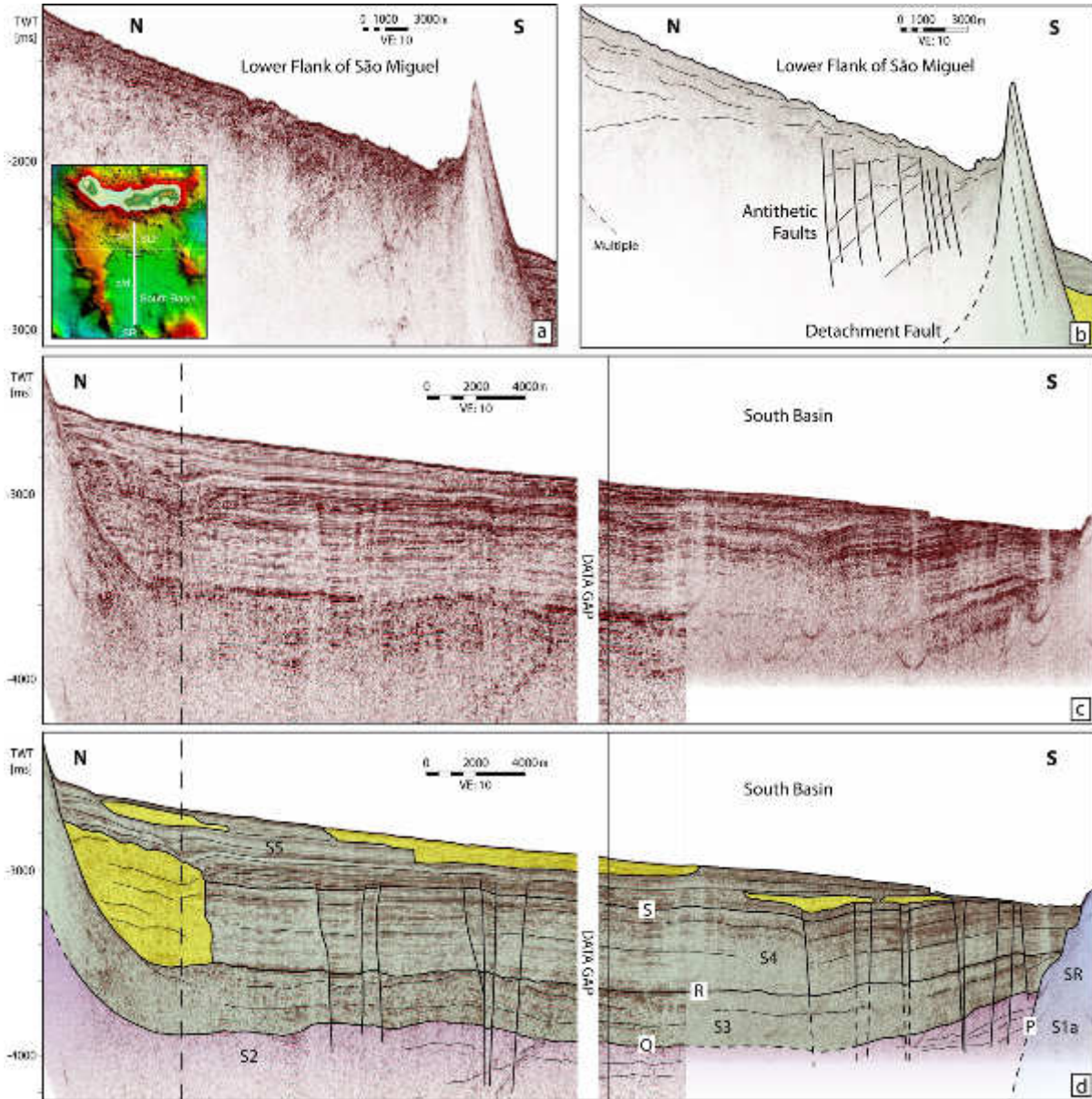


Fig. 2.9: Seismic sections and corresponding interpretations covering the southern slope of São Miguel Island (a, b) and the South Basin (c, d) in a N-S direction. Yellow color indicates mass transport deposits. SLF: Southern lower slope of São Miguel; SR: South Ridge. VE: Vertical Exaggeration. For the section's location see inset, Fig. 2.2 or 2.5. Vertical dashed line marks intersection with the W-E directed profile (Fig. 2.10). Vertical black lines indicate intersection of profiles.

unit S5 reveals a parallel reflection pattern and overlies unit S4 concordantly (Fig. 2.9c/d and Fig. 2.10). In the south reflections converge, onlap the tilted part of unit S4 and the unit pinches out (Fig. 2.9c/d). At the northwestern and eastern basin margins, reflection pattern changes to a contorted and/or lenticular facies (Fig. 2.10). Several packages of mostly chaotic and/or contorted reflections are embedded in or overlain by S5 (marked with yellow in Figs. 2.9d, 2.10b and 2.11b). Close to the eastern package showing a chaotic reflection pattern, reflections

2.4. RESULTS AND INTERPRETATION

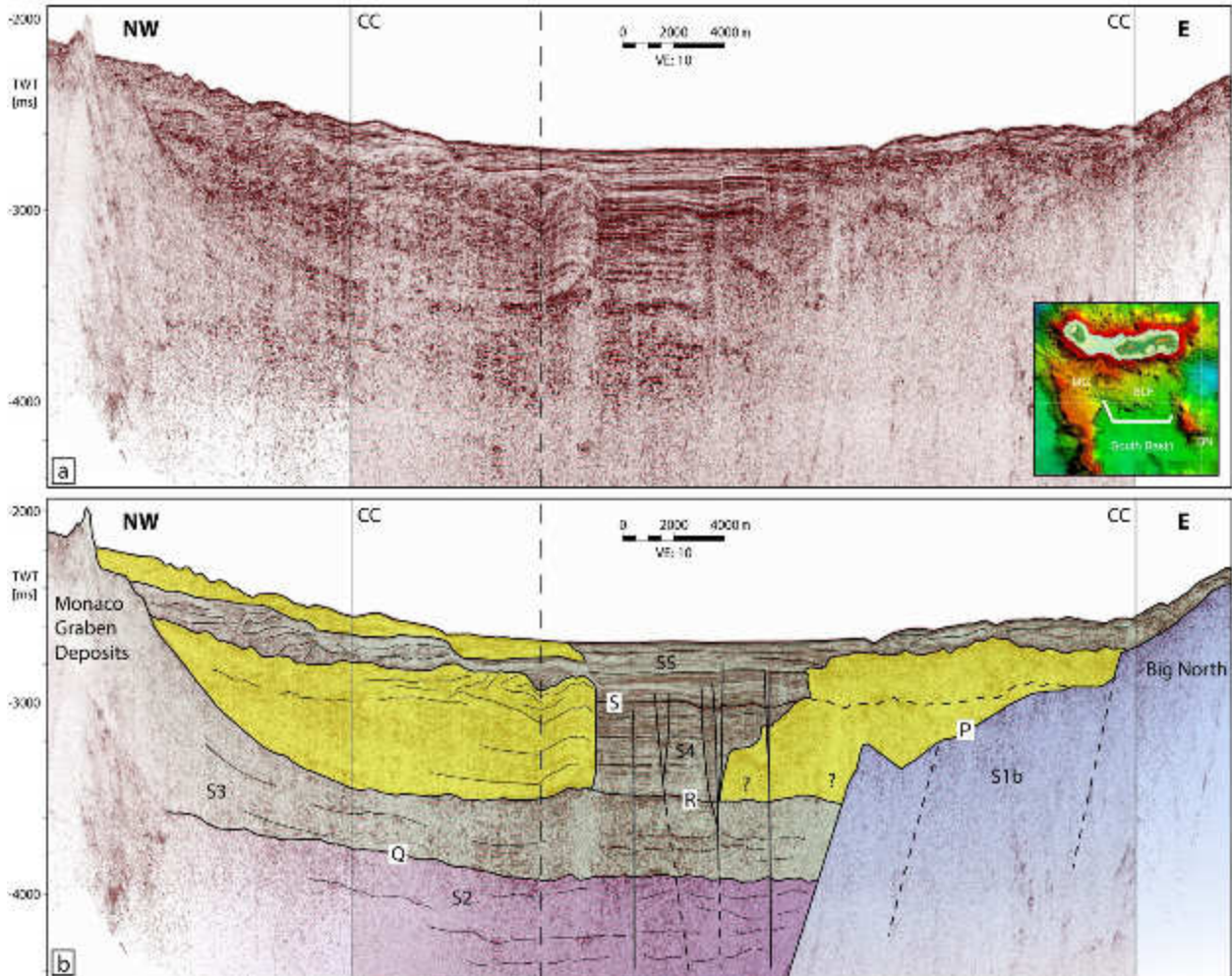


Fig. 2.10: Seismic section (a) and interpretation (b) covering the South Basin in a W-E direction. Yellow color indicates mass transport deposits. SLF: Southern lower slope of São Miguel; MG: Monaco Graben; BN: Big North. VE: Vertical Exaggeration. For the section's location see inset, Fig. 2.2 or 2.5. Dashed line marks intersection with the N-S directed profile (Fig. 2.9). Vertical black lines indicate course changes (CC).

of S5 get more irregular (Fig. 2.10b). A set of faults are traceable in the basin, most of them terminating at the base of or inside unit S5. Faults piercing the seafloor are not observable.

2.4.4.3. Combined interpretation of bathymetric and seismic data

Due to the poor penetration of S1a and S1b, these units are interpreted as magmatic basement, which has been erupted/deposited during the evolution of the South Ridge beside Santa Maria Island and Big North High, respectively (Fig. 2.9c/d, Fig. 2.10). In both cases, the poorly resolved internal stratification of S2 terminates against S1a/b. Therefore, we interpret that horizon Q (which is the stratigraphic continuation of the flank of Monaco Bank and top of S2) onlap horizon P (which is the top of the magmatic basement). This implies that Monaco Bank is geologically younger than these corresponding structures. The onlap configuration of horizon R

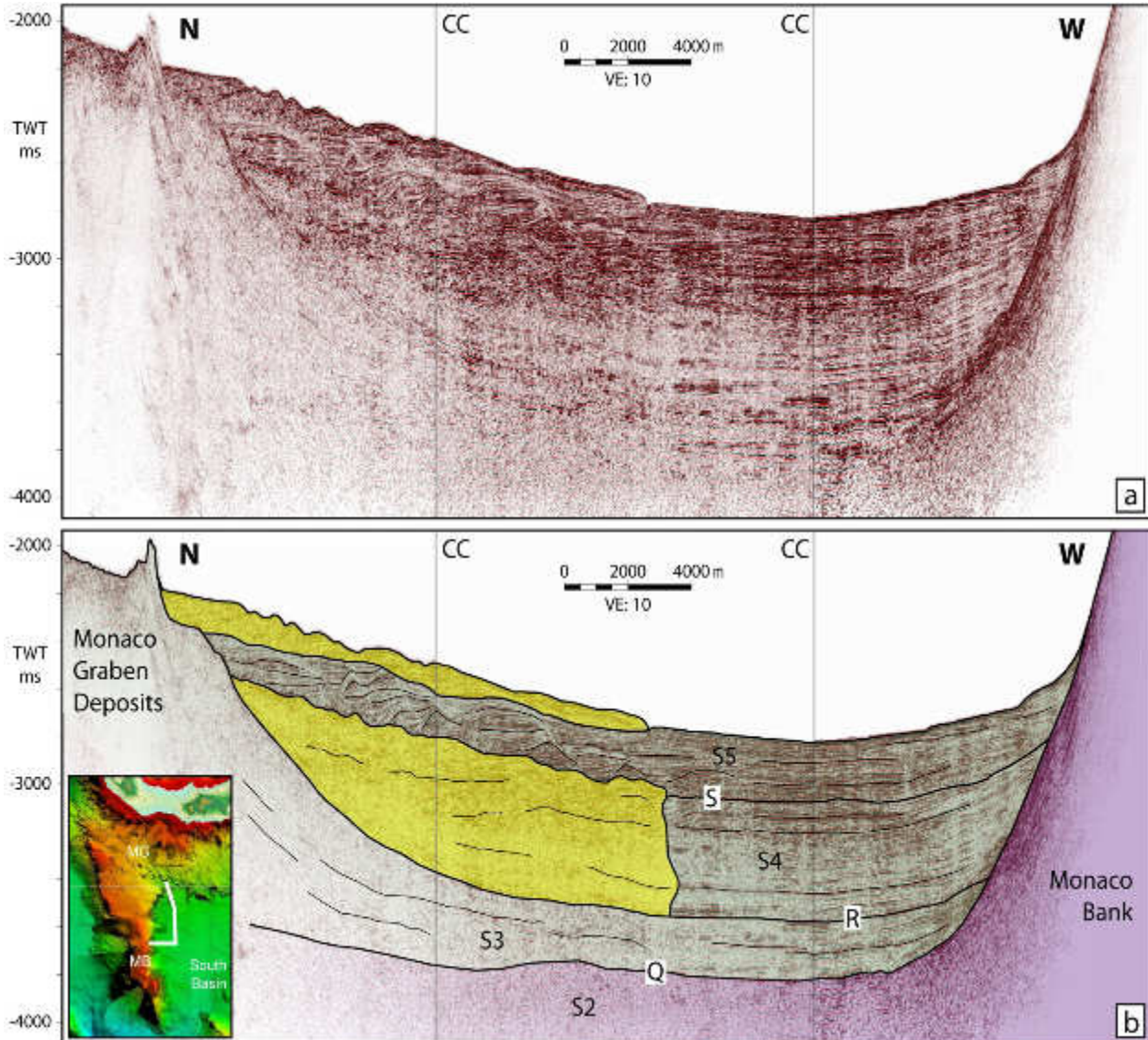


Fig. 2.11: Seismic section (a) and interpretation (b) showing the temporal relationship of Monaco Graben and Monaco Bank. Yellow color indicates mass transport deposits. MG: Monaco Graben; MB: Monaco Bank. VE: Vertical Exaggeration. For the section's location see inset, Fig. 2.2 or 2.5. Vertical black lines indicate course changes (CC).

(which is the stratigraphic continuation of the northwestern basin margin flank and the out pinching Monaco Graben, respectively) at the flank of Monaco Bank (horizon Q, Fig. 2.11) shows that unit S3 was deposited after the formation of Monaco Bank but during the formation of Monaco Graben. The southern flank of the tilted block separating the lower slope of São Miguel and the South Basin (Fig. 2.9a/b) is built up by unit S3 (Fig. 2.9c/d). For this reason, we conclude that the evolution of the block and the adjacent fault system (Fig. 2.5) is linked to the formation of Monaco Graben. Thus, the faults north of the block (Fig. 2.9a/b) could be antithetic branch faults of a north facing detachment fault. After the formation of Monaco

2.4. RESULTS AND INTERPRETATION

Graben, the well stratified unit S4 was deposited in the basin (e.g. Fig. 2.9c/d). Since thickness of unit S4 is constant and faults are neither characterized by an upward increasing offset of internal reflections nor terminating within the unit, sedimentation occurred during isotropic sedimentation conditions and tectonic quiescence. After S4 times, tectonics initiated faulting and tilting of the basin sediments (Fig. 2.9c/d). Due to the fact that faults crop out within S5 and local vertical movements are compensated by S5 sediments, tectonic activity in the basin is interpreted as being limited to early S5 times only. Additionally, maximum thickness (Fig. 2.7b) and the contorted/lenticular reflection pattern of unit S5 in the northwestern and eastern part of the basin (Fig. 2.10) indicate an anisotropic, southward directed sediment transport coming from São Miguel Island. The packages characterized by a chaotic/contorted reflection pattern are again interpreted as mass transport deposits (yellow areas in Figs. 2.9d, 2.10b and 2.11b). The huge deposit in the eastern basin represents a special case (Fig. 2.10b). Since S4 reflections onlap the lower part of the body and S5 reflections are slightly irregular close to the upper part of the body, it is likely that it was generated by several events during S4 and S5 times. Other mass transport deposits can be dated to S5 times, since they are embedded in S5 sediments (e.g. Fig. 2.9d) or since the remobilized material includes S5 sediments (Fig. 2.10b, at the western termination of horizon S). Possible trigger mechanisms could be gravitational load or tectonic events or a superposition of both effects.

2.4.5. Povoação Basin & Big North High

2.4.5.1. *Observations bathymetry*

The Povoação Basin (Pov) links São Miguel Island and East Formigas High, a shoal with a minimum water depth of 100 m and covered with many cones (Fig. 2.12a/b) similar to those observed in the Monaco Graben (Fig. 2.3a). The basin is characterized by a water depth of 2930 m in its center and its conspicuous curved shape. Similar to the South-Hirondelle Basin, the northeastern margin is crosscut by a large number of mostly basinward dipping normal faults occasionally forming small ancillary basins, whereas the southwestern margin is dominated by three fault scarps also dipping basinwards (marked as MF in Fig. 2.12a-c) – one forming the northeastern slope of Big North High, another between Big North and the basin and a further one representing the transition from the margin to the flat basin. To the south, they split up in a set of normal faults (SF in Fig. 2.12a/b). Scarps usually exhibit dip angles of 30° to 40° on both sides. Vertical offsets normally range from 100 m to 300 m at the northeastern margin, but vary up to 700 m at the southwestern one. South of East Formigas High and in prolongation of the northeastern basin margin two dominant fault scarps are observable. They show the same dip direction and similar dip angles, but their vertical offsets reach values of up to 1000 m (marked as DF in Fig. 2.12a).

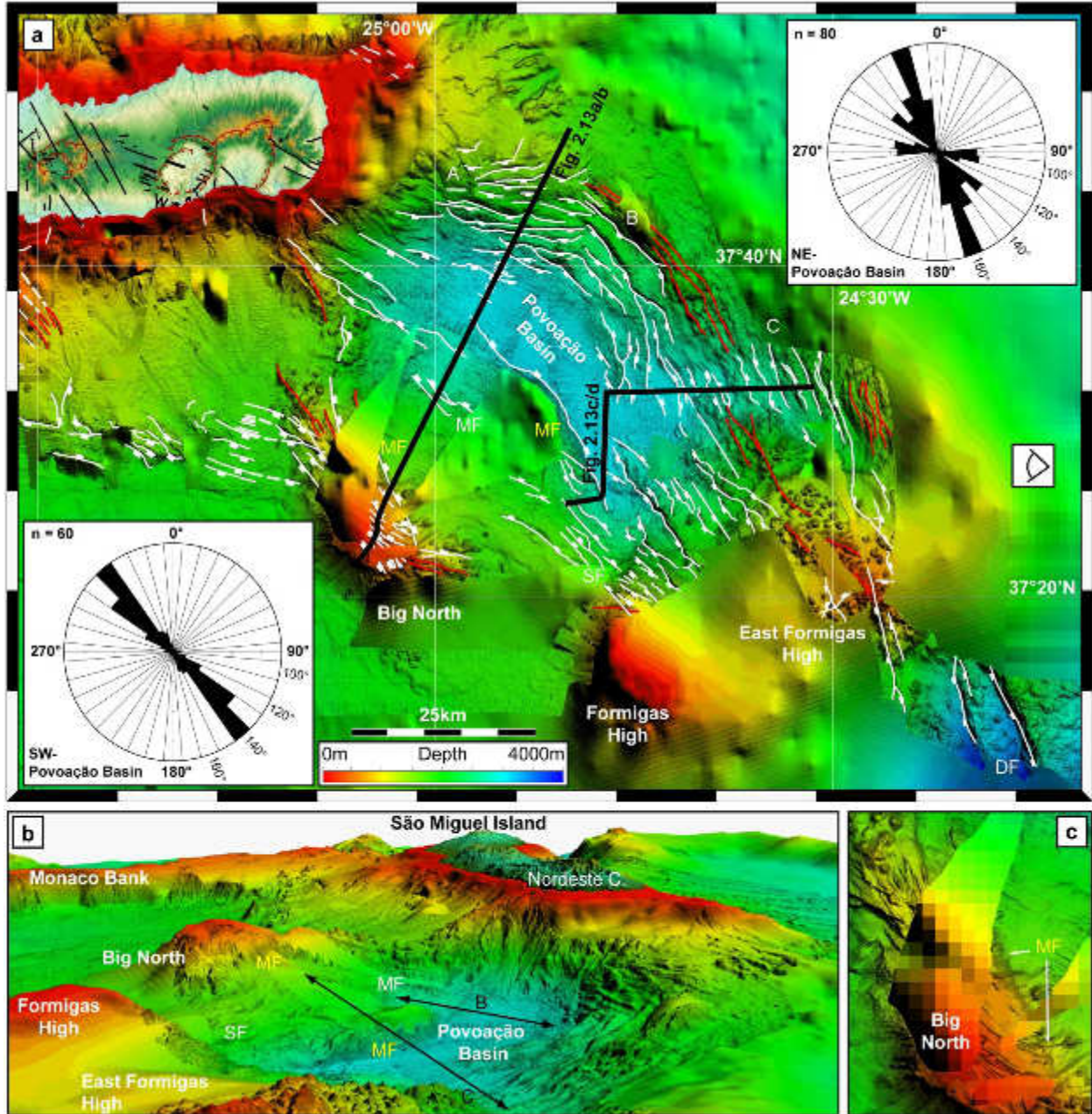


Fig. 2.12: Bathymetry and picked faults in the eastern working area (a), 3D view (b) and zoom of Big North High (c). The northeastern basin margin shows three zones of strike directions: N90° to N110° (A), N130° to N140° (B), N160° (C). Two dominant faults south-east of East Formigas High strike N160° as well (DF). Three major faults are present at the southwestern margin trending N140° (MF, white) and N160° (MF, yellow). To the south these three fault planes split up in a set of normal faults (SF). Onshore faults based on Guest et al. (1999), Carmo (2004) and Carvalho et al. (2006). White line: Fault. Dashed white line: Inferred fault. Red line: Volcanic lineament. Thick black lines indicate seismic profiles. Eye symbol denotes viewing direction of bottom 3D sight. Illumination from N90° with an azimuth of 60°.

2.4. RESULTS AND INTERPRETATION

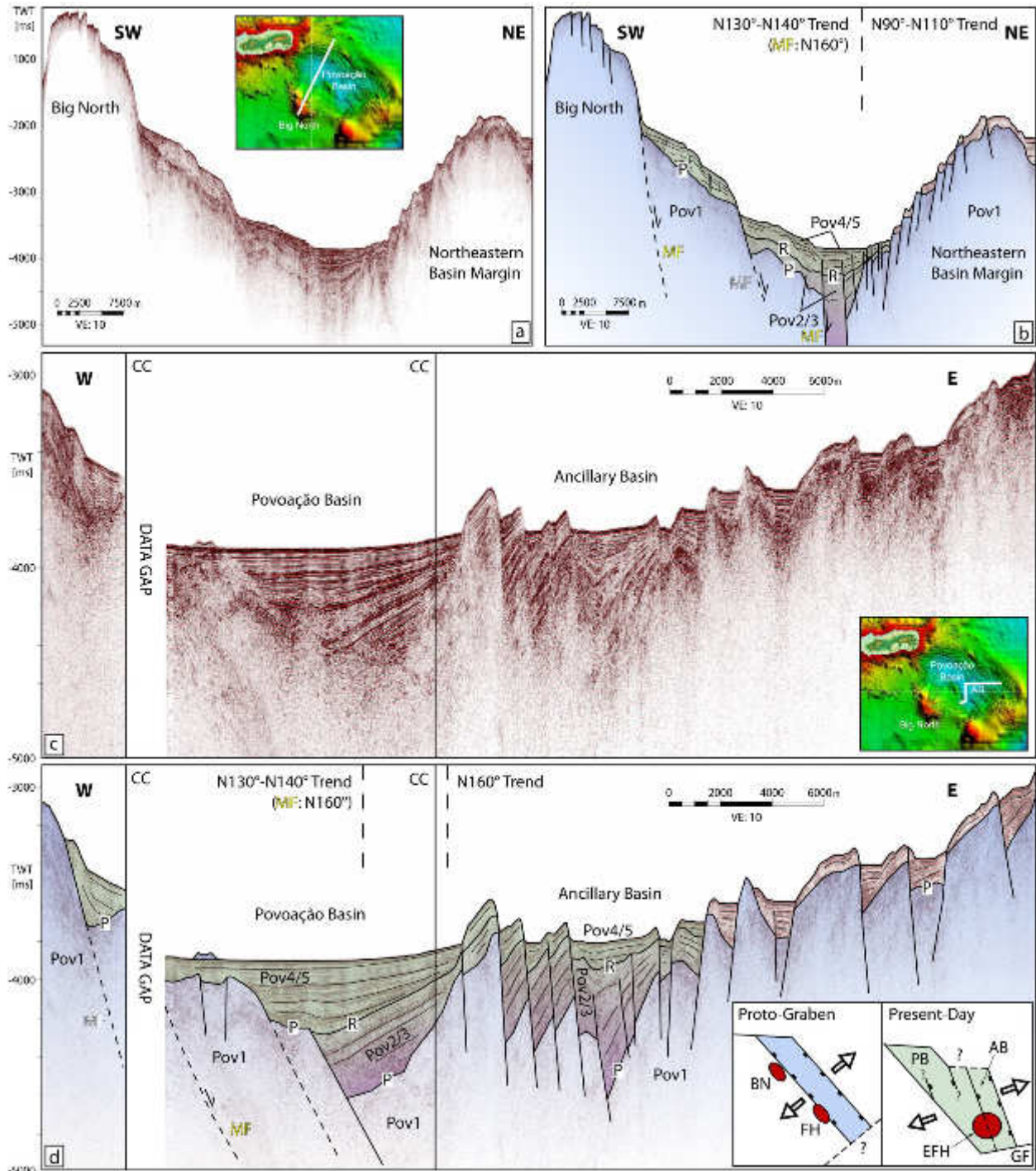


Fig. 2.13: Seismic sections and corresponding interpretations covering the Povoação Basin (PB) south-east of São São Miguel Island. One seismic line crosses the northern part of the basin in SW-NE direction (a, b), another one the southern part and the ancillary basin (AB) in an overall W-E direction (c, d). MF marks major fault planes trending N130°-N140° (white) and N160° (yellow). Dashed line: Inferred faults. VE: Vertical Exaggeration. For the section's location see insets, Fig. 2.2 or 2.12. Vertical black lines indicate course changes (CC).

Southwest of the Povoação Basin, Big North High shows a flat top (Fig. 2.12a) with an average water depth of ~250 m strongly offset by mainly northeast dipping fault scarps (30° to 60°, vertical offsets of 50 m to 100 m).

The dominant strike direction on top of Big North and along the southwestern basin margin is N130° to N140° (lower left rose diagram in Fig. 2.12a). Volcanic lineaments north of Big North and two of the major normal faults (faults marked with yellow MF in Fig. 2.12 and Fig. 2.13) reveal a N160° trend. In contrast, the northeastern basin margin can be divided into three zones of strike directions. North of the basin and close to São Miguel Island, a clear N90° to N110° trend is evident. In the northeast, a set of faults is oriented N130° to N140°. Faults and lineaments east of the basin as well as southeast of East Formigas High are strongly dominated by a N160° trend (A, B, C/DF, respectively, and upper right rose diagram in Fig. 2.12a).

2.4.5.2. *Observations seismics*

Seismic penetration at the basin margins is again very low and the corresponding acoustic basement (Pov1) is characterized by chaotic reflections with high amplitudes (Fig. 2.13). While stratified sediments of unit Pov2/3 concordantly overlie the tilted acoustic basement (Pov1) within the ancillary basin, they discordantly cover unit Pov1 within the main basin. Reflections are usually parallel and tilted but slightly divergent in the inner part of the ancillary basin (Fig. 2.13c/d). Sediments of the uppermost seismic unit Pov4/5 onlap both top Pov1 (horizon P) and top Pov2/3 (horizon R). Pov4/5 is mostly characterized by divergent reflections, but on top of the southwestern margin an oblique sub-parallel to lenticular reflection pattern dominates (Fig. 2.13a/b). Unit Pov4/5 thickens to 150 ms within the ancillary basin and to 450 ms in the main basin (Fig. 2.7d).

2.4.5.3. *Combined interpretation of bathymetric and seismic data*

Due to the seismic characteristics of the unit, we interpret Pov1 to be the magmatic basement, which developed during the evolution of Big North High and the present-day northeastern basin margin. Mostly parallel stratified sediments of unit Pov2/3 filling up accommodation space which had been created by faulting of the magmatic basement (Fig. 2.13b/d), indicate 1) extension of the basement during Pov1 times, and 2) post-tectonic sedimentation during Pov2/3 times (divergent reflections indicate syn-tectonic sedimentation in a small part of the ancillary basin and the northern Povoação Basin only).

East of the basin, N160° trending normal faults offsetting and tilting the seafloor as well as the parallel Pov2/3 sediments (Fig. 2.13d and marked with C in Fig. 2.12a) denote these faults to be active from the beginning of Pov4/5 times until now. On top of Big North High, N130°/N140° faults, terminating eastwards against the N160° oriented fault scarp (marked with yellow MF in Fig. 2.12a,c/2.13b), lead to the suggestion that this scarp is younger than the faults on top.

2.4. RESULTS AND INTERPRETATION

Additionally, diverging reflections of Pov4/5 in the southern basin (Fig. 2.13d) show active subsidence along the N160° trending fault (yellow MF in Fig. 2.13d). Extension could also be partly accommodated at the N140° oriented normal fault west of the N160°-fault (white MF in Fig. 2.13d). However, the northwestern continuation of the N140°-fault (white MF in Fig. 2.12a) seems not to be active, since uppermost unit Pov4/5 shows no evidence of syn-tectonic sedimentation (white MF in Fig. 2.13b).

Therefore, we assume that the Povoação Basin was formed in two phases (see sketch in Fig. 2.13d). First, a N130°-N140° trending (proto-) graben developed during Pov1 times. Corresponding N130°-N140° trending faults can be observed across the southwestern margin and on top of Big North High. Faults with same orientation at the northeastern margin are less dominant but can also be found northeast of the central basin (marked with B in Fig. 2.12a). After a time of reduced extension (Pov2/3), horizon R marks the onset of the second phase (Pov4/5, Fig. 2.13), which is active until today. Extension is mainly accommodated along N160° trending faults and focuses on the southern and the ancillary basin (marked with C in Fig. 2.12a). In the northern part of the basin, less distinct tilted reflections of Pov4/5 within the basin (Fig. 2.13b) possibly indicate that tectonics in this area are more dominated by transfer than slip movements.

2.4.6. Summary of observations

Based on the presented bathymetric and seismic data, we can finally summarize some major results:

1. Strike directions of faults and structural lineaments group into three major categories. Northwest of São Miguel Island, a N140° trend with intercalated N150° trending structures is observable (Fig. 2.3a; marked with red and dark blue in App. 2.2, respectively). The N140° trend is also present southeast of the island, in particular at the southwestern margin of the Povoação Basin and on top of Big North High (Fig. 2.12a). The eastern margin of the Povoação Basin and the East Formigas High are clearly dominated by a N160° trend (Fig. 2.12a; marked with gray in App. 2.2). This trend is also reflected by Monaco Bank and its fault system on top (Fig. 2.5a). In between these two settings, structures mainly strike N90° to N110° (Fig. 2.5a and Fig. 2.12a; marked with light blue in App. 2.2) or reflect the Monaco Graben trend of N120° (Fig. 2.3a; marked with green in App. 2.2).
2. The N160° trending Monaco Bank postdates the evolution of the South-Hirondelle High, the Southwest Ridge, the South Ridge west of Santa Maria Island and the Big North High, all approximately oriented N140°.
3. The Monaco Graben is younger than the Monaco Bank.

4. The Monaco Graben shows no major recent tectonic activity.
5. Since the evolution of Monaco Graben, the South Basin first underwent a tectonically inactive period with uniform sedimentation conditions, followed by a period associated with an N-S directed sediment transport. The transition phase between these periods is characterized by active tectonics.
6. The Povoação Basin evolved in three steps: 1) formation of a N130° to N140° trending proto-basin, 2) sedimentation during reduced tectonics, 3) syn-kinematic sedimentation during a second tectonically active period with distinct extension along N160° trending normal faults. This period is lasting until today.
7. Volcanic cones and several mass waste deposits are observable (these will be addressed in Chapters 3 and 4).

2.5. Discussion

2.5.1. Relative chronostratigraphy

Within the South Basin and Southwest Basin, sediments deposited prior to or during the evolution of Monaco Bank are separated by horizon Q from younger sediments (Figs. 2.8-2.11). Horizon Q coincides with the top of the acoustic basement on top of Monaco Bank and the stratigraphic continuation of its flanks. Pre/Syn-Monaco-Bank sediments (represented by the purple units numbered “2” in Figs. 2.8-2.11 and Tab. 2.1) onlap the magmatic roots of the South-Hirondelle High (Fig. 2.8b/c), the Southwest Ridge (blue unit SW1 in Fig. 2.8e), the South Ridge (blue unit S1a in Fig. 2.9d) and the Big North High (blue unit S1b in Fig. 2.10b). Units numbered “1” are therefore representing the time of these structures’ evolution. S2 and SW2 are postdating this period and predating the end of Monaco Bank formation.

Monaco Bank and Monaco Graben are characterized by a strongly sheared and offset acoustic basement (Fig. 2.6). Since volcanism did not overprint the faults, we can assume that first Monaco Bank evolved during MG2 times (purple unit in Fig. 2.6b). Afterwards, its northern part was rifted and Monaco Graben was formed. Lowermost unit MG3 in the graben (Fig. 2.6b) therefore represents early Post-Monaco-Bank sediments (green colored units in Figs. 2.6, 2.8, 2.9 and 2.10) syn-tectonically deposited during graben formation. In the Southwest Basin, reflection pattern (Fig. 2.8) and thickness distribution (Fig. 2.7e) of the lowermost Post-Monaco-Bank unit SW3 identify the northeastern basin margin between South-Hirondelle-High and Monaco Bank as major sediment source, where the elevated Monaco Graben’s northwestern continuation is located. Top of lowermost Post-Monaco-Bank unit S3 in the South

2.5. DISCUSSION

Evolutionary Stage	Seismic Horizon	Time [Ma]	Description	M. Graben	SW. Basin	S. Basin	Pov. Basin	S.H. Basin
Stage III	S	≥ 0.9	S-Basin first tectonically active, later inactive; Subaerial evolution of São Miguel	MG4/5	SW4/5	S5	Pov4/5	SH2/5a SH2/5b SH2/5c
			Uniform sedimentation during tectonic quiescence in the S-Basin; Tectonic reactivation of the Povoação-Basin			S4		
	R	5.3 - 4.37	Formation of Monaco Graben; Evolution of early Santa Maria Island?	MG3	SW3	S3		
	Q	≤ 5.9	Onset of N70° extension; Formation of Monaco Bank; Pov.-Basin inactive; Evolution of early Santa Maria Island?	MG2	SW2	S2	Pov2/3	
Stage II	P	~10						
Stage I			N50° extension	-	SW1	S1a/S1b	Pov1	SH1

Tab. 2.1: Overview of the stratigraphic units, seismic horizons and associated evolutionary stages of the southeastern Terceira Rift. Colors indicate the stage of N50°-spreading (blue), the Pre-/Syn-Monaco-Bank stage (purple) and the Post-Monaco-Bank stage (green). Stratigraphic units with two colors could not be correlated with one single stage only. Color code is the same as shown in the line drawings of Figs. 2.4, 2.6, 2.8, 2.9, 2.10, 2.11 and 2.13 as well as in the sketches presented in Fig. 2.13 and 2.14.

Basin is defined by horizon R - the stratigraphic continuation of the northwestern basin margin (Fig. 2.11b), where S3 shows its maximum thickness (Fig. 2.7e). Hence, it was deposited after the evolution of Monaco Bank but during the formation of the northwestern basin margin, which is the out-pinching elevated Monaco-Graben. We therefore assume that units MG3, SW3 and S3 altogether reflect the time of Monaco Graben formation.

In the Monaco Graben and Southwest Basin, these units are overlain by unit MG4/5 (Fig. 2.6b) and SW4/5 (Fig. 2.8b/e), both reflecting present-day sedimentation conditions. In contrast, the synchronously deposited sediments in the South Basin can be sub-divided into two units: one characterized by homogeneous sedimentation and tectonic quiescence (S4) and a second one (S5) caused by early tectonics and a high sediment flux from the north lasting until today (Figs. 2.9, 2.10 and 2.11).

Low extension rates during Pov2/3 times in the Povoação Basin (Fig. 2.13) indicate either a general phase of reduced extension along the Terceira Rift or that extension was mainly accommodated elsewhere. Since there is no evidence for higher and lower extension rates in the sedimentary infill of the South-Hirondelle Basin (Fig. 2.4), we suggest a region between the South-Hirondelle Basin and the Povoação Basin which accommodated stress during that time. Three regions come into consideration: 1) the area of present-day São Miguel Island, which is too far north, 2) the South Basin, which in fact underwent tectonic stress in the past but with

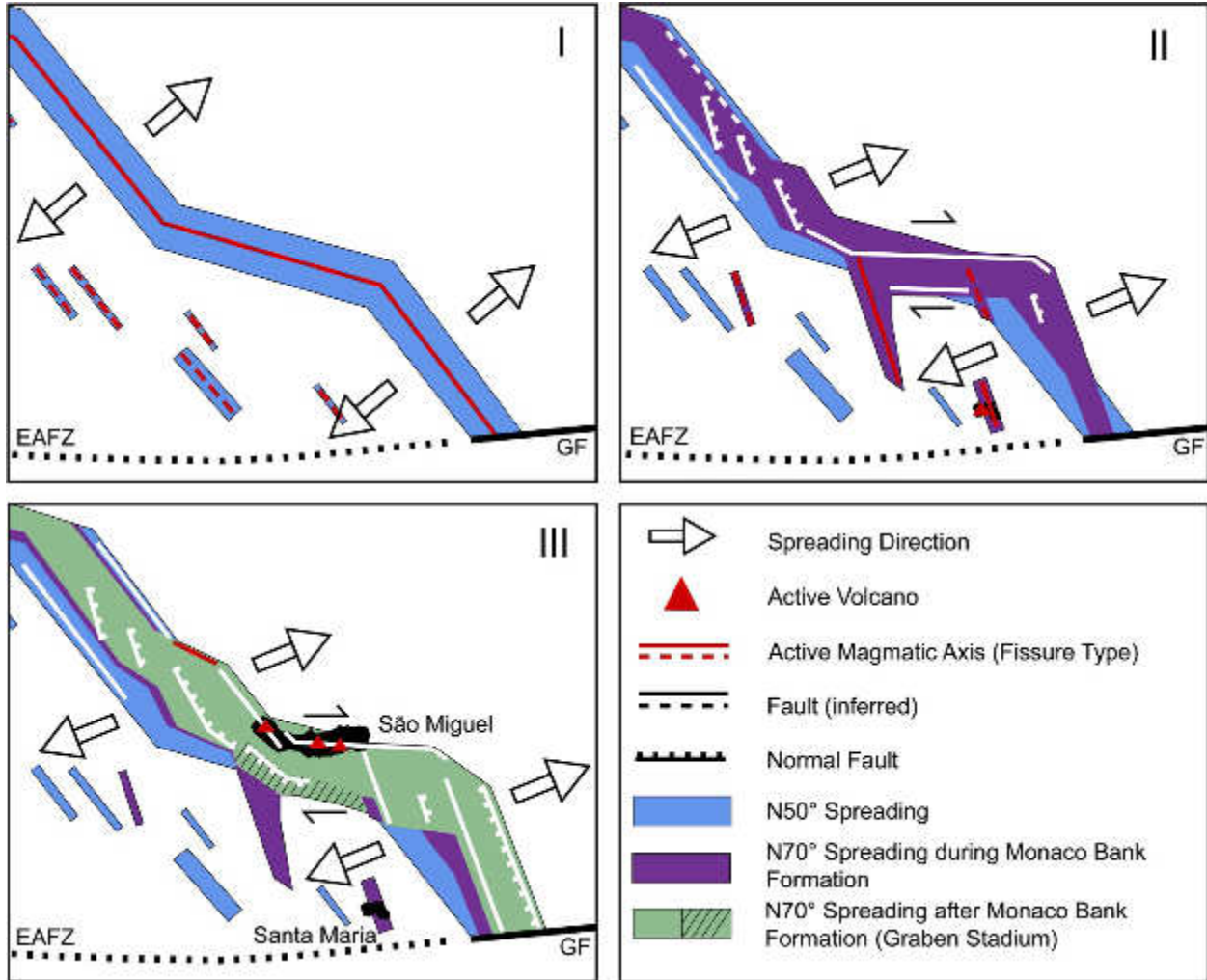


Fig. 2.14: Sketch of evolutionary stages of the southeastern Terceira Rift. Terceira Rift started to evolve under SW-NE rifting conditions ca. 25 - 20 Ma years ago. Fissure type magmatism occurred synchronously southwest of the plate boundary (I). After rifting has changed to WSW-ENE direction ca. 10 Ma years ago (II), Monaco Bank and early Santa Maria Island rose up. New faults west of São Miguel were formed in the inherited NW-SE setting. In the east, NNW-SSE trending faults developed. Ceasing magmatism at Monaco Bank at ~5 Ma led to the formation of Monaco Graben (III, graben stadium). Afterwards, extension was mainly accumulated by normal faulting in the southern Povoação Basin and its ancillary basin (III). Subaerial evolution of São Miguel Island started before 0.9 Ma. See Chapters 2.5.2./2.5.3. for further details. EAFZ: East Azores Fracture Zone; GF: Gloria Fault.

insignificant extension only (Figs. 2.9, 2.10), and 3) the Monaco Bank and Monaco Graben region. Both are indicating distinct extension, since tectonic stress generates pathways for magma ascent and initiates rifting, respectively. Therefore, we chronologically correlate Pov2/3 with the time of Monaco Bank and Graben evolution. Accordingly, syn-tectonic unit Pov4/5 is the temporal equivalent of MG4/5, SW4/5 and S4/S5 in the Povoação Basin, where extension focuses again after the formation of Monaco Bank and Graben had ended.

2.5. DISCUSSION

2.5.2. Evolution of the South-Eastern Terceira Rift

Structures consisting of the earliest units numbered “1” (marked with blue in Figs. 2.4, 2.8-2.11, 2.13; see also Tab. 2.1) either predominantly reveal a N140° trend (e.g. Southwest Ridge, see App. 2.2) or are overprinted by faults with an equivalent orientation (e.g. Big North High, see Fig. 2.5). Additionally, it was shown that the Povoação Basin initially evolved along N130°-N140° normal faults (see Chapter 2.4.5.3.). For these reasons, we suggest that the Azores Plate Boundary here primarily developed within a N40°-N50° extensional regime, which is reflected by N140° trending structures of the southeastern Terceira Rift (Stage I, Fig. 2.14). Following Neves et al. (2013), the ridges southwest of the Terceira Rift (Fig. 2.1/App. 2.2) result from volcanism along fissures synchronous with the Rift evolution. Most of them reveal a N140° trend indicating a time of N50° extension as well, since fissures open perpendicular to the minimum stress axis and do not sustain shear. Furthermore, an early direction of extension of N50° was proved based on an analysis of a high resolution magnetic data set (Luis and Miranda, 2008).

In contrast, younger structures like Monaco Bank (Fig. 2.5) or the active faults east of the Povoação Basin (Fig. 2.12) reveal a N160° orientation indicating a rotation in extension to N70°, which is the present-day extensional direction (Luis and Miranda, 2008; DeMets et al., 2010). This led to a rearrangement of the tectonic regime within the inherited N130° to N140° setting (Stage II, Fig. 2.14). West of São Miguel Island, the kinematics of the inherited faults probably changed from extension to right-lateral transtension and new faults developed being clockwise rotated by 5°-15° (see faults in the South-Hirondelle Basin in Fig. 2.3). A similar phenomenon was discussed by Lourenço (2007) for southeast Terceira Island. Both, reactivated and new faults thus developed the N140° to N150° major trend that was described by Lourenço et al. (1998). Southeast of São Miguel, extension in the Povoação Basin decreased and Monaco Bank was formed south of the island, but Monaco Bank has never acted as an independent plate boundary since there is no connection to the East Azores Fracture Zone and Gloria Fault observed in the bathymetry. This possibly indicates Monaco Bank to be caused by a kind of fissure type volcanism as well – a further evidence for a formation linked to N70° extension.

After volcanic and tectonic processes at Monaco Bank had ceased, extension first accumulated north of it causing the opening of the oblique Monaco Graben (graben stadium of Stage III, Fig. 2.14). Then, tectonic stress again concentrated in the Povoação Basin (Stage III, Fig. 2.14), where it is still predominantly sustaining rifting along N160° faults. This thesis is in agreement with focal mechanisms presented by Borges et al. (2007) also describing present-day normal faulting here, although they obtained a more SW-NE direction of extension. In the South Basin, the transition from isotropic sedimentation conditions to an N-S directed sediment transport (S4 and S5 in Figs. 2.9-2.11, respectively) is assumed to indicate the time of subaerial exposure

of São Miguel Island. Since Monaco Bank acts as a bathymetric barrier hampering a direct transport of material from São Miguel into the Southwest Basin, this transition cannot be traced there. Tectonic movements in the South Basin could be caused by rearrangement of the volcanic system associated with the major formation phase of São Miguel Island.

Distribution of present-day seismicity (App. 2.1), the absence of remarkable tectonic activity in the Monaco Graben (see Chapter 2.4.2.3.) and the lack of active faults in the seismic/bathymetric data of the Southwest Basin and South Basin support the assumption that present-day extension accumulates along the South-Hirondelle Basin, São Miguel Island and the Povoação Basin only (Gente et al., 2003; Vogt and Jung, 2004; Fernandes et al., 2006; Luis and Miranda, 2008). In this context, the W-E trending central and eastern part of São Miguel Island seems to act as a kind of overstep structure linking the re-organized fault setting of the Hirondelle domain and the “pure” N160° setting in the Povoação Basin. This could be caused by a deep rooted Eurasia/Nubia plate boundary related transtensional (leaky) transform. The associated extensional component could therefore facilitate the ascent of magma, which ultimately led to the formation of the volcanic body of São Miguel Island. Leaky transform faults and accompanying volcanism has been described by Favela and Anderson (1999) and references therein. A similar transform fault has also been discussed by Marques et al. (2014b) for the Pico-Faial area.

2.5.3. Age Constrains

At 25 – 20 Ma, a major change in the kinematics of the Azores Triple Junction occurred when Iberia was finally welded to Eurasia (Luis and Miranda, 2008). This initiated the northward jump of the triple point and the evolution of the Terceira Axis. The subsequent rotation in extension from N50° to ~N70° (associated with horizon P) is stated to ~10 Ma (Luis and Miranda, 2008). This implies that formation of Monaco Bank started earliest at ~10 Ma (Tab. 2.1) and since a rock sample from the southern top of Monaco Bank was dated 5.9 Ma (Beier et al., 2015), it was active at least until that time (horizon Q). (In this context, a second sample with an age of 39 Ma from the very northwest of Monaco Bank should be mentioned. According to magnetic data, the MAR was located in the area of São Miguel during that time (Gente et al., 2003; Luis and Miranda, 2008) casting the dating into doubt.)

Fig. 2.8 and Fig. 2.9 show a band of low reflection amplitudes with a thickness of ca. 180 ms at the base of units SW4/5 (Southwest Basin) and S4 (South Basin). This possibly corresponds with transparent upper Miocene hemipelagic sediments within the Atlantis Basin south of the Azores Plateau described by Alves et al. (2004). Hence, the top of the band could represent a time marker within the South Basin and Southwest Basin indicating that formation of the Monaco Bank and Graben ended prior the Pliocene (~5.3 Ma). However, difference in reflection amplitude is weak, less noticeable in the other two profiles covering the South Basin

2.5. DISCUSSION

(Fig. 2.10/2.11) and possibly reflects attenuation of the seismic signal over depth only. In any case, the base of the Miocene unit cannot be inferred in the working area, since sedimentation during formation of Monaco Bank and Graben did not reflect hemipelagic sedimentation conditions.

Sibrant et al. (2015a) recently postulated a change in the regional stress field of Santa Maria Island between 5.3 and 4.3 Ma, which was possibly linked to the ceasing tectonic activity at Monaco Graben (horizon R). According to this, the older part of the island evolved prior to 5.3 Ma and synchronously to the Monaco Bank and Monaco Graben.

Maximum ages of 0.9 Ma onshore São Miguel Island are reported by Johnson et al. (1998). Therefore, the subaerial island evolution started at or before that time (horizon S).

2.5.4. Implications for the Azores Plateau Evolution

The model presented above allows us to draw some general implications for the ongoing debate, whether the genesis of the Azores plateau is driven by processes inside the upper mantle or if it is controlled by rigid tectonic plate kinematics.

The chronological order in the evolution of the N140° and N160° trending structural lineaments (and the intermediate trend), which could be correlated with modelled relative plate movements with extension in N50° and N70° direction, give clear evidence that the tectonic and magmatic evolution of the Azores Plateau is strongly controlled by stress due to the differential plate movement of Nubia and Eurasia. This confirms the conclusion of Neves et al. (2013), who assume that mantle processes are eventually responsible for the high magma support, but arrangement and temporal evolution of the volcanic ridges are mainly driven by plate movements. Therefore, mantle convection may account for the initiation of the Terceira Rift (e.g. Gente et al., 2003; Yang et al., 2006), but it contradicts Adam et al. (2013) who argue stress induced by mantle upwelling being the prevalent factor for the tectonic regime. On the other hand, the dependency on plate movements shows that the evolution of the tectonic architecture is less forced by plate boundary effects as expected by Neves et al. (2013). However, plate boundary effects could account for the fact that the “pure” N160° trend solely developed at the outermost eastern pinnacle of the Azores Plateau.

Between Terceira and São Miguel, new faults with an intermediate orientation of N140°-160° evolved within the pre-existing N140° setting. This “new” trend is also described based on focal mechanisms (Miranda et al., 1998), bathymetric data (Lourenço, 1998) and data from onshore Terceira, where it is reflected by faults and volcanic lineaments interacting with mainly N110° trending structures (Navarro et al., 2003; Montesinos et al., 2003; Lourenço, 2007). Hence, N110° and N140°-N160° trending structures as described by Miranda et al. (1998) as well as

inherited (N140°) and new faults (N145°-N160°) may define small isolated blocks, which possibly show minor clockwise rotation. This addresses the fact that sinistral seismicity along NNW-SSE rupture planes within an overall dextral setting has been recorded (Hirn et al., 1980; Grimison and Chen, 1986; Matias et al., 2007; Borges et al., 2007).

2.5. Conclusion

The southeastern Terceira Rift marks the Nubian-Eurasian plate boundary and comprises the South-Hirondelle Basin and the Povoação Basin. These basins are rift valleys whose southwestern and northeastern margins are defined by few major normal faults and several minor normal faults, respectively. In between, São Miguel Island presumably evolved above a leaky transform that links both basins. South of the island and separated by the N120° trending Monaco Graben system, the Monaco Bank represents a flat topped volcanic ridge dominated by tilted fault blocks.

Based on the characteristics of up to six seismic stratigraphic units per basin, a relative chronology of the tectonic and magmatic processes in the working area were deduced revealing three major stages (Tab. 2.1): I) the early volcano-tectonic evolution of N130°/N140 oriented structures before horizon P time, II) the formation of the N160° trending Monaco Bank, and III) the Post-Monaco-Bank stage including the formation of the Monaco Graben and the subaerial evolution of São Miguel after horizon Q times.

Referring to the more detailed stratigraphy of the Post-Monaco-Bank sediments and in consideration of published age data (Johnson et al., 1998; Luis and Miranda, 2008; Beier et al., 2015; Sibrant et al., 2015a) and extension rates (Luis and Miranda, 2008; DeMets et al., 2010), we postulate a model for the volcano-tectonic evolution of the southeastern Terceira Rift. It includes the following steps:

- Volcano-tectonic evolution of the early Terceira Rift in a N50° orientated extensional setting (seismic units numbered “1”; I in Fig. 2.14).
- At ~10 Ma, rotation in extension to N70°. Subsequent formation of Monaco Bank (and early Santa Maria Island?). Rearrangement of the fault systems in the South Hirondelle Basin (seismic units numbered “2”; II in Fig. 2.14). Tectonics in the Povoação Basin decreased.
- At ≤ 5.9 Ma, formation of Monaco Bank ended. Subsequent opening of Monaco Graben (seismic units numbered “3”; III in Fig. 2.14, Graben Stadium).

2.5. CONCLUSION

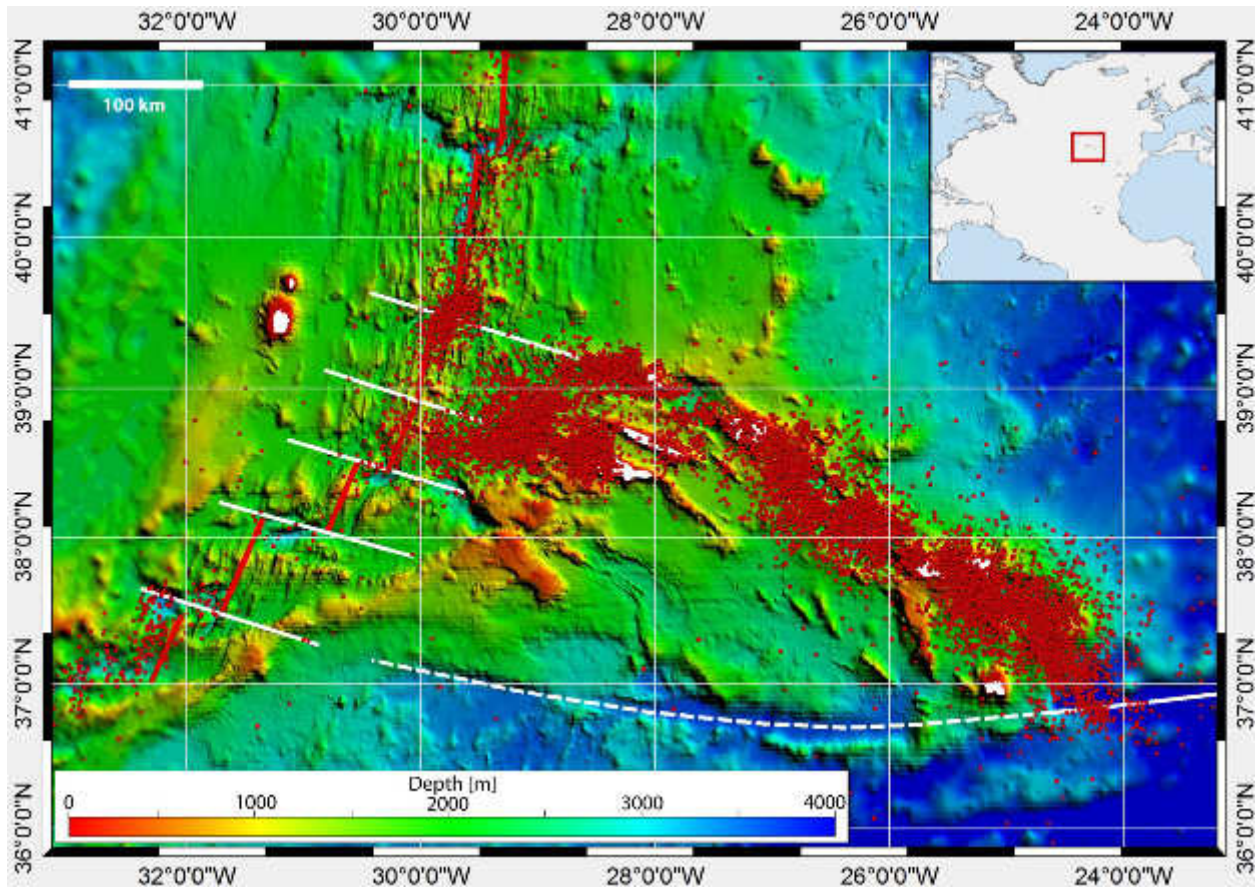
- After rifting at Monaco Graben had ended (5.3 – 4.3 Ma?), tectonics of the Povoação Basin became reactivated. Uniform sedimentation during tectonic quiescence in the South Basin (seismic units numbered “4”; III in Fig. 2.14).
- At ≥ 0.9 Ma, subaerial evolution of São Miguel Island started initiating a N-S directed sediment flux into the South basin. A possible rearrangement of the corresponding volcanic system caused minor tectonic activity in the South Basin at the beginning of this period (seismic units numbered “5”; III in Fig. 2.14).

Hence, the evolution of the southeastern Terceira Rift domain is predominantly controlled by plate kinematics and lithospheric stress forming a kind of a re-organized rift system.

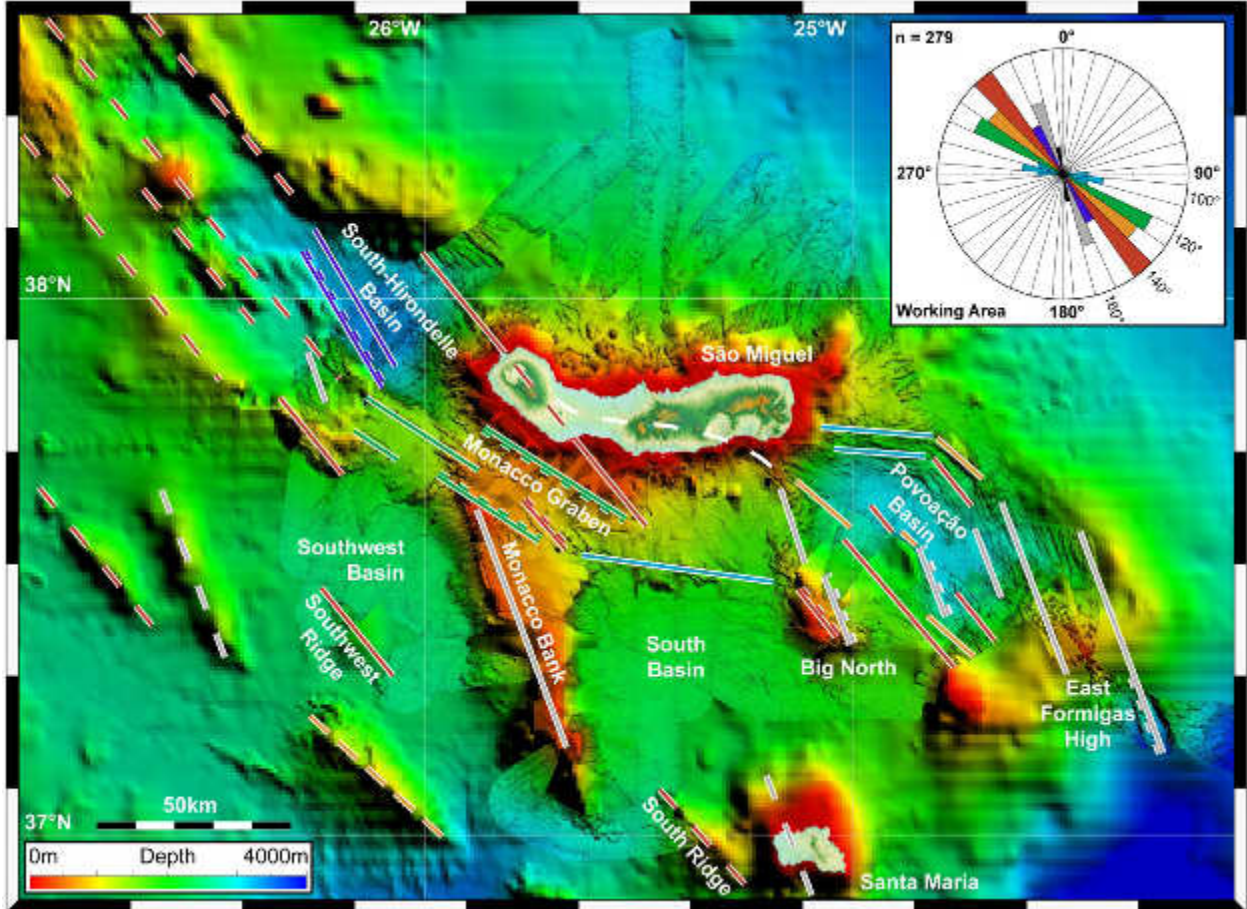
Acknowledgements

We sincerely thank Captain Thomas Wunderlich and his outstanding crew of *RV Meteor* for their support during the M79/2 cruise. We are grateful for the financial support of the German Research Foundation (DFG, grant Hu698/19-1). Additional acknowledgements go to the companies Halliburton-Landmark and Schlumberger for providing university grants for the seismic processing software ProMAX and seismic interpretation software Petrel, respectively, as well as to the NASA's Earth Science Data Systems program for providing the ASTER Global DEM data. Special thanks go to Sönke Reiche for all the helpful discussions. Finally, we want to thank F.O. Marques and N.C. Mitchell for reviewing the manuscript. Their suggestions helped a lot to enhance the quality of this publication.

Appendix



App. 2.1: Recorded seismicity since 1900. Data from International Seismological Centre (2011). Since the magnitude is known for the younger events only, they are shown without any threshold applied.



App. 2.2: Simplified fault map of the working area. Normal faults symbol denotes areas with major vertical offset. Colored dashed lines indicate trends inferred based on bathymetric data published by Lourenço et al. (1998), which are not considered in the rose diagram. White dashed line represents major onshore trends (after Queiroz (1997), Guest et al. (1999), Ferreira (2000), Carmo (2004)).

3. Submarine explosive volcanism in the southeastern Terceira Rift

Abstract

Morphologic studies with sonar data and in situ observations of modern eruptions have revealed some information suggesting how submarine volcanic cones develop, but the information only addresses the modern surfaces of these features. Here, we describe a study combining morphological data with high-resolution seismic reflection data collected over cones within the southeastern Terceira Rift - a succession of deep basins, volcanic bathymetric highs and islands (e.g. São Miguel) representing the westernmost part of the Eurasian-Nubian plate boundary.

The cones (252) are distributed in depths down to 3200 m and exhibit an average diameter of 743 m, an average slope of 20° and heights mainly between 50 and 200 m. The cones are here classified into three different categories by physiographic or tectonic setting (we find no particular morphometric differences in cone shapes between these areas). First, numerous cones located at the submarine slopes of São Miguel's Sete Cidades and Fogo Volcano are considered to be parasitic structures. Second, in the southeast of the island, they form a superstructure possibly reflecting an early submarine stadium of a posterior subaerial stratovolcano. Third, some cones are controlled by faults, mostly in a graben system southwest of the island. High-resolution multi-channel seismic data indicates that the graben cones evolved synchronously with the graben formation. Bottom currents then probably removed the surficial fine grain-size fraction, leaving rough surface textures of the cones, which backscatter sonar signals strongly in the data recorded here. However, a young cone investigated in detail is characterized by a smooth surface, a marked increase of internal stratification with increasing distance from the summit and upwards concave flanks. Others exhibit central craters, suggesting an explosive than an effusive evolution of these structures. The morphological characteristics of these submarine cones show that they have similar sizes and shapes to cinder cones onshore São Miguel.

3.1. Introduction

The Terceira Rift is located in the middle of the Atlantic Ocean roughly 1500 km west of continental Portugal. It is defined by a succession of deep transtensional rift basins and bathymetric highs of volcanic origin, which are distributed along the westernmost tip of the Eurasian-African plate boundary (Fig. 3.1a/b). Few of the bathymetric highs pierce the sea surface, representing the islands of São Miguel and the Formigas islets in the southeastern domain of the Terceira Rift (Fig. 3.1c). Therefore, this area offers unique study conditions for submarine volcanism encompassing a wide range of water depths from shallow to more than 3000 m, which implies a strong diversity of eruption conditions. For example, volcanism close to the sea surface causes steam driven explosions (phreatomagmatism) forming tuff rings. This type of volcanism is called Surtseyan named after the island of Surtsey off the southern coast of Iceland (e.g. Moore, 1985). Such tuff rings are also described in the Azores region, e.g. the Capelas tuff cone at São Miguel (Solgevik et al., 2007) or Capelinhos at Faial (Cole et al., 2001). In water depths of a few 100 m, the effect of sea water boiling predominates (instead of vaporization; Moore, 1985) and the eruption column is concentrated within the submarine domain interacting with surface currents and the sea surface (Cashman and Fiske, 1991). Since every 100 m of water depth corresponds to an increase of pressure by 1 MPa (10 bar), exsolution and expansion of magmatic volatiles - which force explosions at water depths of several hundred meters – are reduced in deeper domains (White et al., 2015). Hence a critical depth has been assumed in the past, below which explosive volcanism is not possible and an effusive type of volcanism (e.g. pillow lavas) is expected only. However, observed deep sea deposits contradict this assumption (e.g. Hekinian et al., 2000).

The submarine domain of the Azores is dominated by several linear volcanic ridges, a very common geomorphological feature in extensional settings like e.g. the Mid-Atlantic Ridge (e.g. Smith and Cann, 1999; Tempera et al., 2013). They are characterized by heights of >1500 m and built up by individual lava terraces, fissure eruption deposits as well as small volcanic cones with diameters <3000 m. These kinds of cones have been described by several authors e.g. in case of the Azores region (Stretch et al., 2006; Mitchell et al., 2012b; Casalbore et al., 2015), the Mid-Atlantic Ridge (Smith et al., 1995a), the Reykjanes Ridge south of Island (Smith et al., 1995b; Magde and Smith, 1995) and the Puna Ridge, Hawaii (Smith and Cann, 1999), all of them based on bathymetric, backscatter and/or side-scan data only.

In contrast, in this chapter we present the first combined analysis of hydroacoustic (bathymetry and backscatter data) and high resolution multi-channel seismic data in the Azores domain focusing on submarine volcanic structures. 252 volcanic cones were observed in the southeastern Terceira Rift, mainly concentrated in the vicinity of São Miguel Island and northeast of the Formigas Islets (Fig. 3.1c). 39 of them are covered by seismic data, although

3.1. INTRODUCTION

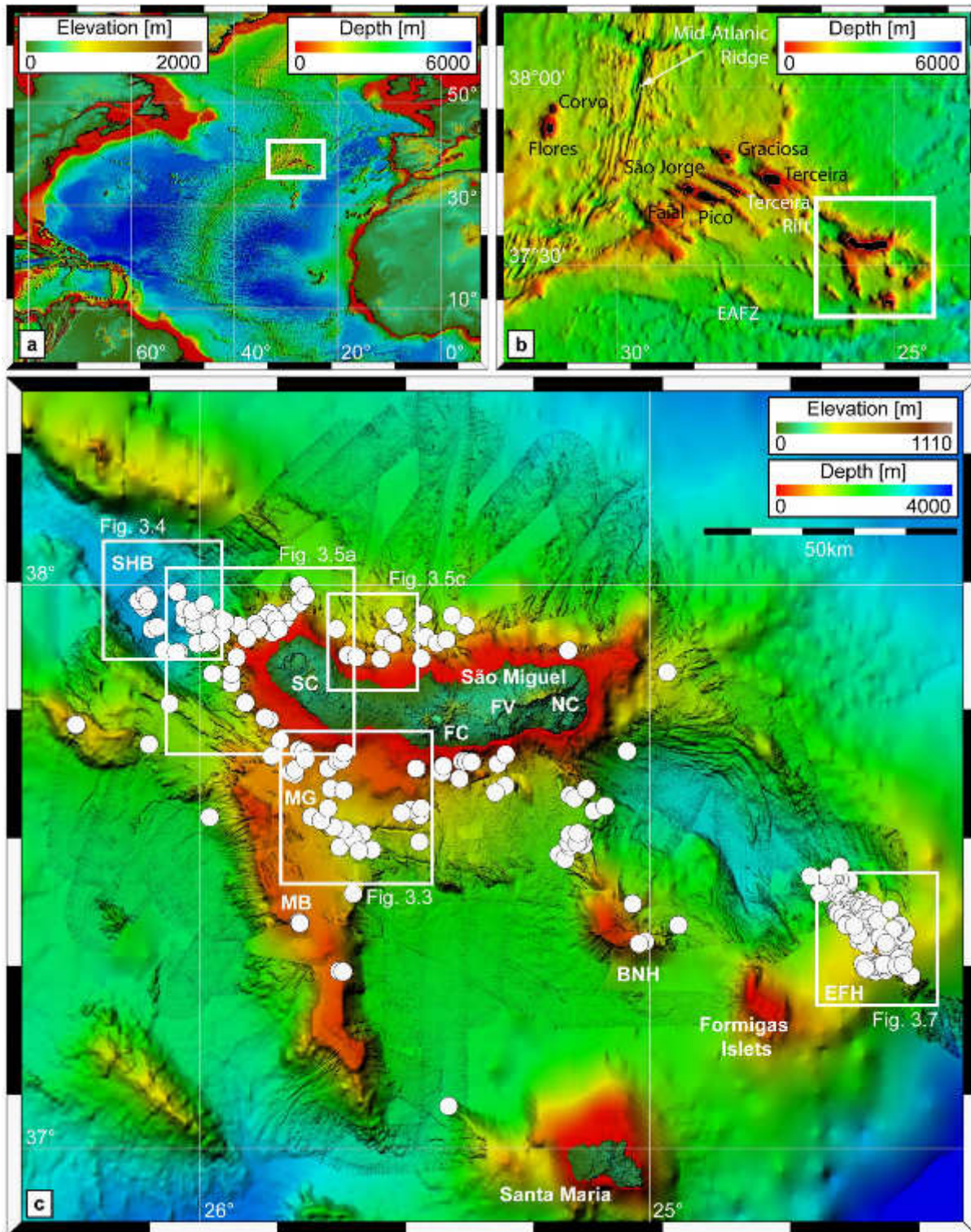


Fig. 3.1: Bathymetric map of the working area. Location of the Azores (a) and the distribution of the islands within the Azores archipelago (b). White dots mark mapped volcanic cones in the working area (c). Lighting from Az320°/Alt70°. EAFZ: East Azores Fracture Zone. Volcanos: SC: Sete Cidades Volcano; FC: Fogo Volcano Complex; FV: Furnas Volcano; NC: Nordeste Complex. SHB: South-Hirondelle-Basin; MG: Monaco Graben; MB: Monaco Bank; BNH: Big North High; EFH: East Formigas High. Background bathymetric data is from Lourenço et al. (1998) and ETOPO (Amante and Eakins, 2009). Topographic data is from ASTER GDEM.

not all of them have been crossed centrally. Most of the cones were assigned to one of three different geographical domains. The cones within each domain were characterized in terms of topographic characteristics, backscatter facies and seismic image (as far as available) before a general statistical overview of the topographic properties like water depth, width, height and slope angle will be given. Finally, the evolution of the cones, the surface texture and its implication as well as the different geological settings will be discussed.

3.2. Regional setting

The Terceira Rift is the Eurasian-Nubian plate boundary with a WSW-ENE directed extension of 4 mm/a (Fernandes et al., 2006). It is located at the northeastern rim of the Azores Plateau, an area where the seafloor is abnormally elevated and roughly defined by the 2000 m contour line (Fig. 3.1b). West of Faial and Graciosa Island, the Terceira Rift merges with the Mid-Atlantic Ridge (MAR) forming the diffuse Azores Triple Junction (Marques et al., 2013, 2014a; Miranda et al., 2014). To the south, the East Azores Fracture Zone (EAFZ) forms the southern rim of the Azores Plateau representing the fossil trace of the Eurasian-Nubian plate boundary (Krause and Watkins, 1970; McKenzie, 1972; Searle, 1980; Luis and Miranda, 2008). During northward migration of the triple junction, the accretion of large volumes of extrusives and intrusives as well as underplated material (Luis et al., 1998; Cannat et al., 1999; Gente et al., 2003) caused the creation of thickened crust (Luis and Neves, 2006; Dias et al., 2007; Georgen and Sankar, 2010; Silveira et al., 2010) resulting in the abnormal elevated seafloor of the Azores Plateau.

Recent studies suggest the initiation of the evolution of the plateau and the Terceira Rift to be strongly controlled by rigid response of the lithosphere to changes in the regional stress field induced by tectonic plate kinematics (Chapter 2; Miranda et al., 1998; Lourenço et al., 1998; Luis and Miranda, 2008; Navarro et al., 2009; Neves et al., 2013). Additionally, the existence of a hot spot (Schilling, 1975; Cannat et al., 1999; Escartín et al., 2001; Gente et al., 2003; Yang et al., 2006) interacting with the MAR or a melting anomaly (Bonatti, 1990; Beier et al., 2008; Métrich et al., 2014) due to an abnormal high volatile content in the mantle (wet spot) may explain the strong volcanism, which has formed the Azores Plateau, the volcanic islands of the Azores Archipelago and submarine linear volcanic ridges.

Several submarine ridges in the Azores have been studied in detail (Mitchell et al., accepted and references therein), e.g. the Condor Seamount west of Faial (Tempera et al., 2013) and a volcanic ridge southeast of Pico (Stretch et al., 2006; Mitchell et al., 2012b). They evolved on top of a system of fissures caused by lithospheric extension along the ridge axis. Ridge volcanism is associated with basaltic magma forming a wide range of different volcanic features such as magma terraces, solidified lava flows, crater and collapse structures, linear volcanic

3.3. DATA AND METHODS

chains as well as isolated small circular volcanic cones. These cones are typically characterized by diameters of 300 m to 3000 m and slope angles of roughly 15° to 25°. Photos taken from similar cones e.g. on top of the median ridge of the Mid-Atlantic Ridge near 34°50'N (south of the Azores Plateau) show hyaloclastites and pyroclastic deposits of unsorted irregularly fragmented rocks (Hekinian et al., 2000), which suggests that the magma was disaggregated during explosive eruptions. Since cones on the submarine Pico Ridge, in contrast, show both smooth as well as rough surface textures in backscatter data, some authors suggest different eruption rates and/or effusive as being responsible for the different surface properties (e.g. Stretch et al., 2006).

In the southeastern domain of the Terceira Rift, three large subaerial active volcanoes are located at São Miguel Island (Fig. 3.1c). From west to east, these volcanoes are the trachyte stratovolcano of Sete Cidades Volcano, the trachyte Fogo Volcano Complex (also known as Água de Pau) and the trachyte Furnas Volcano (Wood, 1980; Moore, 1990; Moore and Rubin, 1991). The youngest and smallest one, Furnas, started to evolve about 100 ka ago (e.g. Moore, 1990) and overlies the remnant Nordeste Volcano Complex, which shows reliable ages of maximum 0.8 – 0.9 Ma (Sibrant et al., 2015b; Johnson et al., 1998). Formation of Fogo and Sete Cidades started about 200 ka (e.g. Moore, 1990). In between these active main volcanoes, fields of alkali basalt lava flows and cinder cones are situated revealing Upper Pleistocene and Holocene ages. Cinder cones usually form during monogenetic explosive eruptions (Schminke, 2005) and resemble submarine volcanic cones in size and shape.

3.3. Data and methods

This work is based on high resolution bathymetric, backscatter and multi-channel seismic data collected by University of Hamburg scientists on board of *RV METEOR* during cruise M79/2 in 2009 (Hübscher, 2013). For the bathymetric and backscatter data measurements the Kongsberg EM120 and EM710 multibeam echosounders installed on board were used. These systems emit 12 kHz and 70-100 kHz acoustic signals, respectively, and soundings from the backscattered signals were recorded over approximately four times water depth over an area elongated perpendicular to the vessel track. Both, travel time and backscattered energy per signal are recorded in fixed receiver beams of known geometry. Based on velocity information of the water column and the travel time, water depth is calculated. The amount of backscattered energy depends on the seafloor's roughness – the rougher the seafloor, the higher the backscattered energy is (black in the backscatter maps presented here). During processing, segments lacking navigation due to errors were filled with interpolated positions, depth information was corrected based on revised water velocity profiles and each recorded beam was edited to eliminate spikes. Grid node spacing was mostly chosen as 30 x 30 m, but smaller

spacings were chosen for detailed views as mentioned in figure captions. However, as the sonar acoustic footprint is equal to $\sim 2\%$ of water depth, effective resolution can be less than the grid spacing. To fill areas where we had not surveyed, a background bathymetric map was created from data of a 1x1 km grid presented by Lourenço et al. (1998), which can be found under http://w3.ualg.pt/~jluis/acores_plateau.htm, and ETOPO1 data ($\sim 1.9 \times 1.9$ km) published by Amante and Eakins (2009). The onshore topographic data shown is originated from the ASTER GDEM, which is a product of METI and NASA. It contains a 1 arc sec (30 m) grid of elevation postings. For visualization purposes the different data sets have been imported to an ArcGIS 9.3 system. Using this system as well as the QPS Fledermaus 3D software high resolution bathymetric data were screened for topographic positive structures with a maximum width of 5 km. To distinguish between volcanic cones and potential blocks of debris avalanches only structures with a circular to oval shape in plan view and a domed vertical profile have been mapped. Each mapped structure were characterized by the following properties: (1) water depth of the summit; (2) basal diameter measured orthogonal to the gradient of the submarine slope the cone lies on; (3) height given as elevation difference of summit and interpolated seafloor below; and (4) slope angle calculated from the arc tangent of height and half basal diameter.

39 cones are covered by high resolution 2D multi-channel seismic data. The corresponding seismic signals were generated by two clustered GI-Guns with a generator volume of 45 cubic inch and an injector volume of 105 cubic inch each. For data recording a 600 m long asymmetric digital streamer was used, containing 144 channels with an average spacing of 4.2 m. Shots were fired every 25 m at a speed of 5 kn. Data processing involved trace editing and CMP sorting with a CMP increment of 5 m as well as the application of several bandpasses with 10/20/300/400 Hz, a spike & noise burst filter and a FK-filter (e.g. Hübscher and Gohl, 2014). Finally, NMO-correction, stacking and a post stack time migration has been performed. For the detailed studies of one volcanic cone (Fig. 3.6) 144 channels were first stacked so that they formed a group of 96 effective channels with a regular spacing of 6.25 m. This data has been filtered by a bandpass of 10/15/150/300 Hz, CMP increment has been decreased to 3.125 m and NMO-correction has been applied based on picked velocity profiles.

3.4. Observations and interpretation

The cones were grouped into different categories according to their location (Fig. 3.2). One category is orientated along faults and bathymetric lineaments (blue area in Fig. 3.2). A second group was chosen around the submarine slopes of Sete Cidades Volcano as well as north and south of the Fogo Volcano Complex (green area in Fig. 3.2). Further cones cluster on top of

3.4. OBSERVATIONS AND INTERPRETATIONS

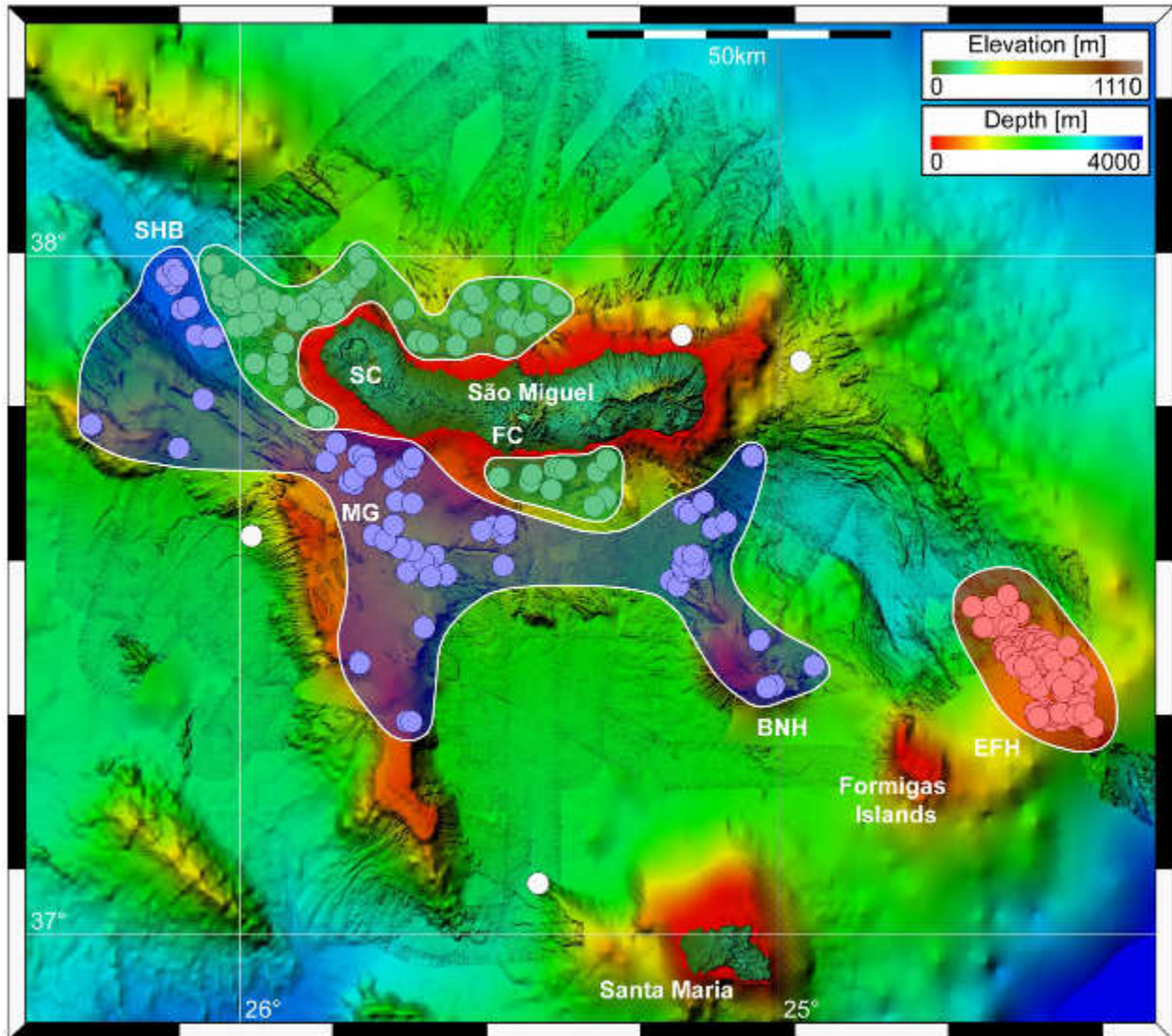


Fig. 3.2: Categories of submarine volcanism according to location. Blue: Volcanism along structural lineaments; Green: Volcanism at the submarine domain of Sete Cidades and Fogo; Red: Volcanism at East-Formigas High. Lighting from Az320°/Alt70°. Volcanos: SC: Sete Cidades Volcano; FC: Fogo Volcano Complex. SHB: South-Hirondelle-Basin; MG: Monaco Graben; BNH: Big North High; EFH: East Formigas High.

East-Formigas High where the density of cones is highest in the working area (red area in Fig. 3.2), which was chosen as a third group. Each of these categories represents a specific volcanic setting controlled by distinct volcanic mechanisms. Below, they will be presented in detail.

3. SUBMARINE EXPLOSIVE VOLCANISM IN THE SOUTHEASTERN TERCEIRA RIFT

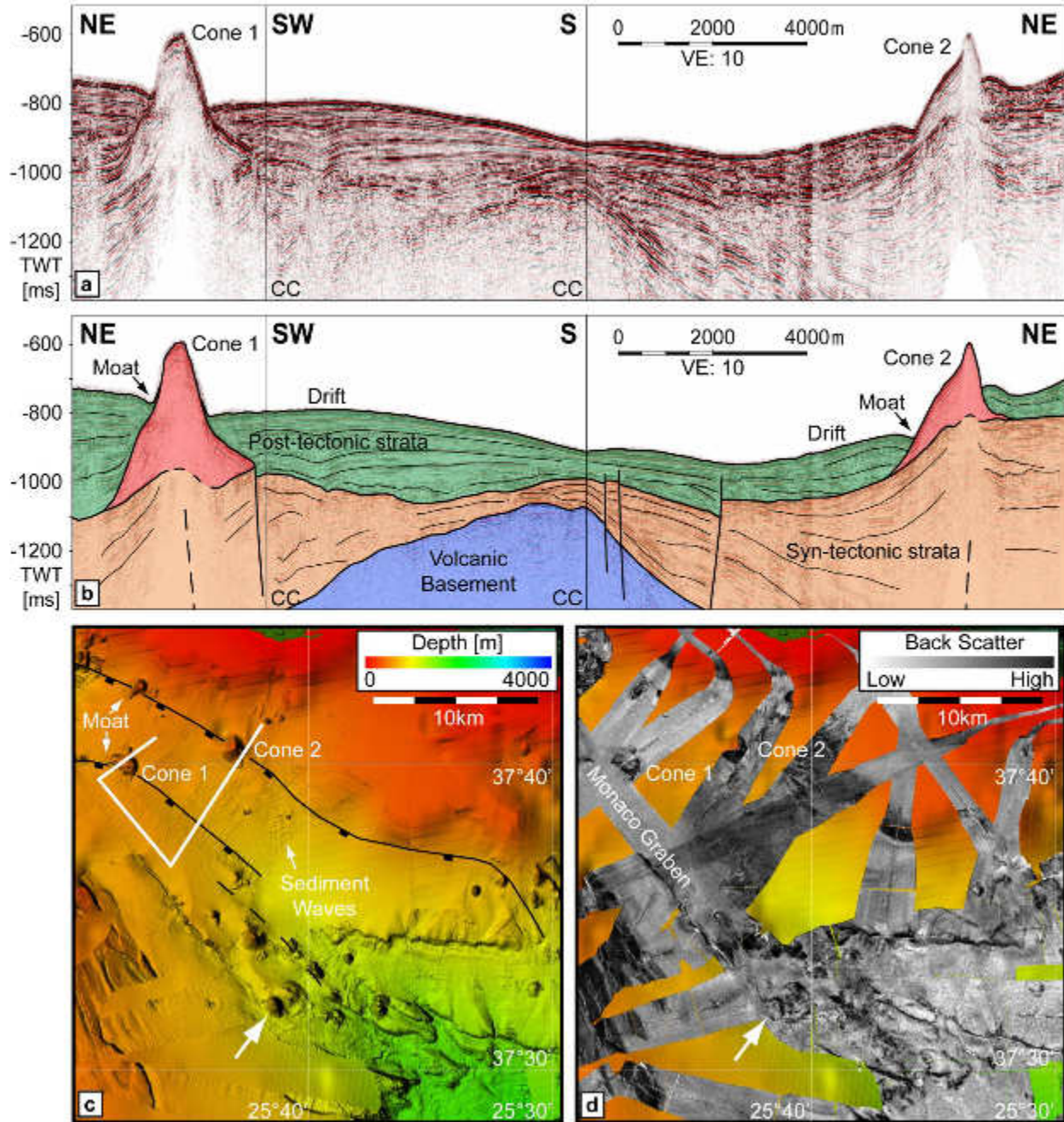


Fig. 3.3: Fault controlled volcanism. Seismic section (a), its interpretation (b), bathymetric (c) and backscatter data (d). Black vertical lines in (a, b) indicate the course changes (CC), white line in (c) shows the location of the profile. White arrows in (c) and (d) indicate the cones with a crater. For detailed location of (c) and (d) see Fig. 3.1. Lighting from Az270°/Alt70°. VE: Vertical Exaggeration. Normal faults (black) and volcanic lineaments (black dashed line) in (c) after Chapter 2.

3.4. OBSERVATIONS AND INTERPRETATIONS

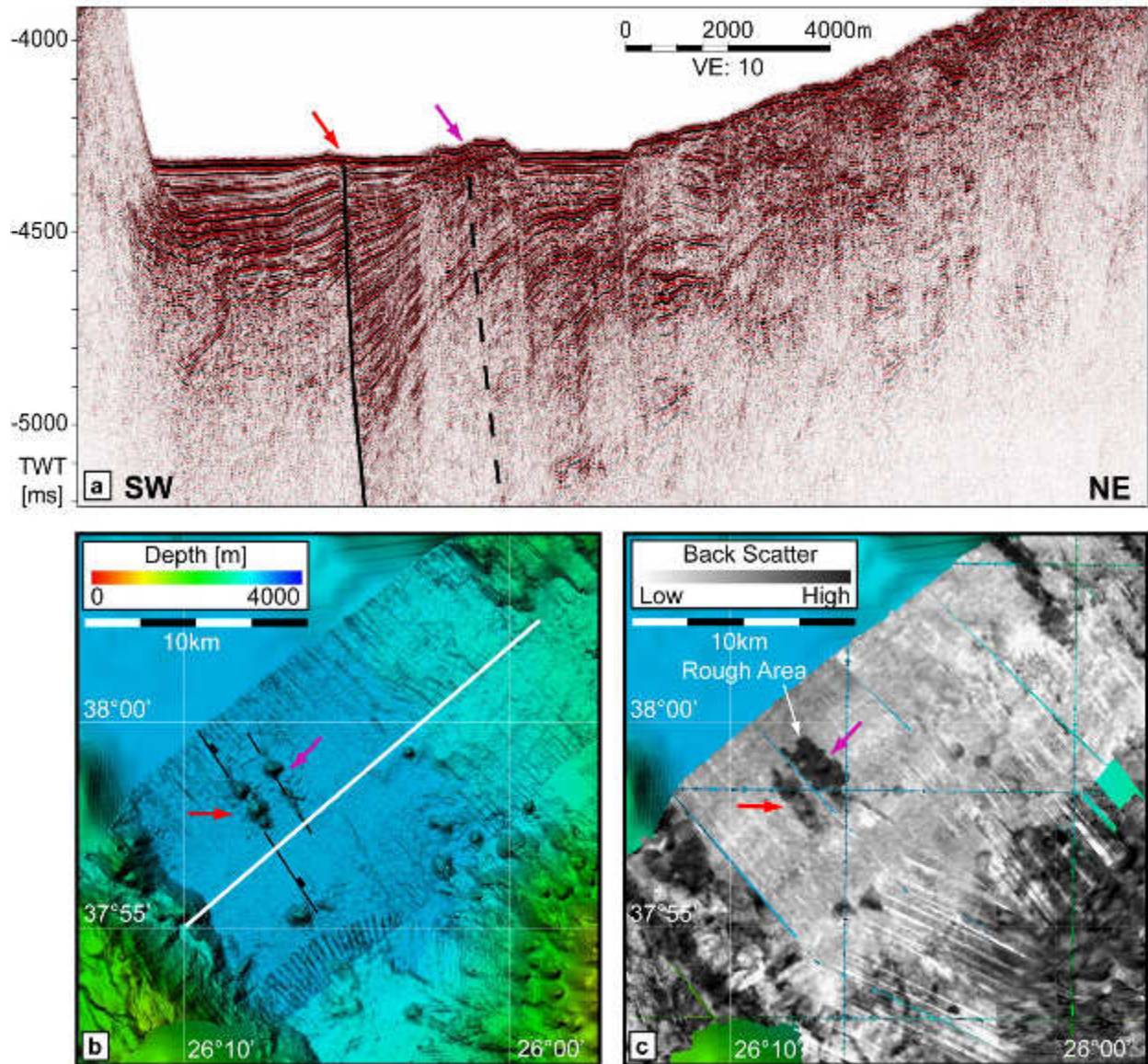


Fig. 3.4: Fault controlled volcanism in the deep areas. Seismic section (a), bathymetric (b) and backscatter data (c). White line in (b) shows the location of the profile. Colored arrows trace the two volcanic lineaments in the deep sea domain of the South-Hirondelle Basin. For detailed location of (b) and (c) see Fig. 3.1. Lighting from Az320°/Alt70°. Grid spacing in (b, c) 40x40 m. VE: Vertical Exaggeration. Normal (black) and inferred (black dashed line) faults in (b) after Chapter 2.

3.4.1. Volcanism along structural lineaments

South of São Miguel Island, many volcanic cones are either distributed along faults and magmatic lineaments or form volcanic chains (blue area in Fig. 3.2). Most cones are located in the vicinity of Big North High and in the Monaco Graben in water depths of 400 m to 2000 m (Fig. 3.3a-d). A further cluster of aligned cones is within the South-Hirondelle Basin where water depth reaches 3200 m (Fig. 3.4a-c). In the backscatter data (Figs. 3.3d, 3.4c), the cones appear

3. SUBMARINE EXPLOSIVE VOLCANISM IN THE SOUTHEASTERN TERCEIRA RIFT

as circular to elongated structures which most of them differ from their surroundings by a higher backscatter (rougher surface). Furthermore, two cones in the South-Hirondelle Basin are located on top of a small area producing high acoustic backscatter, which is also recognizable in the bathymetry (marked with purple arrow in Fig. 3.4b-c).

Cones in the Monaco Graben reveal a transparent and occasionally layered seismic reflection pattern. As illustrated by the two cones in Fig. 3.3a/b, all cones crossed with seismic lines within the graben terminate on the same reflection horizon, which is also a prominent boundary between mainly (sub-) parallel to divergent reflections onlapping each cone's flanks and a sub-parallel, contorted and tilted reflection pattern below. Underneath, a strong amplitude reflection marks the transition to the acoustic basement and the corresponding area of low seismic penetration. Both, basement and overlaying unit are disrupted by faults, but none of them penetrating the seafloor. Faults below the cones are not clearly observable, though tilted and offset reflections suggest their presence.

Following the results of Chapter 2 we interpret the acoustic basement as the volcanic basement, which has been offset during the formation of the Monaco Graben. Faults active during extension thus partly acted as magmatic pathways controlling the distribution of the cones within the graben. Therefore, the unit overlaying the acoustic basement represents the corresponding syn-rift deposits. Since the flanks of the cones terminate on top of this unit and the reflection of the uppermost unit onlap these flanks, the cones were active during the end of graben formation. This agrees with the lack of seismicity in this region (appendix of Chapter 2), indicating that there is neither recent extension nor recent magmatic ascent taking place. The uppermost unit reflects current controlled sedimentation conditions during tectonic quiescence. It forms mounded elongated patch drifts and associated moats, flanking the cones where the bottom currents are intensified (Fig. 3.3a/b).

Cones in the South-Hirondelle Basin have not been directly crossed by seismic data, but an area with a remarkably rough surface is covered by seismic data. It is characterized by strong chaotic and disrupted reflections indicating a volcanic origin (purple arrow in Fig. 3.4a). Since the high acoustic impedance of this area hampers seismic imaging of deeper structures, the existence of a fault plane beneath this structure remains uncertain. Nevertheless, the shape and orientation of the high backscattering area and the strike direction of the corresponding volcanic lineament parallel to the southwestern one support this interpretation. Therefore, the northeastern volcanic lineament is interpreted as being located on top of a small volcanic plateau which has been formed during effusive fissure eruptions. In contrast, the southwestern volcanic lineament clearly correlates with the prominent normal fault identifiable in the seismic data (red arrow in Fig. 3.4).

3.4. OBSERVATIONS AND INTERPRETATIONS

3.4.2. Parasitic Volcanism

Cones assigned to this category occur on the submarine slope of Sete Cidades Volcano as well as north and south of the Fogo Volcano Complex (Fig. 3.5a-d). They comprise the largest cones which have been measured in the working area, with diameters of 1500 m or more. Examples are the northernmost cone north of Fogo (marked with a black arrow in Fig. 3.5c) and a cone southeast of Sete Cidades (also marked with a black arrow in Fig. 3.5a) described in detail later on (Fig. 3.6). The water depth commonly ranges from 400 m to 1200 m but reaches maximum values of 3200 m west of Sete Cidades Volcano, where its slope extends down to the South-Hirondelle Basin floor. Most of the cones are distributed without any obvious pattern or organization. Solely on the northwestern slope of Sete Cidades Volcano (Fig. 3.5a), cones group along faults crosscutting the northeastern margin of the South-Hirondelle Basin and continuing across the main body of Sete Cidades Volcano and the western island of São Miguel, respectively (Chapter 2 and references therein). The seafloor in the Sete Cidades domain produces high backscattering amplitudes and hence appears to be rough before it reaches the South-Hirondelle Basin floor characterized by a smooth sediment surface (Fig. 3.5b). Since the contrast in roughness between most of the cones and the surrounding seafloor is low, it is difficult to identify cones based on backscatter data information only. Nonetheless, a few cones are present, which are characterized by gray in Fig. 3.5b and therefore suggesting smooth surfaces. Examples are the cone southwest of Sete Cidades crossed by seismic reflection data and a cone northwest of that edifice with a small summit crater (both marked with B in Fig. 3.5a/b). Aside from the second mentioned cone, two collapsed cones are observable. In each case, a new cone has grown up within the collapse structure (marked with C in Fig. 3.5a/b). In contrast to the submarine slope of Sete Cidades, the northern slope of São Miguel between the Sete Cidades and Fogo domain (Fig. 3.5c/d) is generally characterized by a brighter backscatter facies and a smooth seafloor, respectively. Volcanic cones commonly appear as black anomalies, but also cones defined by a smooth surface are observable.

One possible reason for the highly backscattering Sete Cidades could be the steep slope ($>10^\circ$) of this area, which may impede sediment deposition. In contrast, north of the Fogo Volcano Complex a lower slope angle ($< 6^\circ$) allows sediment bodies to accumulate, covering most of the volcanic effusive and explosive.

South of Sete Cidades Volcano, a cone showing a low backscattering surface has been covered by a slope-parallel and a slope-perpendicular seismic line (Fig. 3.6a-d), the latter one also covering an adjacent cone. They are located on top of a seismic unit revealing distorted and chaotic reflections. Internally, the cones are mostly seismically transparent in the proximal region, but showing few reflections. Distally, internal stratification increases and the slope is

3. SUBMARINE EXPLOSIVE VOLCANISM IN THE SOUTHEASTERN TERCEIRA RIFT

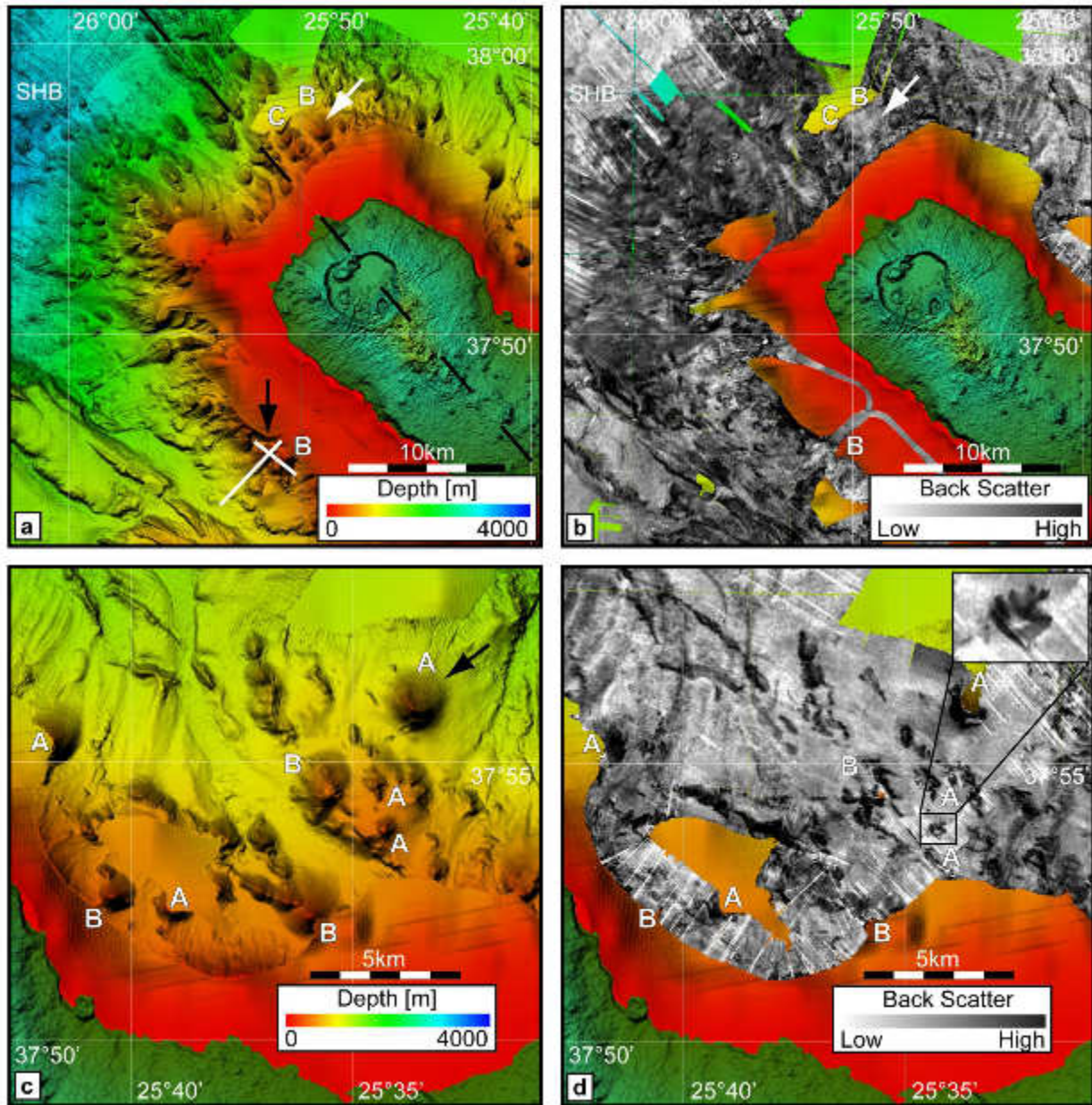


Fig. 3.5: Parasitic volcanism. The submarine slope of Sete Cidades Volcano is covered with numerous volcanic cones (a). Cones as well as the adjacent seafloor show a dark backscatter facies (rough surface) (b). In contrast, the seafloor north of Fogo Volcano Complex (c, d) is much brighter (smoother), but most cones keep their dark backscatter characteristics (marked with A). Few of the cones in (b) and (d), however, show a bright backscatter facies/smooth surface (marked with B). This category of cones reveals the largest structures mapped in the working area (black arrow in a, c). White arrow in (a) and (b) indicate a cone with a crater. For detailed location see Fig. 3.1. C: Collapse structure and cone within; SHB: South-Hirondelle Basin; White lines in (a): Seismic profiles presented in Fig. 3.6; Dashed black line in (a): Simplification of the South-Hirondelle Basin margin faults and their onshore continuation after Chapter 2. Lighting from Az320°/Alt70°.

3.4. OBSERVATIONS AND INTERPRETATIONS

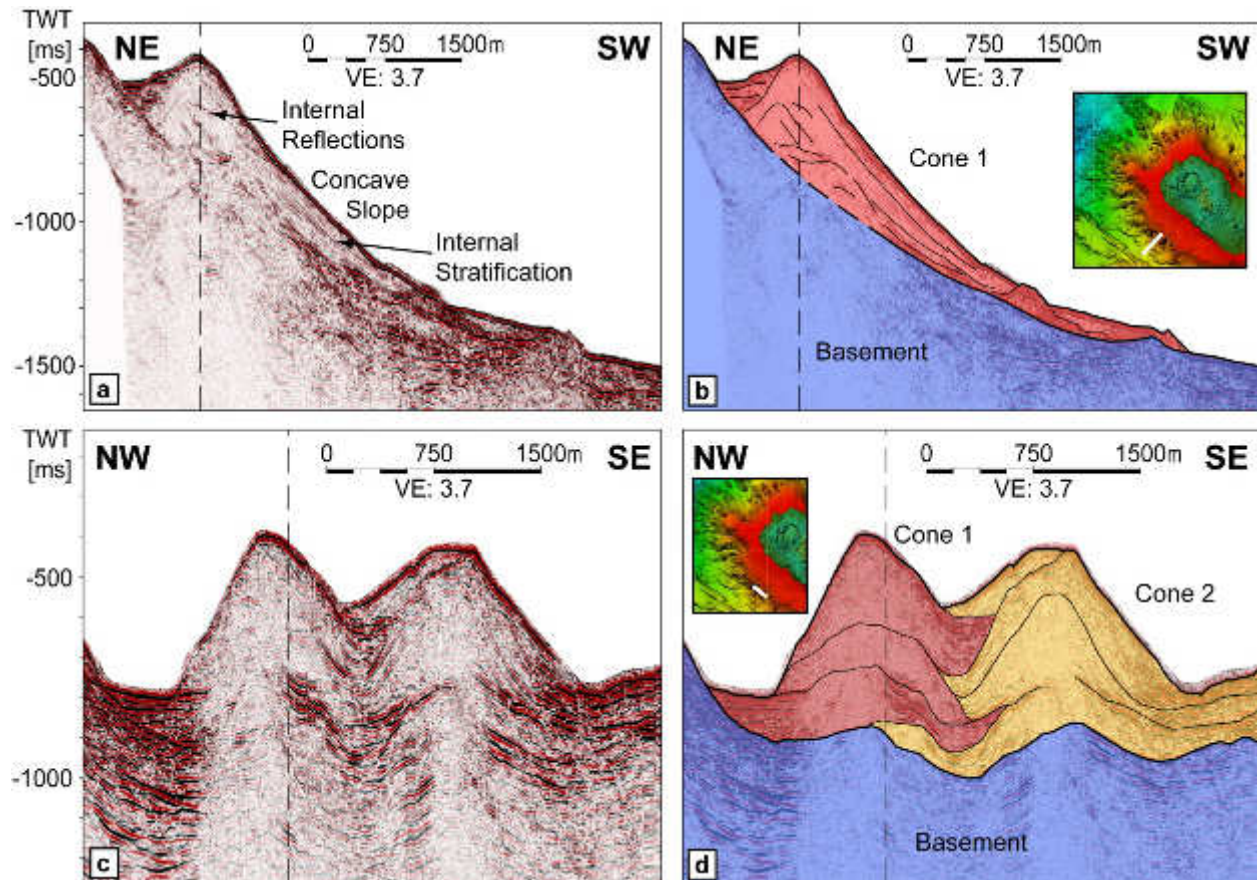


Fig. 3.6: Parasitic volcanism. Seismic sections (a, c) and corresponding interpretation (b, d). Note the concave shape of the flank and the distal increasing stratification of cone 1 illustrating its explosive nature (b). Depositions of cone 1 and 2 interfinger indicating a synchronous evolution (d). For location of profiles see inset or Fig. 3.5a. Dashed black vertical lines indicate the intersection of profiles. VE: Vertical Exaggeration.

concave (Fig. 3.6a/b). In the transition to the nearby cone, volcanic deposit interfinger (Fig. 3.6c/d).

Both cones overlie the southern slope of São Miguel Island, where the substrate presumably consists of successions of coarse rock sediments, lava flows and volcanoclastics deposited during the formation of Sete Cidades Volcano. The concave shape of the slope and the arrangement of internal stratification of the cones indicate deposits with a distally decreasing grain size. We therefore interpret the distal domain of the cone as comprising disaggregated volcanoclastic material. Inter-fingered reflections thus represent multiple eruption phases or overlapping depositions of explosive and effusive volcanic material. Since the deposits of the adjacent cone interfinger, the two cones emerged synchronously, but their corresponding eruption phases alternated in time.

3. SUBMARINE EXPLOSIVE VOLCANISM IN THE SOUTHEASTERN TERCEIRA RIFT

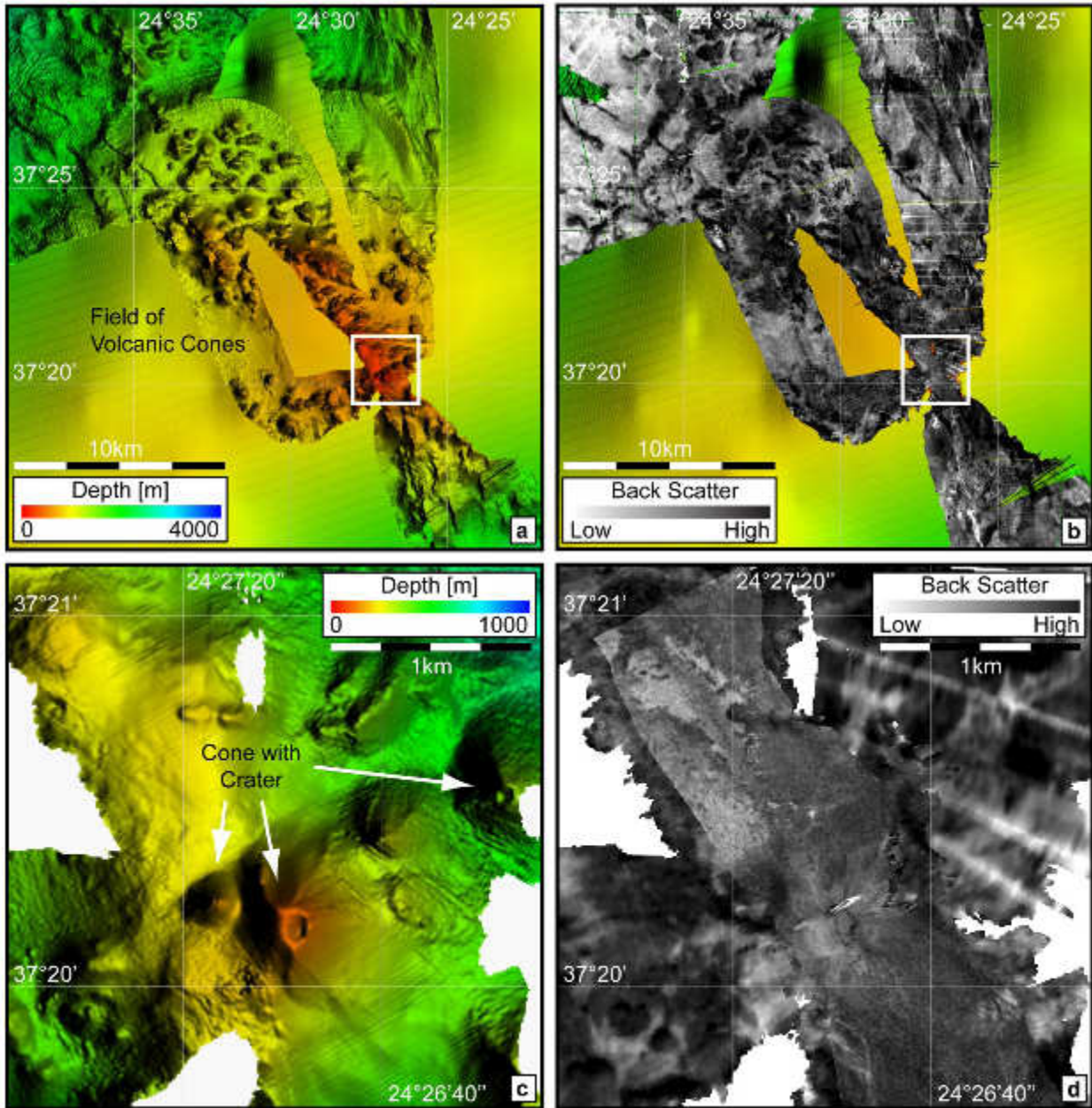


Fig. 3.7: Constructive volcanism. Bathymetric (a, c) and backscatter data (b, d). White boxes in (a) and (b) indicate the location of blow-ups in (c) and (d), respectively. The East-Formigas High is covered with many volcanic cones (a) and several revealing craters (c). In general, this area is characterized by rough surface (high backscattered energy) and roughness of volcanic cones does not strongly differ from their surroundings. For detailed location see Fig. 3.1. Lighting from Az90°/Alt70°. Grid spacing in (c, d) 10x10 m.

3.4. OBSERVATIONS AND INTERPRETATIONS

3.4.3. Volcanism at East-Formigas High

More than hundred volcanic cones have been picked on top of the East-Formigas High (Fig. 3.7a-d). They are distributed in water depths of 200 m to 2000 m. The shallowest point in this region is the crater rim of a cone rising up to a minimum water depth of 110 m (Fig. 3.7c). This one and two adjacent cones clearly show evidence of summit craters. Again, the locations of the cones do not follow organized patterns, such as would occur if erupted above faults. Nevertheless, faults are present and crosscut the entire East-Formigas High. Into shallow water, the seafloor shows higher acoustic backscattering. Thus, the identification of volcanic cones purely based on backscatter data becomes less straightforward, since many of them show a rough surface as well. A special case is the shallowest cone (Fig. 3.7d) which indeed does not show a significantly brighter backscatter facies than the surrounding seafloor, although it lacks a distinct cone-seafloor boundary. For that cone, only the crater rim appears as a well-defined structure.

3.4.4. Morphometrical characteristics and depths of volcanic cones

In total, 252 submarine volcanic cones could be identified in the area covered by our high-resolution multibeam data (Fig. 3.1c). The mapped summits are distributed in water depths from 110 m on top of East Formigas High down to 3200 m in the South-Hirondelle Basin. One of the largest cones is located at the southwestern submarine slope of Sete Cidades Volcano (previously presented in Chapter 3.4.2.). It shows a diameter of 3000 m, a height of 500 m and a water depth of its summit of 265 m. In contrast, one of the smallest structures which could be identified as a volcanic cone is located on top of Monaco Bank in a water depth of 485 m. It is 110 m in diameter and 14 m high. The average width of all measured cones is 743 m with a standard deviation of 405 m, the average height is (139 ± 77) m with an average slope angle of $(20\pm 4)^\circ$ and they are located in water depths of (1023 ± 705) m. In comparison, cones observed onshore São Miguel – in particular between Sete Cidades Volcano and the Fogo Volcano Complex – are smaller. They have an average width of (484 ± 215) m, a height of (73 ± 36) m and show slightly lower slope angles of $(17\pm 4)^\circ$.

Fig. 3.8a shows the distribution plot of size over depth. Water depths of the cones are assigned to ten 300 m bins. Corresponding average diameter and standard deviation per bin are indicated by circles and vertical lines, respectively. One can notice that the average cone width is not a function of the water depth but alternates around an average of 743 m. In contrast, the standard deviation tends to decrease with increasing water depth, declining from 520 m to 70 m (only one cone lies within the 2400 m bin so no standard deviation is given there), before increasing again at 3000 m depth. These cones, which are all located on the floor of the South-Hirondelle Basin, show again an increased variation in size of 250 m. The total number of cones

3. SUBMARINE EXPLOSIVE VOLCANISM IN THE SOUTHEASTERN TERCEIRA RIFT

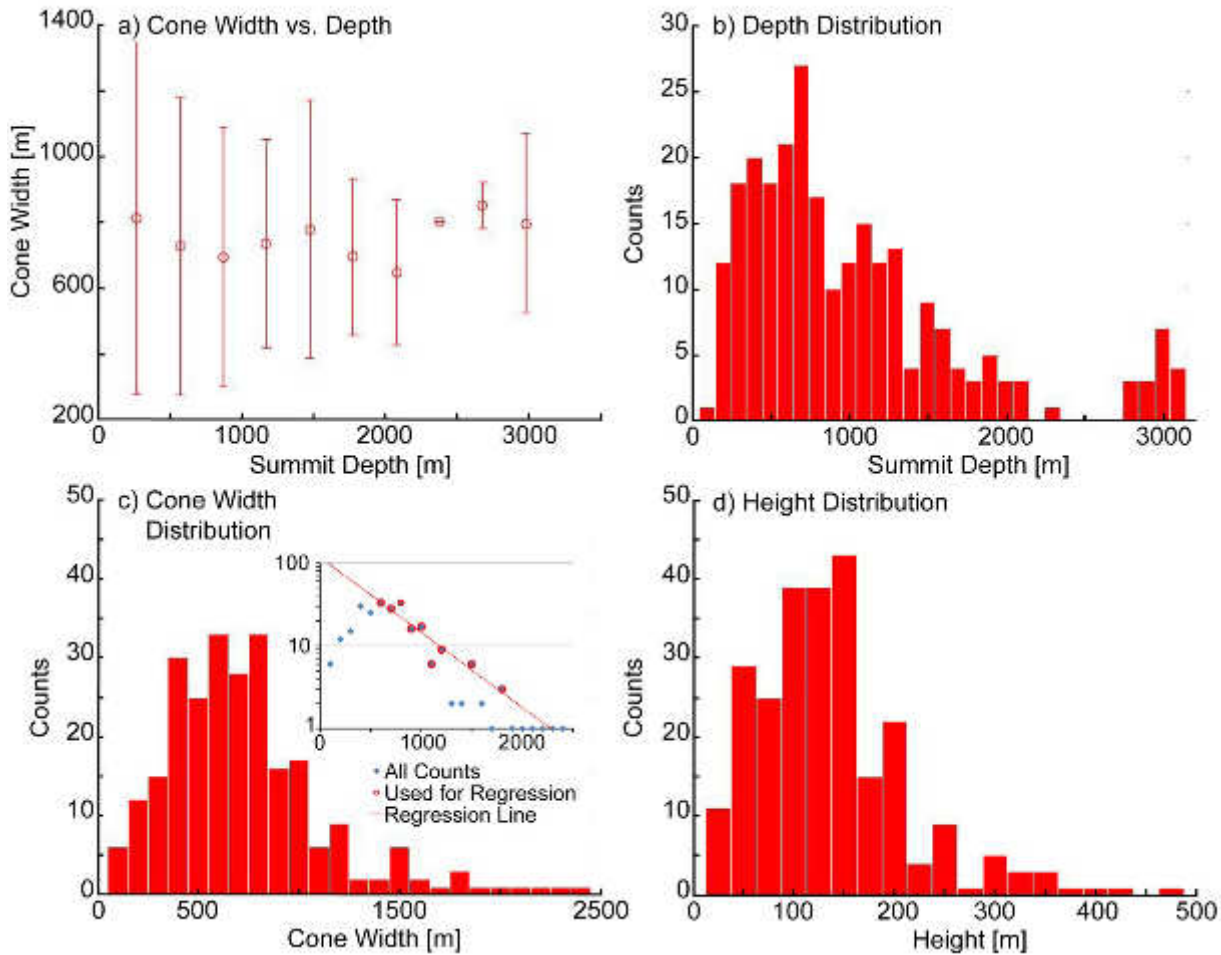


Fig. 3.8: Cone morphometrical characteristics and depths. Distribution of cone diameters with depth (a). Circles indicate the average and vertical lines the standard deviation of all cones within 300 m water depth bins. Note that the average shows no dependency on water depth, whereas the standard deviation tends to decrease. Total number of cones in a certain water depth (100 m bins, b), with a certain diameter (100 m bins, c) and a certain height (25 m bins, d). Please note that cone size distribution shows an exponential trend when considering cones wider than 500 m and bins with more than 4 counts only (red circles in (c), inset). Blue squares show the original values on a logarithmical scale as also shown by the linear red histogram.

per 100 m depth bin as well as number of cones of a distinct diameter (100 m bin) and height (25 m bins) are presented in Fig. 3.8b-d. The cone width distribution, when considering cones with a minimum width of 600 m and bins with more than 4 counts (less is expected not to be statistically relevant) only, shows an exponential decrease of cone numbers with increasing size (Fig. 3.8c, inset). The inverse exponential coefficient of the exponential regression line (red dotted line) is 480 m. Both distribution and exponential coefficient are in a good agreement with observations at and close to the MAR south of the Azores as well as south of Iceland (Smith, 1996). In Fig. 3.9a the relation between cone heights and cone widths (H/W ratio) is presented. With one exception, all cones are characterized by slope angles lower than the angle

3.4. OBSERVATIONS AND INTERPRETATIONS

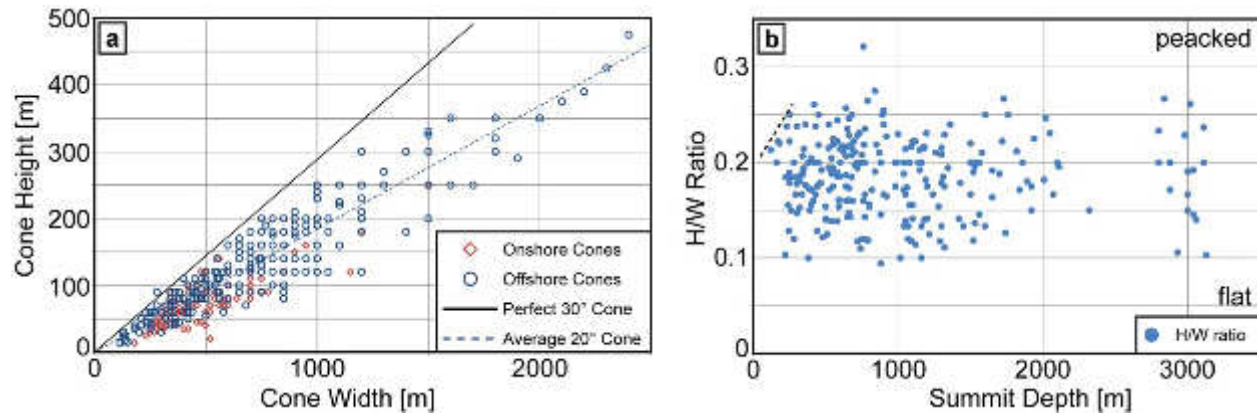


Fig. 3.9: Relation between cone width and height. Both offshore cones and cones onshore São Miguel are underneath the line describing a perfect cone with 30° slopes (a). Ratio of height and width (H/W) of cones deeper than 300-400 m is independent of the water depth (b). Dotted line in (b) indicates a decrease of the maximal H/W ratio values in shallow water depths (<300-400 m).

of repose of granular material, expected to be 30°. For comparison, the H/W values of cinder cones onshore São Miguel also have been included. Measurements were taken in the same way as for the offshore domain but were based on ASTER GDEM topographic data. It becomes obvious that the onshore cones are smaller and that they tend to reveal lower slope angles than the offshore structures. The ratio of cone height and width plotted against water depth shows that for the offshore cones there is no correlation between cone shape and the water depth of the summits below 300-400 m (Fig. 3.9b). Above this level, cones tend to be flatter as indicated by the black dashed line.

Most of the submarine cones in the working area have a peaked summit and less of 4% reveal an identifiable crater. This is similar to the onshore cones, but craters of various sizes are much more common here. However, the lack of craters - especially in the deep sea domain - could rather be a problem of horizontal resolution than reality (effective resolution after processing and gridding is e.g. ~75 m in a depth of 3000 m or ~25 m in a depth of 1000 m).

The backscatter data suggests a little majority of cones characterized by high acoustic backscattering (111 of 252), appearing as dark spots like in the Monaco Graben (upper left part of Fig. 3.3d) and the South-Hirondelle Basin (Fig. 3.4c) or as an intensely dark speckled area (e.g. marked with A in Fig. 3.5d). In contrast, 100 of 252 cones show an overall bright backscatter facies (marked with B in Fig. 3.5b/d). But apart from the backscatter characteristics, both types of cones do not remarkably differ in their topographic characteristics (width, height, slope angle). However, several cones could not reliably be assigned to one of the two categories (41 of 252) since they partially show both low and high backscattered energy or due to their location in an overall “darker” setting, where the contrast between a cone and its surroundings is generally low (Figs. 3.5b/3.7b).

3.5. Discussion

3.5.1. Explosive or effusive evolution of volcanic cones?

Several observations allow concluding on possible information on the eruption process. Even if several cones include or overprint elongated structures (e.g. Fig. 3.5c), the cones are predominantly circular and tapered (Figs. 3.3-3.7), which reminiscent of a sandheap. This pattern indicates that the deposits of the cones originate from a central vent (which is sometimes part of a volcanic fissure system).

An almost transparent reflection pattern partially revealing some weak internal stratification within the proximal domain of a cone (Fig. 3.6a) indicates clastic but irregular and unsorted deposits, which are deposited close to their origin, possibly revealing minor effusive/intrusive. In contrast, stratification is clearly observable in the distal domain. Hence, we conclude on an outwards fining sediment composition which was farther distributed by the water column before it settled down. Deposits which mainly have been formed by runout of particles or, in particular, by disaggregation of downslope lava flows producing breccias (Sansone and Smith, 2006) would result in a more irregular to chaotic reflection pattern and, hence, are unlikely. Anyway, reflection pattern rules out a composition of effusive (Hübscher et al., 2015), even if a minor presence cannot generally be excluded (e.g. Fig. 3.5d, inset).

Few cones show summit craters (Figs. 3.3c, 3.5a and 3.7c). Generally, such craters may result from explosions or collapses. Onshore, craters at volcanoes similar in size (cinder cones) are commonly the result of explosive eruptions (Schmincke, 2004; Wood, 1980). These volcanoes are formed by monogenetic volcanism resulting from propagation of small batches of magma (Németh et al., 2003). In contrast, pit craters (collapse features) typically occur at much more complex volcanic systems characterized in particular by internal magma reservoirs/flows and rift zones usually causing collapses. Examples for such volcanic systems are e.g. the shield volcanoes of Hawaii (Okubo and Martel, 1998) or the adjacent Lō`ihi Seamount (Garcia et al., 2006). Hence, we suggest that the observed craters were formed by submarine explosive eruptions similar to those studied in detail by e.g. Chadwick et al. (2008).

Based on these interpretations and since the H/W ratio is nearly uniform (implying nearly uniform slope angles) over all mapped cones (Fig. 3.9a), we conclude on volcanoclastic particles deposited near the angle of repose being the main component of these structures. Associated hyaloclastites and pyroclasts were described e.g. for the East Pacific Rise region (Smith and Batiza, 1989), the Mid-Atlantic Ridge (Hekinian et al., 2000) and the Aegean Sea/Mediterranean (Nomikou et al., 2012). Meyer et al. (1996) observed tuffs, lapilli and pillow breccias at obducted seamounts of similar (estimated) size in the Masirah island ophiolite (Oman) also concluding on explosive eruptions during formation of these cones. In contrast, a remnant

3.5. DISCUSSION

seamount in the Troodos ophiolite (Cyprus) consists of pillow lavas and lava tubes, which is flat but still close to the lower limit of the H/W ratios observed in this study (Eddy et al., 1998). However, it is part of a much more complex and wider tectono-magmatic system (including a caldera) and is subaerially exposed since upper Miocene (Robertson, 1998). Hence, erosion may have washed away the unconsolidated volcanoclastics leaving an early effusive core of a larger edifice.

Since the H/W ratio displays no dependency on the water depth below 300-400 m (Fig. 3.9b), the process of cone formation is assumed not to be controlled by depth or ambient water pressure, respectively. These analogies in the topographic characteristics indicate that there is only one common eruption mechanism driving the genesis of the cones. This is in accordance with other studies conducted in the Azores (Stretch et al., 2006; Mitchell et al., 2012b; Tempera et al., 2013; Casalbore et al., 2015), where the same deduction for submarine volcanic cones southeast of Pico, west of Faial and in the vicinity of Terceira Island is drawn, based on bathymetric and side-scan data.

In shallow waters of less than 300-400 m the upper limit of the H/W ratio slightly decreases to a maximal value of 0.21 at 120 m (Fig. 3.9b) indicating a trend to flatter structures. Corresponding observations at shallow cones in the Pico and Terceira region has also been described by Mitchell et al. (2012b) and Casalbore et al. (2015), respectively. Following Cashman and Fiske (1991), the reduced height is interpreted as the result of eruption columns, which spread along the close sea surface boundary leading to a wider area influenced by volcanic fallout. Therefore, the eruption mechanism in the shallow domain is the same as in deeper waters, but the cone shape is affected by a direct interaction of corresponding submarine explosive eruptions and the water surface. Such eruptions likely produce emissions into the air above the water level, so the inflection point of the upper H/W ratio in depth can be considered as the regional critical water depth above which submarine eruptions pose a hazard potential to people and environment above the sea level (Hübscher et al., 2015). However, this critical water depth is a rough estimation only, since the time of the eruptions and, therefore, the associated sea levels are unknown.

Cones with a diameter of ≤ 500 m do not follow an exponential size distribution (Fig. 3.8c, inset), which indicates that there is an additional factor affecting the evolution of small cones. One explanation could be that there is a critical volume of melt needed to be able to reach the seafloor and erupt. Since resolution of our bathymetric data is high enough, an underestimation of these cones appears to be unlikely (Smith, 1996).

In summary, the cones described in this study resemble the cones that have been measured in other regions of the Azores in height and diameter (Stretch et al., 2006; Mitchell et al., 2012b; Tempera et al., 2013; Casalbore et al., 2015). Hence, the measured dimension seems to be

typical for the Azores Plateau, but has also been reported e.g. from the slow spreading Reykjanes Ridge north and the slow spreading Mid-Atlantic-Ridge at 24°-30°N south of the Azores domain (Magde and Smith, 1995; Smith et al., 1995a/b), the Puna Ridge, Hawaii (Smith and Cann, 1999) as well as in the Mediterranean near Santorini/Aegean Sea (Nomikou et al., 2012).

In comparison with the submarine structures, cones onshore São Miguel Island are smaller and show slightly lower slope angles (Fig. 3.9a). This is relevant to observations on- and offshore Pico (Stretch et al., 2006) and is probably caused by a higher erosion rate in the subaerial domain. But due to the general similarities, we consider the offshore cones to be the submarine equivalent of the onshore cinder cones, which are a typical result of monogenetic alkali-basaltic volcanism on São Miguel Island (Wood, 1980; Moore, 1990; More and Rubin, 1991; Schmincke, 2004).

Finally, the question may rise up why less than 4% of the cones show a noticeable crater although they are interpreted as structures with an explosive origin. Possible explanations could be that either the craters in deep water are commonly below resolution as mentioned above, that former craters have been filled up by late eruptive and younger sediments or that the crater rims are often unstable and tend to collapse after the eruption cycle has ended (Chadwick et al., 2008; Hübscher et al., 2015).

3.5.2. Backscatter facies of young and old cones

It is commonly assumed that a smooth or rough texture of submarine lava flows is a relative marker for high or low eruption rates, respectively (e.g. Griffiths and Fink, 1992; Gregg and Fink, 1995; Batiza and White, 2000). According to studies at the Mid-Atlantic-Ridge (Magde and Smith, 1995; Smith et al., 1995a), Stretch et al. (2006) therefore correlated the surface characteristics of the submarine cones near Pico Island with the corresponding magma supply. Hence, the predominance of smooth cones in the Pico area accounts for the hypothesized magma upwelling in the Azores domain. On the contrary, the rough cones (in that study described as hummocky) are supposed to be caused by different eruption styles, lower eruption rates and/or effusive like pillow lavas. Therefore, their reported larger size may result from subsequent lower feeding rate eruptions of primary smooth cones, reflecting a variability of the eruption rate over time. But in contrast to these authors, our measurements did not reveal a majority of smooth cones. Therefore, the increased number of rough cones suggests a minor magma supply in the southeastern Terceira Rift compared with the Pico area. However, the observation of rough cones being systematically larger than smooth cones was not confirmed in this study. Since the cones do not show a difference in the topographic features in general and particularly in size, e.g. a higher content of effusive appears to be more unlikely. Indeed, lobe like features in the foot region of a few cones (e.g. inset of Fig. 3.5d) indicate effusive eruption

3.5. DISCUSSION

phases in between, but we propose the interpretation that the different surface textures do not reflect diversity in the eruption mechanisms.

Due to the following evidence, we rather suggest that a smooth cone corresponds to a young one, whereas matured cones are characterized by a rough surface. (1) All verifiably extinct volcanic cones reveal a dark backscatter facies (as indicated by overlapping sediments on the cone flanks in the Monaco Graben, Fig. 3.3). (2) The seismically covered cone at the southwestern slope of Sete Cidades is both smooth and young, since it onlaps the slope sediments (Figs. 3.5b/3.6). (3) Both smooth and rough cones occur together. The vicinity of recent and long-time extinct structures seems to be more likely than different volcanic mechanisms forming the same kind of topographic structures. (4) The seismic data shows no difference in reflection pattern between cones with the two types of surface. A change in reflection pattern (e.g. resolution of internal structures and transparency) is occasionally dependent on the profile orientation only (e.g. Fig. 3.6a/c) and can be observed at both smooth and rough cones.

Following this assumption, winnowing as observed by Kokelaar and Durant (1983) is a possible explanation for the increased slope roughness of matured cones. Current controlled sedimentation structures, such as moats (Fig. 3.3b) and sediment waves (Fig. 3.3c) e.g. in the Monaco Graben suggest the presence of bottom currents, which may remove the fine grain content of the volcanoclastic sediments exposing bare rocks and effusive over time.

3.5.3. Submarine volcanic domains

Submarine volcanism producing the described cones clusters in three different domains (Fig. 3.2), each of them reflecting a specific mechanism of magma supply.

A first category of cones is located on top of faults that represent magma migration pathways (Figs. 3.3 and 3.4). Hence, volcanism is most likely controlled by regional tectonics. An example is the Monaco Graben, where the evolution of the volcanic cones is assigned with the graben formation (Chapter 2, Fig. 3.3). However, since graben formation and seismicity ceased, no recent volcanism is observable here.

The second category of cones is distributed on top of the submarine slopes of Sete Cidades Volcano and the Fogo Volcano Complex (Fig. 3.5). Their existence is interpreted as being linked to magmatic processes of the main volcanic bodies and as parasitic structures, respectively. Both dike and fissure related secondary magmatism are probably feeding the submarine cones. Elsewhere, lava tubes or channels have been described feeding submarine effusive eruptions from e.g. onshore magma sources (Smith and Cann, 1999). But since low viscous and degassed magma is necessary for their evolution, it is implausible to assume tubes etc. feeding explosive

structures. The absence of these kinds of lava flows is also in agreement with the lack of tumuli structures as observed e.g. around the shelf of Pico (Mitchell et al., 2008).

Finally, a high concentration of cones is found on top of East-Formigas High (Fig. 3.7). Isolated from subaerial volcanism and not controlled by faults they superimpose a huge magmatic underwater body, which might represent a juvenile formation phase of a subaqueous seamount ultimately resulting in a new volcanic island. Therefore, the magma source of the cones is associated with the growth of the main body. But in contrast to parasitic volcanism, the cones do not represent a secondary feature of a major subaerial volcano as already mentioned. However, it remains unclear if a major volcano will develop later on in the case of subaerial exposure and – as a consequence - if the distributed explosive volcanism is caused e.g. by the enhanced cooling of the surrounding water. An increased seismicity in this region (Chapter 2) is most likely reflecting both tectonic processes and magma ascent.

3.5.4. Pyroclastic deep sea volcanism

For a long time, explosive eruptions in the deep sea have been assumed to be unlikely, since the high ambient pressure hampers the dissolution of gas in the magma (e.g. Schmincke, 2004). However, in recent years several studies have been published describing explosion deposits or observations of active pyroclastic activity in maximum water depths of 4000 m (e.g. Davis and Clague, 2006; Sohn et al., 2008; Rubin et al., 2012 and references therein). We therefore contribute to this discussion since the deepest mapped volcanic cone is located at the seafloor in a water depth of 3200 m. Indeed its explosive origin is deduced by its topographic characteristics only. But again, comparing the cones in the submarine domain of Sete Cidades Volcano distributed in water depths of 400 m to 3000 m, no change in their characteristics is traceable that would indicate different eruption mechanisms (Fig. 3.5a). In any case, the deepest cone with a noticeable crater is located in a water depth of ca. 1000 m (marked with a white arrow in Fig. 3.3c/d).

Deep sea explosive volcanism is usually associated with the exsolution of carbon dioxide (e.g. White et al., 2015). A more detailed explanation was given by Hekinian et al. (2000), who investigated volcanic cones of similar size on the Mid-Atlantic Ridge culminating at depths of 1500 m to 1900 m. There, explosive eruptions were suggested to have been driven by the superposed effect of magma degassing, first of the carbon dioxide then of the water content. Since a high volatile content in the Azores magma is described by e.g. Bonatti (1990) and Beier et al. (2012), this mechanism may also be responsible for explosive eruptions in a water depth of >3000 m as postulated in this study. Therefore, deepest explosive structures or deposits in a volcanic setting could generally represent a marker of the volatile content of the corresponding magma source. As an alternative, seawater could be trapped within the cones and vaporized during pulsating magma ascents (Hekinian et al., 2000).

3.6. Conclusion

252 submarine volcanic cones have been mapped in the submarine domain of the southeastern Terceira Rift. They reveal an average size of (743 ± 405) m in width and (139 ± 77) m in height correlating with slope angles of $(20\pm 4)^\circ$. They are distributed in water depths of 120 m to 3200 m. Based on a combined morphological and seismic interpretation, all of them are associated with explosive eruptions. Since the cones resemble monogenetic alkali-basaltic cinder cones onshore São Miguel in their topographic appearance, they are assumed to be their submarine equivalent with comparable eruption histories.

Backscatter data shows both a smooth and a rough surface texture, which we expect to be a marker for young or long-time extinguished cones. Currents erode the finer grain-size fraction, so the older the cones are the rougher they become.

The majority of cones can be assigned with one of the following volcanic settings: (1) Fault controlled volcanism, where fault planes provide pathways for ascent of magma; (2) parasitic volcanism, where the cones are secondary features of a major subaerial volcanic system; and (3) constructive volcanism, where the cones superimpose a huge submarine volcanic body possibly reflecting a kind of proto-island.

Acknowledgments

We sincerely thank Captain Thomas Wunderlich and his outstanding crew of *RV Meteor* for their support during the M79/2 cruise. We are grateful for the financial support of the German Research Foundation (DFG, grant Hu698/19-1). Additional acknowledgements go to the companies Halliburton-Landmark and Schlumberger for providing university grant's for the seismic processing software ProMAX and seismic interpretation software Petrel, respectively, as well as to the NASA's Earth Science Data Systems program for providing the ASTER Global DEM data. Finally, we want to thank P. Nomikou and N.C. Mitchell for reviewing the manuscript. Their suggestions helped a lot to improve this publication.

4. Submarine sedimentation processes in the southeastern Terceira Rift

Abstract

Most case studies dealing with the evolution of volcanic islands concentrate on the easily accessible onshore domain and neglect the interplay of constructional and destructive processes in the offshore domain. Combining bathymetric and multi-channel seismic data recorded during the RV Meteor cruise M79/2, this study focuses on the impact of volcanism, erosion, tectonics, time-variant sediment support and climatic/oceanographic conditions on the submarine sedimentation processes in the southeastern Terceira Rift - a succession of deep rift basins, volcanic bathymetric highs and islands (e.g. São Miguel) along the westernmost part of the Eurasian-Nubian plate boundary. The shelf of São Miguel Island (shelf break at ~140 m) was formed by erosion during the Last Glacial Maximum and has been subsided by approximately 0.6 mm/a. While the western island slope below the shelf is characterized by submarine volcanism, the northern slope is affected by unconfined density currents most likely induced by North-Atlantic storm swell along the entire shelf (line source). The resulting lobe deposits are incised by a widespread system of channels. At the upper slope, the channels merge with retrograde canyons and gullies, which drain the terrestrial sediment load (point source). In contrast, turbidity currents at the southern slope are caused by a uniform coastal erosion and fluvial sediment flux generating cyclic steps, chutes-and-pools and turbidity lobes. These turbidity currents follow morphological features and enter the sedimentary basins via gateways. Fine grained sediments and volcanic fall-out are transported or re-mobilized by ocean currents. Currents are controlled/deviated by volcanic bathymetric highs or fault scarps where they cause the deposition of drift bodies. High local accumulations of sediments caused by a channelized sediment flux, bottom currents or onshore volcanism are partly remobilized resulting in slumping/slide events and a volcanic ridge partly collapsed due to tectonic stress and/or gravity spreading.

4.1. Introduction

Having a look at major volcanic islands from above the sea level, they often provide an imposing view due to their massive shape, their volcanic features and their erosional structures caused by e.g. local tectonics, waves and weather conditions. In the Azores Archipelago, this interplay of constructive (volcanic) and destructive (erosional) processes is well analyzed in the onshore (e.g. Costa et al., 2015; Hildenbrand et al., 2012a/b; Sibrant et al., 2014, 2015a) but only locally documented in the offshore domain (Costa et al., 2014, 2015; Mitchell et al., 2012a, Sibrant et al., 2015b).

However, the main bodies of these islands are located below the sea surface. So, much of the interaction of construction and destruction occurs on the shelf close to the water surface and below (e.g. Casalbore et al., 2015; Quartau et al., 2014) without being overprinted by vegetation or weather effects. Hence, bathymetric data plays a major role in understanding the submarine evolution of islands, in particular where the original magmatic strata crops out. Where it is covered by sediments, multi-channels seismic data allows the widespread analysis of the island's evolution as far as stored in the sedimentary record. For example, what is the evolutionary history of the shelf and the submarine island slope? What are the shelf - deep sea transportation mechanisms? How are these mechanisms influenced by weather and onshore erosional conditions? How do faulting and associated fault scarps affect bottom currents and sedimentation pathways? Is sedimentation influenced by bottom currents and how are those currents affected by the rise of volcanic lineaments? Did tectonic events trigger mass wastings? In this context, our study aims for an overview of the prevalent submarine sedimentation processes and a deeper insight of the interaction of volcanism, tectonics, time-variant sediment support and locally defined sediment accumulation at the southeastern Terceira Rift.

The Terceira Rift is located in the North-Atlantic Ocean roughly 1500 km west of continental Portugal at the westernmost tip of the Eurasian-Nubian plate boundary (Fig. 4.1). Here, strong rifting related volcanism led to the formation of several volcanic ridges and bathymetrical highs (Chapter 2; Cannat et al., 1999; Gente et al., 2003; Luis et al., 1998) with São Miguel Island being the subaerial exposed part of one these highs.

Based on a combined analysis of a hydroacoustic and high resolution multi-channel seismic data set, we mapped the location and depth of the São Miguel Island shelf. Below the shelf edge, the morphology of the upper island slope significantly varies from east to west, whereas the lower slope is characterized by a north-south contrast. We will focus on these variations and discuss the associated processes during formation and erosion of the submarine domain of São Miguel. Over time, large successions of sediments were deposited within the basins southwest

4.1. INTRODUCTION

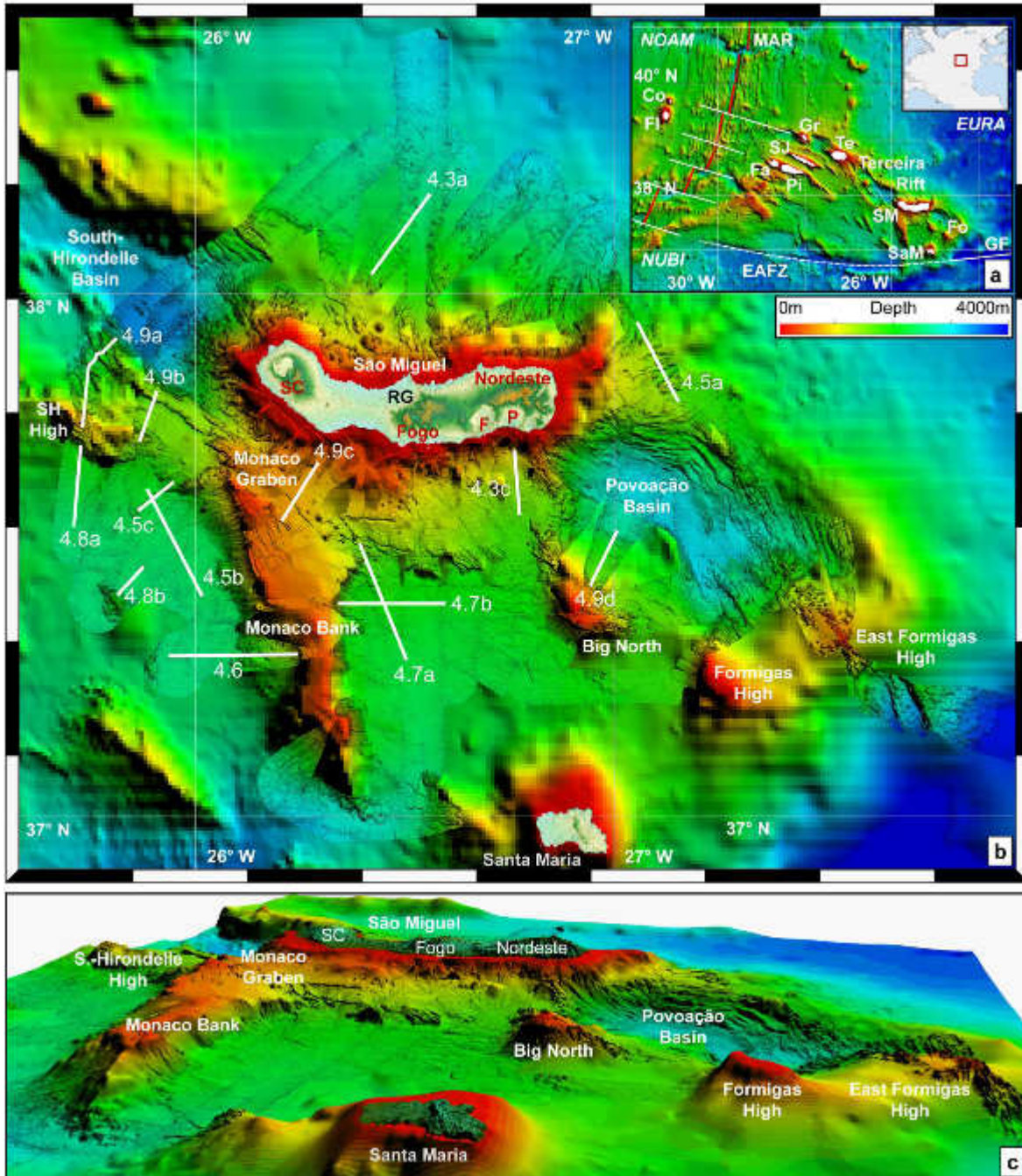


Fig. 4.1: Working area and corresponding structures. Azores Archipelago (a), southeastern Terceira Rift (b) and 3D view of the working area (c). White lines in (b) represent seismic lines shown in this study, corresponding numbers indicate figure numbers. Islands: Corvo (Co), Faial (Fa), Flores (Fl), Formigas Islets (Fo), Graciosa (Gr), Santa Maria (SaM), São Jorge (SJ), São Miguel (SM), Pico (Pi), Terceira (Te); EAFZ: East Azores Fracture Zone; GF: Gloria Fault; MAR: Mid-Atlantic Ridge; NOAM: North-American Plate; EURA: Eurasian Plate; NUBI: Nubian Plate; SH High: South-Hirondelle High. Onshore structures: RG: Ribera Grande Graben; Sete Cidades (SC), Furnas Caldera (F), Povoação Depression (P). Background bathymetric data from Lourenço et al. (1998) and ETOPO1 (Amante and Eakins, 2009). Topographic data is from ASTER GDEM. Structural features after Luis et al. (1994). Illumination from N45° with an altitude of 60°.

and south of the island. Sedimentation occurred while being influenced by oceanic currents, volcanism and tectonic movements, whose consequences will be finally described, interpreted and discussed.

4.2. Geological context

4.2.1. Azores Plateau & Terceira Rift

The Terceira Rift consists of a succession of rift basins, bathymetric highs and volcanic islands, which are – from west to east – Graciosa, Terceira and São Miguel (Fig. 4.1). It links the Gloria Fault (GF) in the east with the Mid-Atlantic Ridge (MAR) where the North American, Nubian and Eurasian plates meet at the diffuse Azores Triple Junction (Marques et al., 2013, 2014a; Miranda et al., 2014). The Terceira Rift defines the northeastern boundary of the Azores Plateau, an abnormal shallow area within the North-Atlantic roughly defined by the 2000 m contour line. To the south, the plateau is bounded by the East Azores Fracture Zone (EAFZ) representing the fossil trace of the GF on the Nubian Plate (Krause and Watkins, 1970; Luis and Miranda, 2008; McKenzie, 1972; Searle, 1980). Synchronous to the final welding of Iberia and Eurasia between at 33-20 Ma (Luis and Miranda, 2008; Srivastava et al., 1990), the Nubian-Eurasian plate boundary moved from this former to the present-day location (Gente et al., 2003; Luis and Miranda, 2008). The realignment of the triple junction involved the accretion of large volumes of magmatic in- and extrusions as well as underplated material (Cannat et al., 1999; Gente et al., 2003; Luis et al., 1998), which finally led to the creation of thickened crust and the Azores Plateau itself (Dias et al., 2007; Georgen and Sankar, 2010; Luis and Neves, 2006; Silveira et al., 2010).

The driving mechanism initiating the northward movement of the triple junction is not definitely identified yet. Interpretations of bathymetric/morphologic (Lourenço et al., 1998; Navarro et al., 2009; Neves et al., 2013), magnetic (Luis and Miranda, 2008), seismological (Miranda et al., 1998) and multi-channel seismic data (Chapter 2) favour a strong association with a rigid response of the lithosphere to changes in plate kinematics, like the readjustment of plate boundaries in the Iberian domain. The strong volcanism of the Azores is stated to be caused by an enriched volatile content in the upper mantle (Asimow et al., 2004; Bonatti et al., 1990; Métrich et al., 2014). However, geochemical data also indicate an interaction of a hotspot with the MAR (e.g. Bourdon et al., 2005; Schilling, 1975; White and Schilling, 1978), which might have initiated the jump of the plate boundary and the increased volcanism. This is supported by the observation of an elevated MAR axis (e.g. Escartín et al., 2001; Schilling, 1985; Thibaud et al., 1998) and seismic velocity anomalies in the Azores region (e.g. Montelli et al., 2006; Silveira et al., 2006, 2010; Yang et al., 2006).

4.2. GEOLOGICAL CONTEXT

4.2.2. Southeastern Terceira Rift & São Miguel region

Volcanism in the São Miguel region is discussed to be strongly controlled by tectonic stress (Haase and Beier, 2003), in particular in relation of the volcanoes' location on top of a more discrete or highly fractured lithosphere (Sibrant et al., 2015b), the latter one possibly reflecting a leaky transform (Chapter 2). The Terceira Rift originally started to develop in a SW-NE extensional setting, before direction changed to WSW-ENE at ~10 Ma (Luis and Miranda, 2008). The first extensional regime is reflected by the main trend of the rift system between Terceira Island and the Formigas region (Chapter 2). After the stress field changed, the formation of Monaco Bank occurred orthogonally to the extensional direction and it was volcanically active at least until 5.9 Ma (Beier et al., 2015). Afterwards, Monaco Graben separating Monaco Bank and present-day São Miguel Island was rifted (Chapter 2). It is still remaining unclear at which time the submarine formation of which part of the island body started. However, reliable ages of maximum 0.8 - 0.9 Ma from onshore São Miguel Island (Sibrant et al., 2015b; Johnson et al., 1998) verify that the subaerial evolution of the island started at or before that time.

São Miguel Island consists of 6 subaerial volcanic units (Fig. 4.1), which are from west to east: (1) the active trachytic stratovolcano of Sete Cidades, (2) a field of alkali-basaltic cinder cones and lava flows (western Waist Zone), (3) the active trachytic stratovolcano of Fogo, (4) another field of alkali-basaltic cinder cones and lava flows (eastern Waist Zone), (5) the active trachytic stratovolcano of Furnas Caldera, and (6) the inactive basaltic shield volcano of Nordeste including the Povoação Depression (Moore, 1990; Sibrant et al. 2015b, and references therein).

The Nordeste Complex represents the oldest part of the island, which has been affected by a large flank collapse towards the south 750 – 500 ka ago (Sibrant et al., 2015b). The resulting scar was partly filled by south dipping lava flows with ages of 500 – 250 ka and massive pyroclastic units of Furnas Volcano, which were deposited between 140 ka and the present (Moore, 1990). The remnant scar of the Nordeste flank collapse and several caldera collapses during the formation history of the Furnas Volcano (Guest et al., 1999; Montesinos et al., 1999) predominantly define the present-day Povoação Depression and Furnas Caldera (Fig. 4.1). Further to the west, Fogo Volcano (also called Agua de Pau) and its caldera (two collapses at 46 and 15 ka; Moore, 1990) shapes the central part of São Miguel Island. Age constraints indicate that the major formation phase of this volcano initiated at least at 200 - 270 ka (Moore 1990; Sibrant et al., 2015b) and ended at about 100 ka (Muecke et al., 1974). Hundreds of meters thick pyroclastic deposits almost exclusively form the southern flank and reflect the explosive eruption history of Fogo. In contrast, at the northern flank thick lava flows are still observable possibly indicating a major sector collapse and/or blast event (and subsequent pyroclastic flows) towards the south (Sibrant et al., 2015b). Sete Cidades Volcano represents the western end of the island. A recent study of Sibrant et al. (2015b) suggests Sete Cidades as the youngest

stratovolcano of São Miguel island since their samples show a maximum age of 91 ka (older ones propose ages of more than 210 ka; e.g. Moore, 1990). It is composed of successions of mafic lava flows as well as pumice, pyroclastic flow and surge deposits (Moore, 1990), whereas the submarine slope (similar to those of Fogo Volcano) is covered by many volcanic cones (Chapter 3). The major formation phase of Sete Cidades Volcano ended at 64 ka when the first of four caldera collapse occurred (Queiroz et al., 2008; Sibrant et al., 2015b).

4.3. Data and methods

This work is based on high resolution bathymetric data and a 2D multi-channel seismic data set collected by University of Hamburg scientists on board of *RV METEOR* during cruise M79/2 in 2009 (Hübscher, 2013). The seismic data set consists of profile lines with a total length of 1000 km spread around São Miguel Island (see Fig. 4.1 for location of profiles shown in this chapter). The seismic signals were generated by two clustered GI-Guns with a generator volume of 45 cubic inch and an injector volume of 105 cubic inch each. For data recording a 600 m long asymmetric digital streamer was used containing 144 channels with an average spacing of 4.2 m. Shots were released every 25 m at a speed of 5 kn. Data processing first encompassed trace editing and CMP sorting with a CMP increment of 5 m (e.g. Hübscher and Gohl, 2014). Subsequently, several bandpasses with 10/20 – 300/400 Hz, a spike & noise burst filter, FX-deconvolution and FK-filter were applied before NMO-correction and post stack time migration. Owing to the relatively small offset to target ratio reliable interval velocities could not be derived and, as a consequence, sediment thicknesses are given in milliseconds [ms] throughout the text. Assuming interval velocities of 2000 m/s within the sedimentary units, milliseconds are equivalent to meters.

High resolution bathymetric data were synchronously recorded using the hull mounted Kongsberg EM710 and EM120 Multibeam echosounders installed on board of *RV METEOR*. During processing, navigation errors were interpolated and depths/positions were recomputed using revised sound velocity profiles. After beam editing was applied for every single swath to eliminate spikes and noisy data, the data was gridded with a spacing of 30 x 30 m. However, since the acoustic footprint is equal to ~2% of water depth, effective resolution in water depth higher than 1300 m is less. Additionally, bathymetry in Fig. 4.3c encompasses new high-resolution bathymetric data, which was recorded by a Kongsberg EM122 Multibeam system on *RV METEOR* during a cruise in early 2015 (grid node spacing of 50 x 50 m). The background bathymetric maps were created from data of a 1 x 1 km grid presented by Lourenço et al. (1998), which can be found under http://w3.ualg.pt/~jluis/acoress_plateau.htm, and ETOPO1 data (~1.9 x 1.9 km) published by Amante and Eakins (2009). The onshore topographic data shown is originated from ASTER GDEM, which is a product of METI and NASA. It contains a 1 arc-second

4.3. DATA AND METHODS

(30 m) grid of elevation postings. For visualization purposes the different data sets have been imported to an *ArcGIS 9.3* system. Measurements of e.g. slope angles, depths, lengths and heights were done using the program *FLEDERMAUS* (© by QPS). For surveying the shelf edge, the edge was assumed to be the area between the gently dipping shelf plateau and the island slope where the seafloor shows its maximum change in slope angle.

The surface/bottom ocean circulation presented in Chapter 4.3 is based on the daily output from an eddy-resolving numerical simulation over the period 2003-2011 obtained with the MIT general circulation model (MITgcm) code (Marshall et al., 1997). The model domain encloses the entire Atlantic Ocean north of 33°S (including the Mediterranean Sea and the Nordic Seas) and the Arctic Ocean. The horizontal resolution is about 4 km and the vertical resolution varies from 5 m in the upper 200 m to 275 m in the deep ocean (in total, 100 vertical levels). The model bottom topography was interpolated from the Smith and Sandwell (1997) 2-minute resolution topography database and the initial stratification (temperature and salinity) from the January 2003 state of an 8-km resolution integration of the same model since 1948, in turn initialized with the World Ocean Climatology 2005 (Boyer et al., 2005). The simulated ocean was forced at the surface by fluxes of momentum, heat and freshwater computed using bulk formulae and the 6-hourly atmospheric state from the ECMWF/ERA-interim reanalysis (Dee et al., 2011). The lateral forcing at 33°S and at the Bering Strait was interpolated from a previous coarse-resolution global integration using the MITgcm. Vertical mixing was parameterized by the KPP formulation, including a background vertical viscosity coefficient of $1 \times 10^{-4} \text{ m}^2 \text{ s}^{-1}$. Horizontally, unresolved mixing was parameterized with a biharmonic operator using a background coefficient of horizontal viscosity of $3 \times 10^9 \text{ m}^4 \text{ s}^{-1}$. The model further includes a dynamic-thermodynamic sea ice model and has an annually-averaged river run-off derived from Fekete (1999) imposed, by adding a corresponding freshwater flux to the precipitation-minus-evaporation term at grid points adjacent to river mouths. More details of the Atlantic-Arctic model configuration and respective validation can be found, e.g., in Serra et al. (2010).

4.4. Submarine sedimentation processes: results and implications

4.4.1 Shelf and slope morphology of São Miguel Island and associated sedimentation processes:

4.4.1.1. Observations

The island shelf of São Miguel is poorly covered by high resolution bathymetric data. Nevertheless, the shelf was passed several times, which allowed us to identify the shelf edge at

4. SUBMARINE SEDIMENTATION PROCESSES IN THE SOUTHEASTERN TERCEIRA RIFT

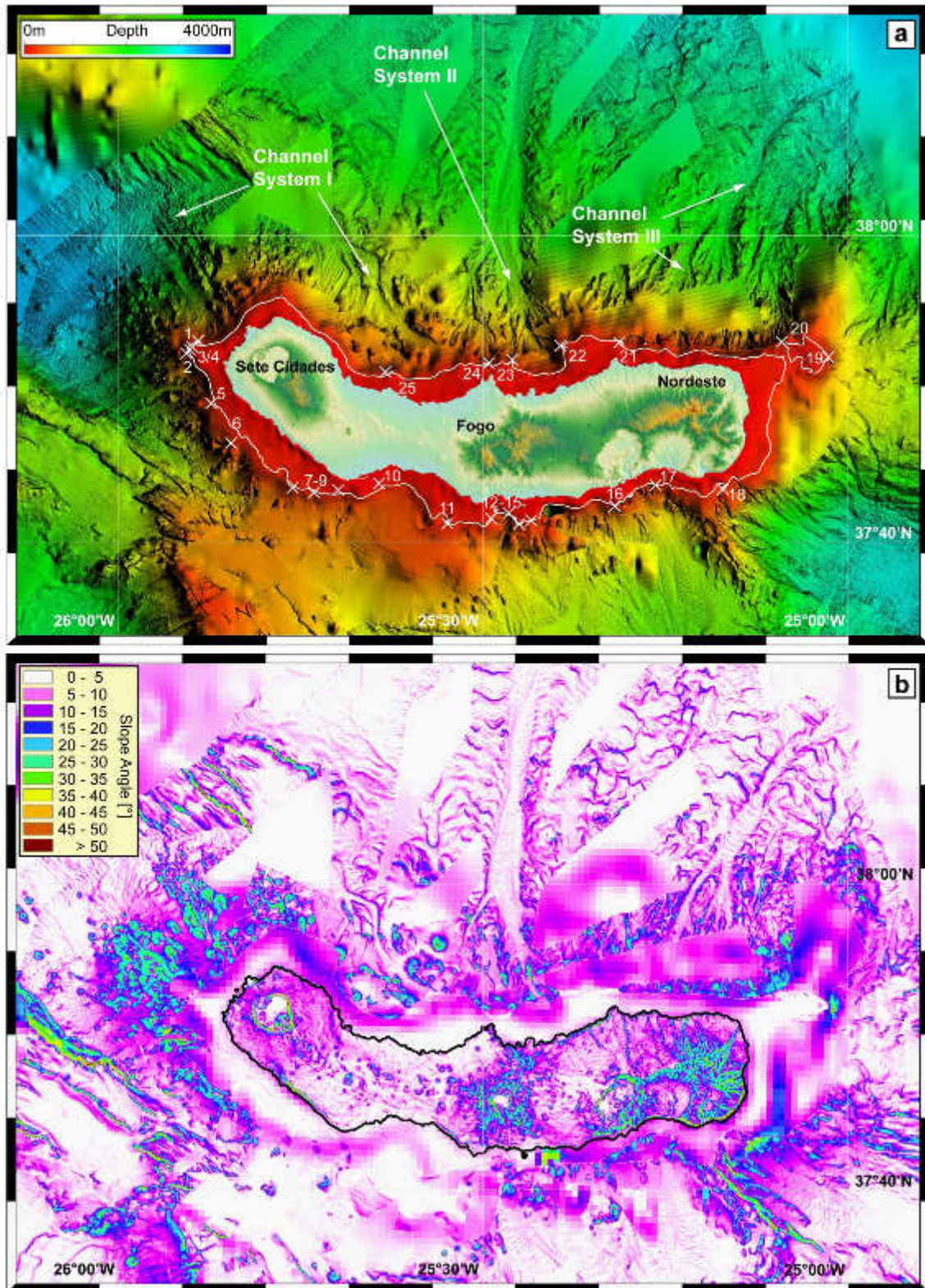


Fig. 4.2: High-resolution bathymetry (a) and slope map (b) in the vicinity of São Miguel Island. The northern slope of the island is characterized by a wavy seafloor expression intersected by three channel systems. White line in (a) indicates the 140 m depth contour reflecting the average depth of the outer shelf edge. White crosses mark the picked shelf edge (based on the high-resolution bathymetry). Illumination is from N90° with an altitude of 60° (a).

4.4. SUBMARINE SEDIMENTATION PROCESSES: RESULTS & IMPLICATIONS

Pick ID	Latitude [°]	Longitude [°]	Depth [m]	Distance to Coast [m]
1	-25,89045	37,88518056	140	5300
2	-25,90668333	37,87160556	180	6000
3	-25,90185833	37,87565833	68	5700
4	-25,89824722	37,87852222	67	5500
5	-25,872725	37,81732222	180	3700
6	-25,84509444	37,77414167	190	5900
7	-25,78069722	37,72534444	150	5200
8	-25,73147778	37,72021667	160	3600
9	-25,698475	37,72287222	75	1300
10	-25,64259722	37,73033333	65	1400
11	-25,54878056	37,68659722	140	4400
12	-25,48878889	37,69187222	130	2300
13	-25,46473333	37,69753333	60	1900
14	-25,45078333	37,68587778	120	3300
15	-25,43369722	37,68984722	120	2800
16	-25,31900556	37,70558889	120	2300
17	-25,26368056	37,72833333	140	1750
18	-25,17093611	37,72355833	150	2400
19	-25,02636667	37,86744444	150	13900
20	-25,09063056	37,88393611	150	8200
21	-25,31327222	37,88311389	100	3000
22	-25,39402778	37,87977778	160	6200
23	-25,45987222	37,86467222	110	4000
24	-25,49166944	37,86115833	100	2300
25	-25,63381389	37,85149444	150	2400
		Ø [100 ≤ Depth ≤ 190]	141,5	4447,5

Tab. 4.1: IDs, locations, water depths and coastal distances of shelf edge picks. See also Fig. 4.2a. Note that given averages are based on picks characterized by a water depth of ≥ 100 m only.

25 locations around the island (Fig 4.2a). Detailed locations, depth and distances to the coast are given in Tab. 4.1. Water depth of the shelf edge around the island ranges from 100 m to 180 m leading to an average depth of approximately 140 m. The shelf edge is deepest southwest of Sete Cidades Volcano (picks 1, 2, 5 – 8 in Tab. 4.1). The distances to the coast line ranges from 1,750 m (17) south of Nordeste to 13,900 m (19) east of Nordeste, whereas the average shelf width is $\sim 4,500$ m. Additionally, east of Sete Cidades (3, 4) and along the southern island shelf (9, 10, 13) terraces in a depth of 60 to 75 m are detectable.

4. SUBMARINE SEDIMENTATION PROCESSES IN THE SOUTHEASTERN TERCEIRA RIFT

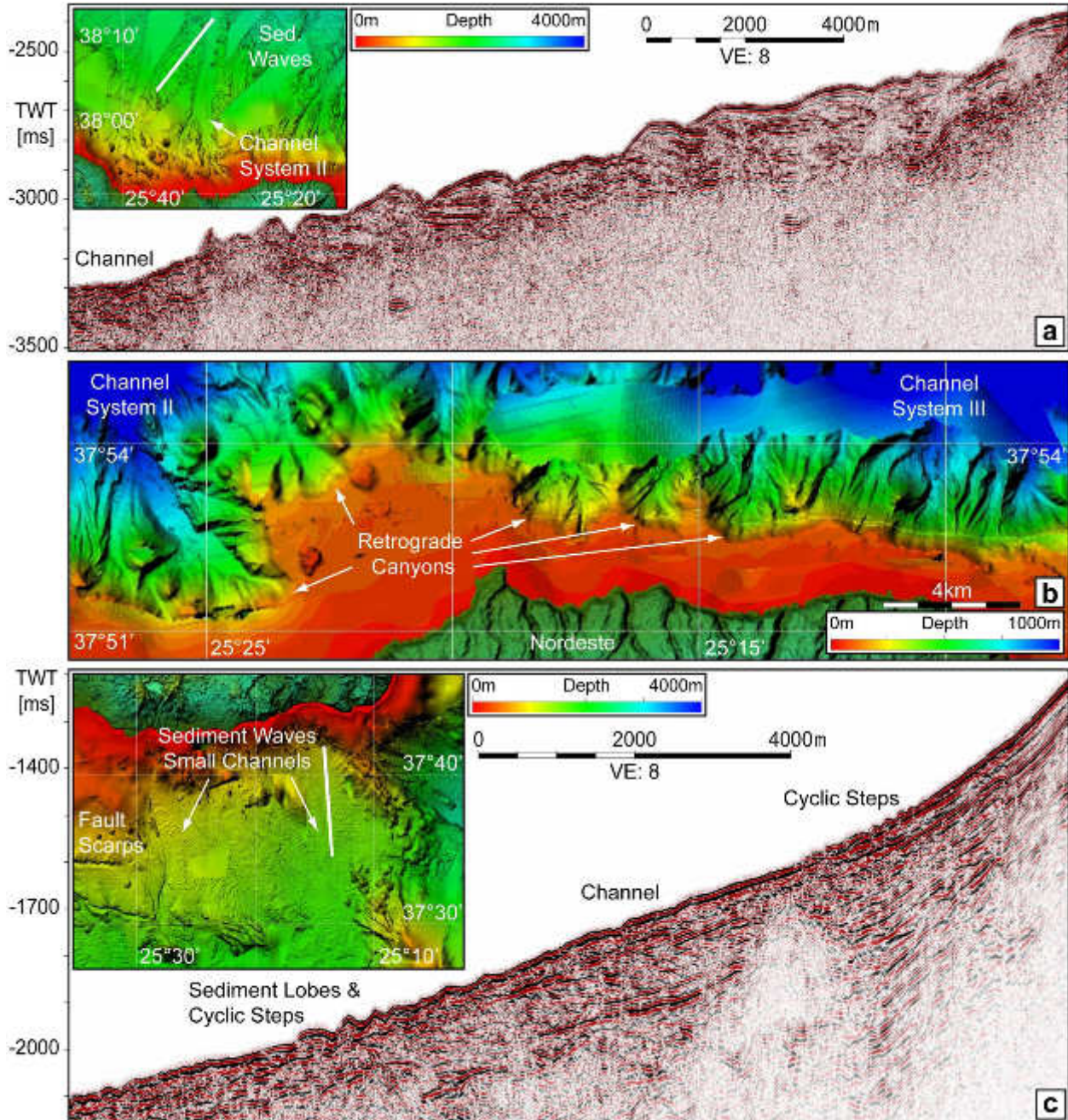


Fig. 4.3: Sediment waves and northern São Miguel Island shelf. Sediment waves at the northern lower slope are 1000 – 4000 m in size and show clear internal stratification (a). The upper northern slope is characterized by canyons and gullies, which pass into three major channel systems (b). At the southern lower slope, in contrast, sediment waves are a few meters in height only and internal stratification is hardly resolvable (c). VE: Vertical exaggeration. Illumination is from N315° with an altitude of 60°.

4.4. SUBMARINE SEDIMENTATION PROCESSES: RESULTS & IMPLICATIONS

The morphology of the slope of São Miguel – where covered by high resolution bathymetry – clearly varies around the island (Fig. 4.2a). In the west, the submarine domain of Sete Cidades Volcano is characterized by slope angles of 10-20° covered by many submarine volcanic cones.

The proximal gradients off the northern coast decrease eastward to 5-15°. Submarine volcanism become less prominent and several canyons crosscut the slope. The submarine morphology of the northern Nordeste Complex is shaped by gullies and canyons revealing maximum slope angles of up to 30° (see also slope map in Fig. 4.2b). Distal of the northern coast, the seafloor is characterized by a strongly undulating topography dissected by three dominant channels systems (Figs. 4.2 and 4.3a/b). The westernmost channel system I initiates northeast of Sete Cidades Volcano below the uniform Sete Cidades Shelf (Fig. 4.2a), follows first a northwestern then a southwestern direction, and terminates within the South-Hirondelle Basin. Channel system II and III initiate north of Fogo Volcano and the Nordeste Complex in the foot region of canyons deeply incised into the slope (Fig. 4.3b), follow a northward direction (Fig. 4.2) and end up in the deep sea (not covered by our data). Dimension of the sediment waves (or hummocks) are 1000-4000 m in wavelength (increasing with water depth) and a few tens of meters to 100 m maximum in height. They reveal an internal stratification, which is well resolved by our seismic data (Fig. 4.3a). Seismic data show a succession of sediments with a maximum thickness of 300 ms on top of the acoustic basement. Sediments are characterized by sub-parallel, oblique and lenticular reflection pattern forming overlapping sub-units.

Between the Povoação Depression and Fogo Volcano, the upper southern slope is incised by several canyons partly revealing gradients of up to 50° (Fig. 4.2). Southwest of Fogo, the slope is smooth and normally dips less than 10° involving a platform in a water depth of 300-400 m gently dipping to southwest by $\leq 2^\circ$. Further to the west, gradients increase (10-15°) before reaching the submarine domain of Sete Cidades Volcano, which is again dominated by volcanic cones. In contrast to its northern counterpart, the lower southern slope is defined by low gradients of less than 10°. Here, the seafloor is partly dissected by fault scarps, but apart from that it is characterized by a smooth surface (west) or small channels and sediment waves (east; Figs. 4.2 and 4.3c). Sediment waves with wave length of 100-200 m and a few meters in height group in the transition area where the slope angle decreases from $>5^\circ$ to 2-3° (Figs. 4.2b and 4.3c). More distal, wave length increases to 300-600 m and sediment waves reveal maximum heights of 20 m. Due to the low spatial dimensions of the sediment waves, vertical resolution of the seismic data is too low to image an internal stratification.

4.4.1.2. *Shelf erosion and subsidence at São Miguel Island*

With an average depth of ~140 m, the depth levels of the shelf breaks at São Miguel Island are comparable to those of Pico (Quartau et al., 2015; Mitchell et al., 2008), Terceira (Quartau et al., 2014) and Faial Island (Quartau et al., 2010, 2012) primarily ranging from approximately

60-200 m as well. Most of the picked shelf break locations at São Miguel are close to or even deeper than 123 m (which corresponds to the sea level minimum during the Last Glacial Maximum after Bintanja et al., 2005). Additionally, the main volcanic formation phases of the coastal areas (with the exception of the northeastern coast) lasted at least until 100 ka (Sibrant et al., 2015b and references therein). Following e.g. Quartau et al. (2015), these facts let us conclude that the shelf was formed by erosion during the Last Glacial Maximum. Shallower shelf terraces (picks 3, 4, 9, 10, 13 in Tab. 4.1), on the contrary, most likely evolved during the post-glacial sea level rise (Quartau et al., 2014).

Based on modelled shelf break depths of ca. 130 m for shelf segments at Faial Island which were formed at the Last Glacial Maximum (Quartau et al., 2010), an average subsidence of ~10 m of São Miguel Island during the last postglacial sea level rise (18 ka after Lisiecki et al., 2005) can roughly be estimated and, as a consequence, a maximum long-term subsidence rate of ~0.6 mm/a. This is within the order of subsidence rates known from Terceira and Faial (Quartau et al., 2014 and 2010) but less than the minimum value of 1 mm/a deduced by Muecke et al. (1974), who encountered subaerial volcanic deposits with an age of 690 ka 786 m below the present-day sea level. However, the drilling location is situated within the Ribera Grande Graben (Fig. 4.1) where local extension (e.g. Oliveira et al., 1990) may possibly account for a locally increased subsidence northwest of Fogo Volcano. Subsidence caused by tectonics can also account for the clearly higher depth level of the shelf southwest of Sete Cidades Volcano (picks 2, 5, 6 in Tab. 4.1), since this part of the island is located on top of normal faults associated with extension at the South-Hirondelle Basin (Chapter 2).

The average shelf width of more than 4400 m at São Miguel is comparably high to those values known from Pico (Quartau et al., 2015) and Faial Island (Quartau et al., 2012), where shelf widths of less than 3200 m are reported. The shelf of Terceira Island, in contrast, shows similar high values with a maximum of 6600 m (Quartau et al., 2014). However, since surveying focused on the deep sea and a minimum distance to the coast of 2000 m was maintained due to security reasons, narrow shelf areas are possibly not covered and the picks are not necessarily representative.

4.4.1.3. Evolution of the upper slope

The presence of many volcanic cones (Fig. 4.2) indicate that the submarine slope of Sete Cidades Volcano below the shelf break mainly consists of in situ generated effusiva and volcanoclastics deposited near the angle of repose (see also Chapter 3). Between Sete Cidades and Fogo Volcano, the bathymetric expression of the northern and southern upper slope becomes less affected by submarine volcanic cones and, hence, submarine (explosive) volcanism seems to play a minor role during slope formation. Rather, deposition of eroded material from the shelf and onshore São Miguel most likely is the prevailing slope shaping

4.4. SUBMARINE SEDIMENTATION PROCESSES: RESULTS & IMPLICATIONS

process, which would also be in accordance with the lower slope angles here (Fig. 4.2b). In contrast, the dominance of retrograde canyons and gullies (Fig. 4.3b) and associated steep slopes (Fig. 4.2a) in the Nordeste domain depicts a rocky nature of the shelf break and the upper slope. This change in slope morphology in combination with the almost overall absence of submarine volcanic cones (Figs. 4.2a and 4.3b) imply different kinds of volcanism during the (submarine) formation of Sete Cidades Volcano in the west and the Nordeste Complex in the east. Whereas the evolution of the trachytic Sete Cidades Volcano (e.g. Moore, 1990) involves distinct distributed submarine explosive volcanism (Chapter 3), formation of the Nordeste Complex appears to be predominantly associated with effusive volcanism and lava flow progradation reflecting Nordeste's basaltic nature (Moore, 1990). Hence, changing morphology of the northern upper slope retraces the variation in magma composition from east to west. However, it is unlikely that gullying around the Nordeste shelf reflects the older age of the shelf. Indeed, an overall west/young-east/old trend along the island is existent, but our data shows no variation in upper slope morphology north and south of Nordeste although the northern coast is much older than the southern coast between picks 16 and 18 in Fig. 4.2a (Sibrant et al., 2015b and references therein).

4.4.1.4. *Downslope sedimentation processes off the São Miguel Island shelf*

The obvious morphological discrepancies at the lower slope north and south of the island (Fig. 4.2a) show that sediment support and downslope transport processes must significantly differ on both sides.

In the south of the island and in particular south of the Nordeste Complex, sediment waves directly below the slope break (Fig. 4.3c) are very similar to those observed e.g. by Betzler et al. (2014) at Great Bahama Bank in terms of height, width and their occurrence in trains (these waves are 150-200 m wide and as high as 3 m). In accordance to these authors we interpret them as cyclic steps (e.g. Kostic, 2011), which verifies the presence of downslope turbidity currents fed by coastal erosion processes and the comparative steady sediment load of the rivers draining the Furnas Caldera and the Povoação Depression (Louvat and Allègre, 1998). Further downslope, the increase in wavelength in combination with a more irregular wavelength spectrum possibly indicates a superposition of strong turbidity events related cyclic steps and sediment lobes of weak turbidity currents running out here.

In contrast, sediment waves north of the São Miguel are irregular, much larger in size and since their spatial distribution is independent from the slope break (Fig. 4.2a), it is implausible to associate them with the hydraulic jump effect (e.g. Kostic, 2011). Since internal stratification lacks tilted blocks as well as extensional or compressional features (Fig. 4.3a), sediment waves neither appear to be the result of gravity driven mass transport like e.g. retrograde slumping

4. SUBMARINE SEDIMENTATION PROCESSES IN THE SOUTHEASTERN TERCEIRA RIFT

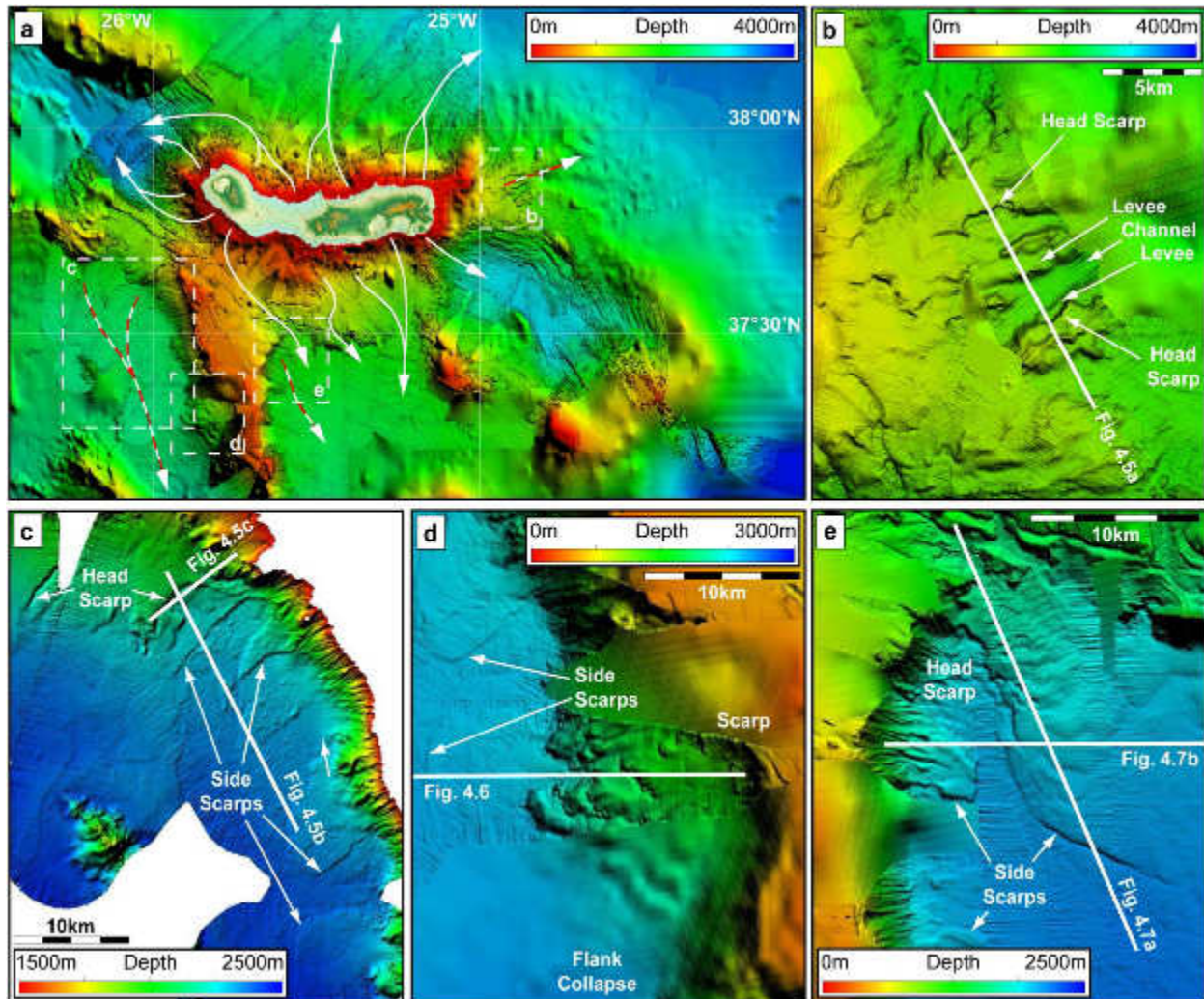


Fig. 4.4: Sediment pathways and mass transport deposits. White arrows indicate main pathway of sediments originated onshore São Miguel, white-red arrows show the direction of mass movements (a). East of the island, sediments were partly remobilized and channel-levee systems developed (b). The bathymetry in the basin southwest of the island reveals several head/side scarps (c) and the deposits of a partial flank collapse of Monaco Bank (d). Head/side scarps are also observable in the southern basin (e). White line show seismic lines presented in Figs. 4.5, 4.6 and 4.7. Illumination from N45° with an altitude of 60° and 30 m grid node spacing (a, b). Revealing a 50 m grid node spacing (c) is illuminated from N315° with an altitude of 45° and (d) from N45° with an altitude of 65°. (e) is illuminated from N15° with an altitude of 55° and reveals a 40 m grid node spacing. Note the different color scales.

(Bull et al., 2009; Mulder and Cochonat, 1996). Hence, we interpret the sediment waves as lobe deposits of unconfined high suspension density currents (e.g. Deptuck et al., 2008; Gervais et al., 2006), which initiate along the northern shelf. Relevant quantities of suspended material are possibly induced by episodic high-energetic long-wavelength swell and their high shallow shelf sediment remobilization and coastal erosion potential creating a line source – in particular during sea level lowstand. Since strong wind events primarily occur in the North-Atlantic

4.4. SUBMARINE SEDIMENTATION PROCESSES: RESULTS & IMPLICATIONS

(e.g. winter storms), the northern shelf and coast of São Miguel is more affected by storm swell than their southern counterparts (e.g. Fan et al., 2014; Woolf et al., 2002; Young, 1999). Channel systems II and III incise into the resulting depo centers indicating a more recent process. The channels are the continuation of retrograding canyons and gullies at the upper northern slope (Fig. 4.3a/b) and, in contrast, result from confined turbidity currents that emerge from point sources. Additionally, the canyons/gullies most likely act as conduits for remobilized shelf sediments or the sedimentary load of rivers, which continuously drain the northern flank of Nordeste (Louvat and Allègre, 1998).

Sedimentary lobes (northern slope, Figs. 4.2a and 4.3a) as well as sediment waves and channels (southern slope, Figs. 4.2a and 4.3c) are more prominent in the east, respectively, so sediment support seems to be higher here. This is possibly due to a higher fluvial sedimentary input, since permanent rivers are existent in the eastern part of São Miguel only (Louvat and Allègre, 1998). Additionally, Nordeste Complex and the northeastern coast represent the oldest part of São Miguel (e.g. Sibrant et al., 2015b) revealing the highest altitudes and slope angles (Fig. 4.2), which is relatively strong affected by erosion over time. An overlook of the main sediment pathways down the shelf are shown in Fig. 4.4a.

4.4.2. Mass failures

4.4.2.1. Observations

Fig. 4.4b-e shows that the seafloor in the working area is shaped by systems of scarps and incisions. Such incisions, for example, are observable east of São Miguel Island (Fig. 4.4b). Corresponding seismic data identify the acoustic basement to be covered by a sediment layer with a maximum thickness of 400 ms (Fig. 4.5a). This layer reveals a mostly parallel internal stratification, which terminates against or appears to be down bended at the flanks of the incisions.

A network of scarps overprints the seafloor south of the South-Hirondelle High and alongside the western flank of Monaco Bank (Fig. 4.4c/d). The sedimentary infill of the corresponding basin reveals a parallel reflection pattern. Seismic lines crossing the scarps (Fig. 4.5b/c) show intercalated units with mostly chaotic, hummocky or contorted reflections. Three spacious units (MTD1, MTD2, MTD3) can be traced throughout the basin (see Fig. 4.5d for locations). In the case of the lowermost unit MTD1, an internal stratification is partly observable but corresponding reflections cannot be correlated between seismic lines. In contrast, MTD2 (similar to MTD 3) is characterized by a more chaotic reflection pattern and reveals a wavy to blocky surface. MTD1 and MTD2 are both traceable down to the very south of our data range.

4. SUBMARINE SEDIMENTATION PROCESSES IN THE SOUTHEASTERN TERCEIRA RIFT

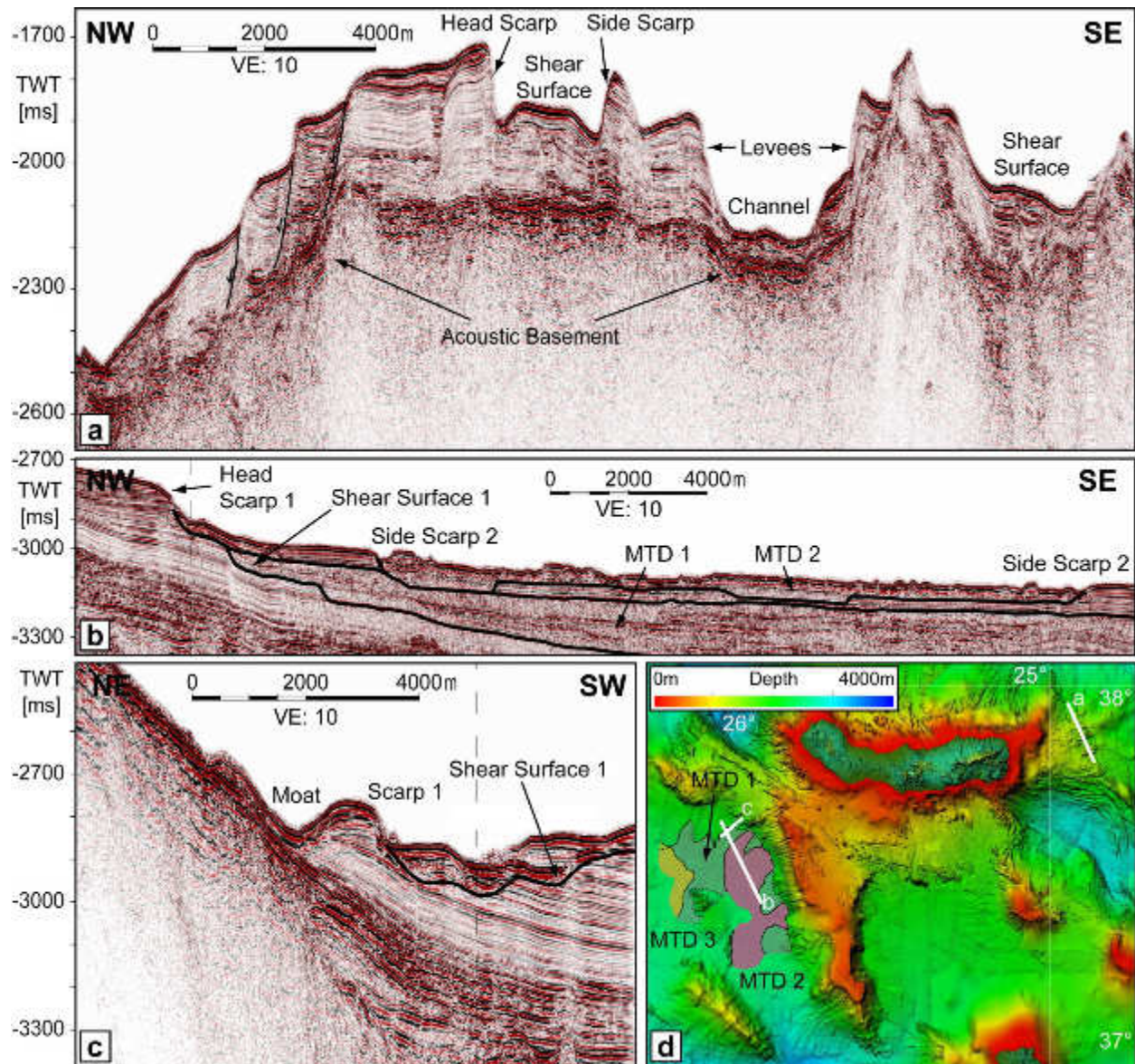


Fig. 4.5: Seismic sections illustrating mass transports. (a) East of São Miguel, an up to 400 ms thick sediment body was partly remobilized initiating the development of a channel-levee system – see also Fig. 4.4b. (b, c) In the southwestern basin, seismic data show mass transport deposits and corresponding scarps – see also Fig. 4.4c. Deposits of at least three distinct events can be traced throughout the basin (d). Dashed black lines indicate intersection of profiles (b, c). MTD: Mass transport deposit; VE: Vertical exaggeration.

Here, the western slope of the southern Monaco Bank is characterized by a ~20 km long concave embayment (Fig. 4.4d), which upslope domain is defined by slope angles of 20-30° revealing a vertical offset of ~500 m. Downslope, a ramp with a wavy surface approximately 250 km² in size dips to WSW with angles of 4-7°. Within the basin and covered by stratified sediments, a triangular shaped unit of chaotic reflections merges with the acoustic basement of

4.4. SUBMARINE SEDIMENTATION PROCESSES: RESULTS & IMPLICATIONS

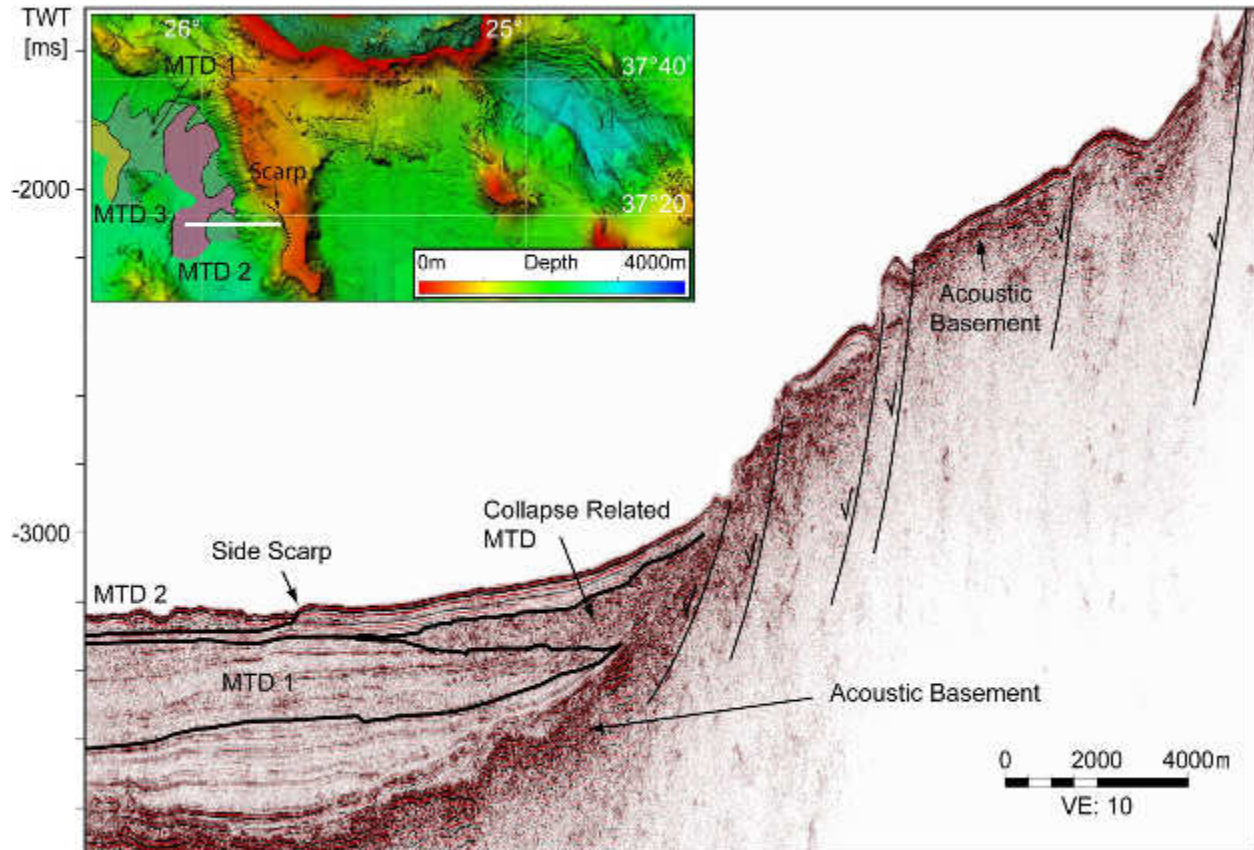


Fig. 4.6: Seismic section covering the partial flank collapse of Monaco Bank. See also Fig. 4.4d for zoomed bathymetry. MTD: Mass transport deposit; VE: Vertical exaggeration.

this ramp (Fig. 4.6). The acoustic basement shows a similar chaotic reflection pattern with higher amplitudes and is offset by several normal faults. It is covered by thin stratified sediment packages whose curved surfaces close to the fault scarps are identical with the wavy structures observable in the bathymetry (Fig. 4.4d).

At the northwestern margin of the basin south of São Miguel Island, where the eroded material of the Sete Cidades region comes down the Monaco Graben (see Fig. 4.4a), 400-500 km³ of deformed sediments have accumulated (bordered by the black line in Fig. 4.7a/b). The sediment deposits reveal a sub-parallel to disrupted reflection pattern in the lower part and rather contorted, tilted and - in the very south (Fig. 4.7a) - wavy reflections in the upper part. To the east, this body is bordered by a front of folded sediments, which terminates against the horizontal layered basin deposits (Fig. 4.7b). In the NW-SE directed crosscut (Fig. 4.7a), overlying sediments show lenticular (proximal) to sub-parallel (distal) reflections. In W-E direction, a sub-parallel reflection pattern dominates and sediments covering the folded front converge (Fig. 4.7b). In contrast, uppermost sediments (separated by the black dotted line in Fig. 4.7) are characterized by a mixture of contorted and chaotic high-amplitude reflections

forming sediment waves (Fig. 4.7a). Distal, amplitudes slightly decrease and sediments become stratified. Close to the flank of Monaco Bank, upper sediments are incised by a depression whose basal sediments reveal contorted/irregular high amplitude reflections. Sediments onlapping the flank of Monaco Bank are wavy but well stratified. The depression belongs to a more widespread system of scarps overprinting the seafloor topography in this part of the basin (Fig. 4.4e).

4.4.2.2. *Submarine slides*

Seismic data show that the channels observed in the bathymetry east of São Miguel Island (Fig. 4.4b) incise a sediment layer (Fig. 4.5a). The origin of these sediments remains uncertain, since the transition area to the island shelf is not covered by our data. It may either be caused by erosion of the spacious easternmost shelf associated with the Nordeste Complex evolution or – more likely due to the uniform stratification – may predominantly consist of a succession of pelagic and aeolian pyroclastic material hurled by subaerial eruptions. This is, at least, in accordance with palaeowind directions during the last 5000 years (Booth et al., 1978), which are generally oriented towards the east. Thus, the area covered by this sediment layer may act as a significant depocenter for volcanic fall deposits. In any case, termination of internal reflections at the northern channel's walls indicates that sediments partly slipped off. Based on the concave and linear shape (Fig. 4.4b), the side walls were identified as head and side scarps, respectively. The deepest incised channel also illustrates a remobilization of sediments, but down bended reflections at the channel walls possibly indicate levee deposits caused by turbidity currents.

In the basin southwest of São Miguel Island, sliding is a very widespread phenomenon. Slides initiated along the South-Hirondelle High and Monaco Bank where several head and side scarps are observable (Figs. 4.4c/d and 4.5b-d). The origin of the remobilized sediments will be further described in Chapter 4.4.3. Corresponding mass transport deposits are verifiable throughout the whole basin. They are typically characterized by chaotic and contorted reflection pattern and a blocky surface (Bull et al., 2009). The existence of continuous reflections within parts of MTD1 indicates that the mass waste deposit was generated either by a successive event or by several slides. However, since these reflections cannot be correlated across the basin, sub-units are not identifiable. Slides and their direction of propagation are illustrated in Fig. 4.4a.

4.4.2.3. *Flank collapses*

The approximately 20 km long escarpment at the southern Monaco Bank represents a collapse of its western flank. Based on the bathymetric and seismic data the maximum detectable extent of the flank collapse related deposit in moving direction (WSW) is ~22 km (Figs. 4.4d and 4.6) resulting in an inline/crossline ratio of ~1. However, flank collapses reported from e.g.

4.4. SUBMARINE SEDIMENTATION PROCESSES: RESULTS & IMPLICATIONS

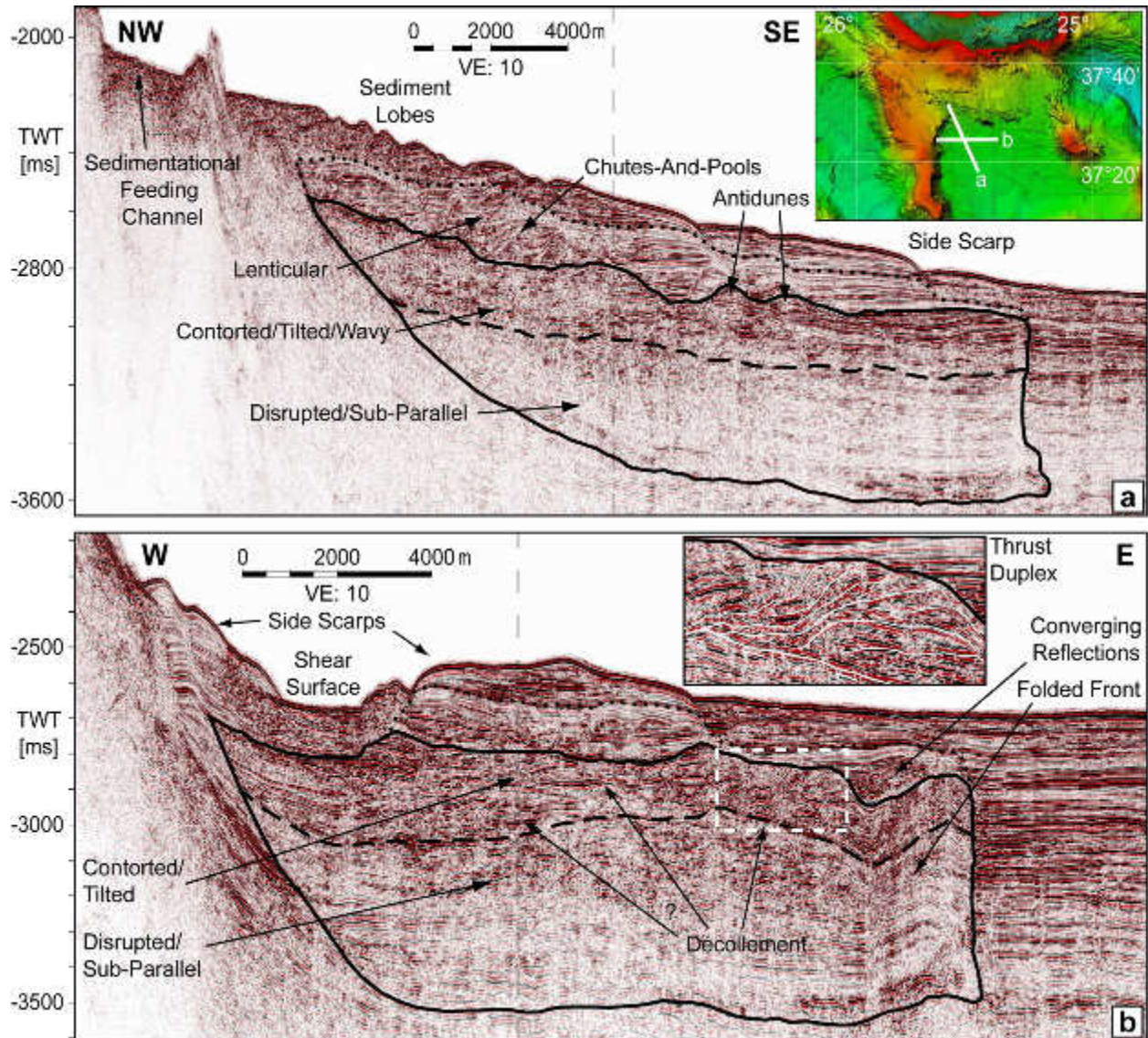


Fig. 4.7: Seismic profiles crossing a sediment body overprinted by distinct mass movements in the basin south of São Miguel. Seismic lines reveal an NW-SE (a) and W-E (b) orientation. Inset in (b) shows a piggy back thrust duplex structure in the upper part of the mass transport deposit (white dashed box). Black dashed line indicates the internal continuation of the horizon marking the onset of the subaerial evolution of São Miguel Island after Chapter 2. Black dotted line shows the transition between the chutes-and-pools facies and recent sediments. See also Fig. 4.4e for bathymetry close-up. Vertical dashed black lines indicate intersection of profiles. VE: Vertical exaggeration.

Hawaii (McMurtry et al., 2004) or Montserrat (Watt et al., 2012) showing ratios which are many times higher than this value. Additionally, neither bathymetric nor seismic data show evidence for blocky debris deposits usually present in these settings. Hence, the collapse appears rather to be the result of slow gravitationally and/or tectonically driven normal faulting (involving small mass wastes only) than being generated by a high energetic event involving large debris

avalanches. On top of the hanging wall blocks, bottom currents trapped by fault scarps cause the formation of small drift deposits and, hence, account for the wavy/undulating surface of the collapse related deposits. This interpretation is somewhat relevant, in the sense that the wavy surface pattern of the deposits may also be reminiscent of a stacked slump complex.

4.4.2.4. Interaction of sedimentation, sediment remobilization and downslope density currents

Remobilized material transported over long distances is usually characterized by its chaotic and blocky deposits (see Sub-chapters 4.4.2.2 and 4.4.2.3 or e.g. Bull et al., 2009). In contrast, the level of internal deformation (e.g. folding, thrusting) inside the sediment body at the northwestern margin of the basin south of São Miguel (Fig. 4.7) indicates mass movement with minor lateral offset of a few hundred meters. Since folded and thrust sediments are particularly observable in the W-E crosscut (Fig. 4.7b), an associated eastward direction of motion is assumed.

The vertical variation in reflection pattern shows that deformation has progressed in different ways. The transition area roughly correlates with the continuation of horizon S (black dashed line in Fig. 4.7) introduced in Chapter 2, which is associated with the onset of the subaerial evolution of São Miguel Island. The horizon, as a consequence, separates marine hemipelagic (below) from hemipelagic and clastic sediments (above). Since the development of décollements (Fig. 4.7b) and thrusting (see piggyback thrust duplex in the inset of Fig. 4.7b) is verifiable in the upper sub-unit only, we conclude that the much higher content of eroded clastic material from onshore São Miguel result in a more brittle behavior of the sediments during deformation. In contrast, deformation of the hemipelagic sediments apparently acts on a scale which is below seismic resolution.

The wavy pattern of the upper southern body (Fig. 4.7a) indicates bottom currents more or less parallel to the corresponding seismic line (NW-SE direction) escaping the Monaco Graben. In contrast to the central Monaco Graben, the basin south of São Miguel Island shows a significantly higher sediment infill (compare Figs. 4.7 and 4.9b or note Fig. 2.7 in Chapter 2.4). Hence, sediment reaching the Monaco Graben is kept in suspension or is remobilized by bottom currents (see also Sub-chapter 4.4.3.3) forming density currents which primarily enter the southern basin (sedimentation in the southwestern basin is associated with a different process – see also Sub-chapter 4.4.3.2). The wavy reflections therefore possibly reflect antidunes (e.g. Kostic, 2011). Further upslope, additional antidunes either never developed or, due to strong deformation, they are not verifiably any longer. Sediments were and are still particularly deposited close to Monaco Graben forming a kind of talus fan at the northwestern basin margin. Additionally, disturbed basin deposits associated with tectonic processes during the early subaerial evolution of the island onlap the slump body (Figs. 2.9 and 2.10 in

4.4. SUBMARINE SEDIMENTATION PROCESSES: RESULTS & IMPLICATIONS

Chapter 2). Hence, both differential load and tectonic events finally initiated the mass movement. In contrast to the slump deposits, the overlying sediments in Fig. 4.7a show no evidence for thrusting or normal faulting and, as a consequence, for post-depositional deformation due to lateral movement. In fact, the lenticular reflection pattern indicates a strong influence of density currents entering the basin from the Monaco Graben, flowing down the basin margin and generating chutes-and-pools where the slope angle abruptly decreased (e.g. Cartigny et al., 2014). However, converging reflections on top of the folded slump front (Fig. 4.7b) proves residual lateral movement of the slump in W-E direction during that time dragging the overlying sediments. At a certain time, the hydraulic jump effect vanished most likely due to the fact that the basin margin sediments reached the level of the Monaco Graben floor forming a uniform ramp since then (Fig. 4.7a). Present-day sedimentation is assumed to be generated by turbidity currents, since the uppermost deposits are characterized by a significant distal increase in stratification. Hence, uppermost sediment waves are interpreted to represent turbidity lobes.

To the west and close to Monaco Bank, recent sediments, chutes-and-pools deposits and the upper part of the slump complex were remobilized and transported basinward by a slide event, whose scarps can be observed in Fig. 4.7b. The corresponding headscarp domain is shown in Fig. 4.4e.

4.4.3. Current controlled sedimentation

4.4.3.1. *Observations*

Alongside the bathymetric highs bordering the basin southwest of São Miguel Island, truncated and converging to parallel reflections within the upper sediments are detectable (Fig. 4.8a). Additionally, converging reflections are also present close to the linear volcanic ridge within the basin, where the seafloor forms a local bathymetric depression (Fig. 4.8b/c). A comparable depression is difficult to infer south of the South-Hirondelle High (Fig. 4.8a), but further to the east such a depression bordered by converging reflections is clearly present close to Monaco Bank where sediments did not slip away yet (Fig. 4.5c). Similar constellations of local depressions and adjacent lenticular sediment bodies showing truncated and/or converging to parallel reflections (even if smaller in size) are present north of the South-Hirondelle High within the elevated graben system (Fig. 4.9a/b). Within the Monaco Graben (Fig. 4.9c), a channel has incised along a fault scarp bordered by convex sediment bodies on both sides. A further lenticular sediment body revealing truncated and converging reflections is located at the northeastern flank of Big North (Fig. 4.9d/e) – on top of an offset and tilted hanging wall block of a major fault. In this case, a local depression is not observable at the edge but in the central part of the sediment body and in prolongation of a normal fault offsetting the acoustic basement.

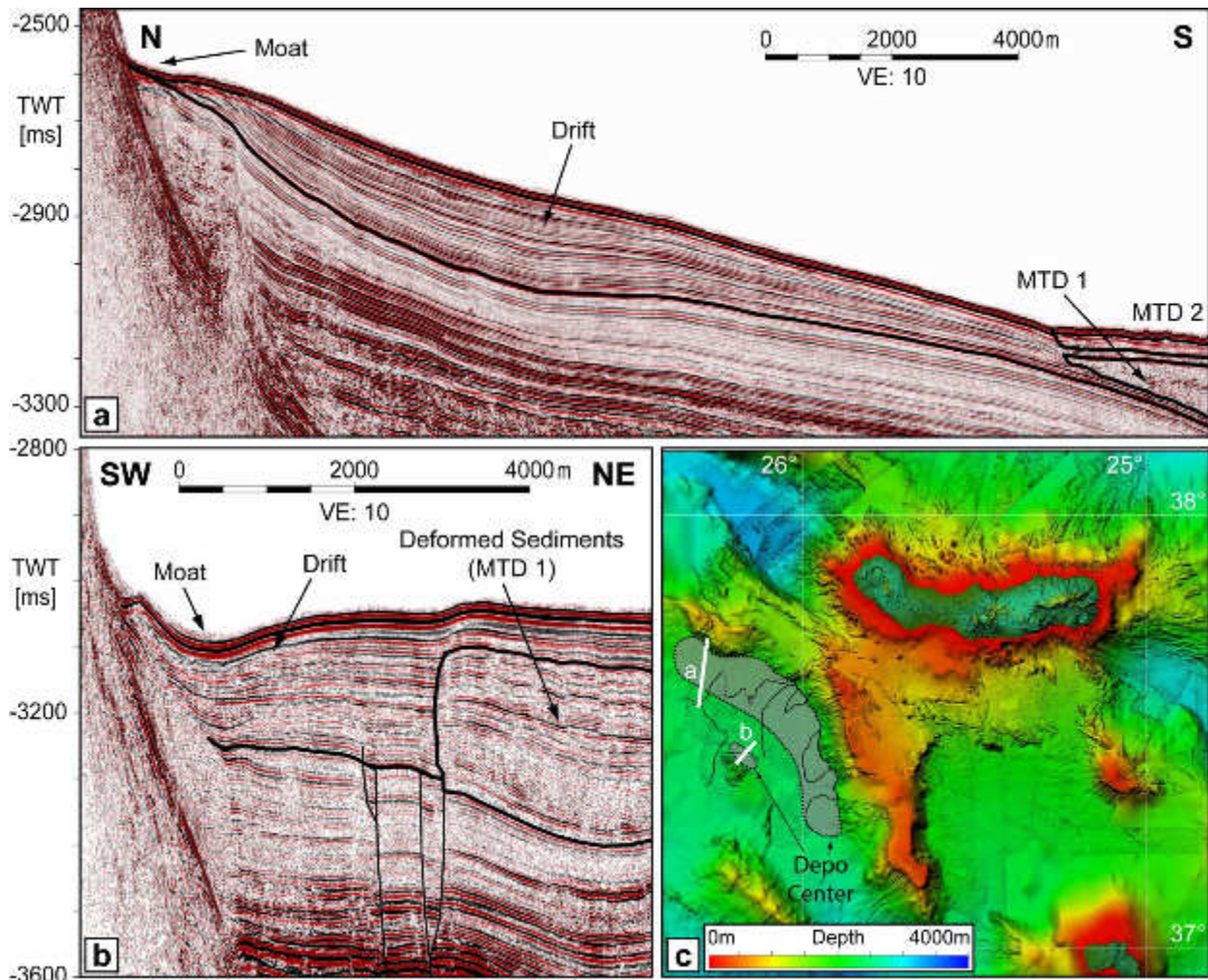


Fig. 4.8: Current controlled sedimentation along bathymetric highs. Seismic data show conturites close to the South-Hirondelle High and Monaco Bank (a) and the volcanic ridge in the basin center (b). Conturites (grey areas in c) are partially remobilized resulting in slump events (black lines in c correspond to scarps also described in Fig. 4.5). MTD: Mass transport deposit; VE: Vertical exaggeration.

4.4.3.2. Conturites in the basin southwest of São Miguel Island

Channels (Figs. 4.5c and 4.8b) following bathymetric features and affiliated convex sediment bodies - representing moats and conturites - generally show that bottom currents affect sedimentation in the basin southwest of São Miguel (Rebesco et al., 2014). In fact, south of the South-Hirondelle High a moat is not well pronounced (Fig. 4.8a), but the truncation of well stratified and converging reflections indicate non-deposition close to the flank and current controlled sedimentation in the distal domain. Conturites are observable at the northeastern basin margin and in the foot region of the linear volcanic ridge in the basin center (Fig. 4.8c).

4.4. SUBMARINE SEDIMENTATION PROCESSES: RESULTS & IMPLICATIONS

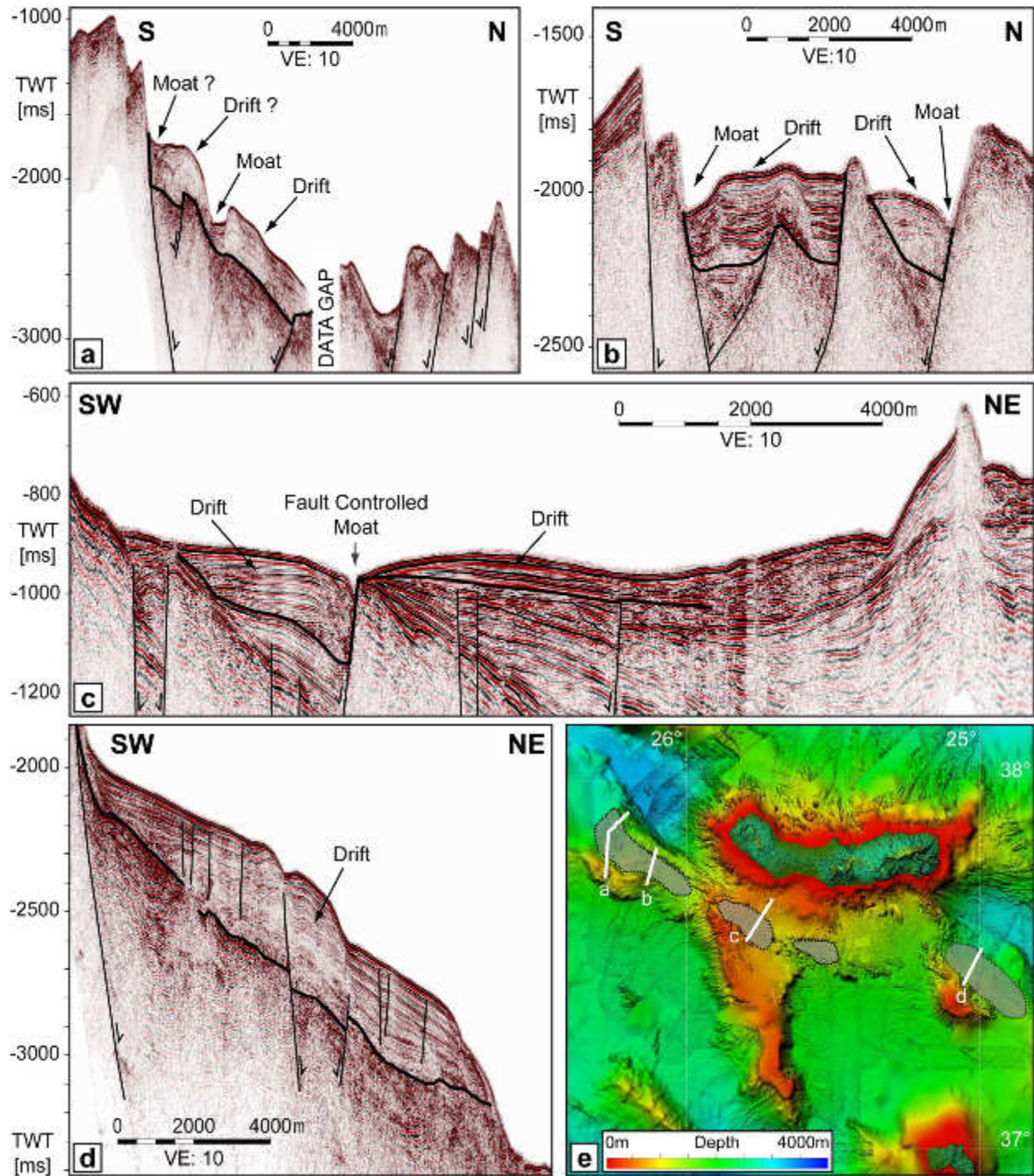


Fig. 4.9: Current controlled sedimentation along fault planes. Drift deposits can be traced in the elevated graben system north of the South-Hirondelle High (a, b), within the elevated Monaco Graben (c) and along the fault scarp defining the northeastern flank of Big North (d). Depocenters are represented by grey areas (e); white lines indicate locations of seismic profiles. VE: Vertical Exaggeration.

4. SUBMARINE SEDIMENTATION PROCESSES IN THE SOUTHEASTERN TERCEIRA RIFT

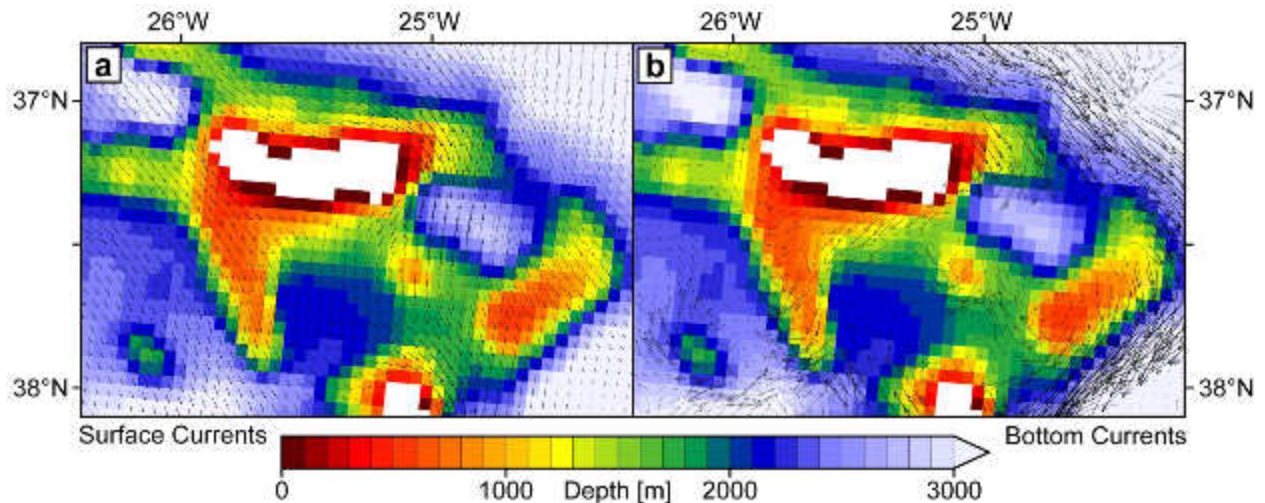


Fig. 4.10: Modelled surface (a) and bottom (b) currents based on the MITcgm. Surface currents in the southeastern Terceira Rift show an overall NW-SE direction. Bottom currents flow around bathymetric highs in a clockwise manner.

If Coriolis-controlled flows (which has the tendency to be concentrated along the right side of its flow path; e.g. Hernández-Molina et al., 2014) were assumed, the geometry of moats/erosional channels and contourites would indicate a SE-NW directed bottom current following the elevated Monaco Bank/South-Hirondelle High (Figs. 4.5c and 4.8a) and a current in opposite direction close to the volcanic ridge (Fig. 4.8b). However, the ridge is a comparatively small structure and the current controlled sediments may rather reflect a patch drift caused by the turbulent interaction of morphology and the bottom current which is predominantly related to the contourite at the northeastern basin margin. This is also in accordance with flow directions calculated based on the MITcgm. Even if the model shows an overall NW-SE directed flow of the surface water (Fig. 4.10a) representing the return flow of the North-Atlantic subtropical gyre (e.g. Dietrich et al., 1975; Reid, 1994; Schmitz 1995), the bottom current in the southwestern basin is SE-NW directed (Fig. 4.10b). This current focuses along the western flank of Monaco Bank and the southern flank of the South-Hirondelle High where it controls the formation of a separated, elongated mounded drift (Fig. 4.8c).

Since the contourites overlie uniformly stratified sediments (Fig. 4.8a/b), the bottom currents must be initiated at a specific point in time. This time possibly correlates with vertical tectonic movements in the region of Iceland and the Greenland-Scotland-Ridge at ~2.5 Ma resulting in an increased influx of North Atlantic Deep Water into the eastern North Atlantic basins (Müller-Michaelis and Uenzelmann-Neben, 2014) and in a potentially increased overflow of the Azores Plateau. Furthermore, this would roughly fit the fact that the contourite represents

4.4. SUBMARINE SEDIMENTATION PROCESSES: RESULTS & IMPLICATIONS

approximately the half volume of the uppermost sedimentary unit defined in Chapter 2, which base is assumed to have an age of 5.3 – 4.3 Ma.

4.4.3.3. *Drifts along fault scarps*

Separated, elongated mounded drift systems are also located within the elevated graben north of the South-Hirondelle High, even if smaller in size (Fig. 4.9a/b) and organized along fault scarps. Within the Monaco Graben, a moat follows a fault keeping the uppermost part of the fault plane free of sediments (Fig. 4.9c). Upwards convex reflections show sedimentation on both sides of the channel rather reminding of a channel related patch drift with a fault controlled moat. Low thicknesses of current controlled deposits depict high bottom current velocities due to the narrow graben resulting in a decreased effective cross section for the water masses to pass. At the northeastern flank of Big North High and on top of an offset tilted block associated with the rifting of the Povoação Basin, a plastered drift shapes the seafloor (Fig. 4.9d). The evolution of the drift involves a significant interaction with faulting of the acoustic basement, which favored the development of a central moat at the top of the fault-generated basement.

The drift bodies northeast of the South-Hirondelle High and Big North as well as the small one east of Monaco Graben are all characterized by a comparable water depth of 1100-1600 m (Fig. 4.9e). In this depth level, bottom currents calculated by the MITcgm show higher velocities, generally follow the topography and flows around bathymetric highs in an anticyclonic (clockwise) manner (Fig. 4.10b). Hence, the drift bodies east of Monaco Bank and on the flank of Big North are located left of the current core (in flow direction), which is typical for Coriolis-controlled flows. In contrast, the flow conditions north of the South-Hirondelle Basin and within the shallower Monaco Graben (550-900 m) are less clear. In these cases, the resolution of the MITcgm bathymetric information (which is ETOPO2) is too low to resolve the graben structures. This is why the model shows bottom current directions oblique/perpendicular to the bathymetric feature, which is unrealistic. Since the sediment accumulation rate at the northwestern margin of the southern basin is comparably high (Fig. 4.7a or Chapter 2.4), we rather assume a NW-SE directed bottom current similar to the movement of the surface water (Fig. 4.10a), which would additionally support a sediment flux towards the southern basin. All these uncertainties show how complex the local current system in the Azores region is. To get a more comprehensive picture of the local oceanography, more detailed studies of the water masses are needed. However, it has to be mentioned that the modelled circulation pattern as well as recent oceanographic measurements do/will reflect the present-day conditions only, and variations in circulation during the last 5 Ma cannot be ruled out.

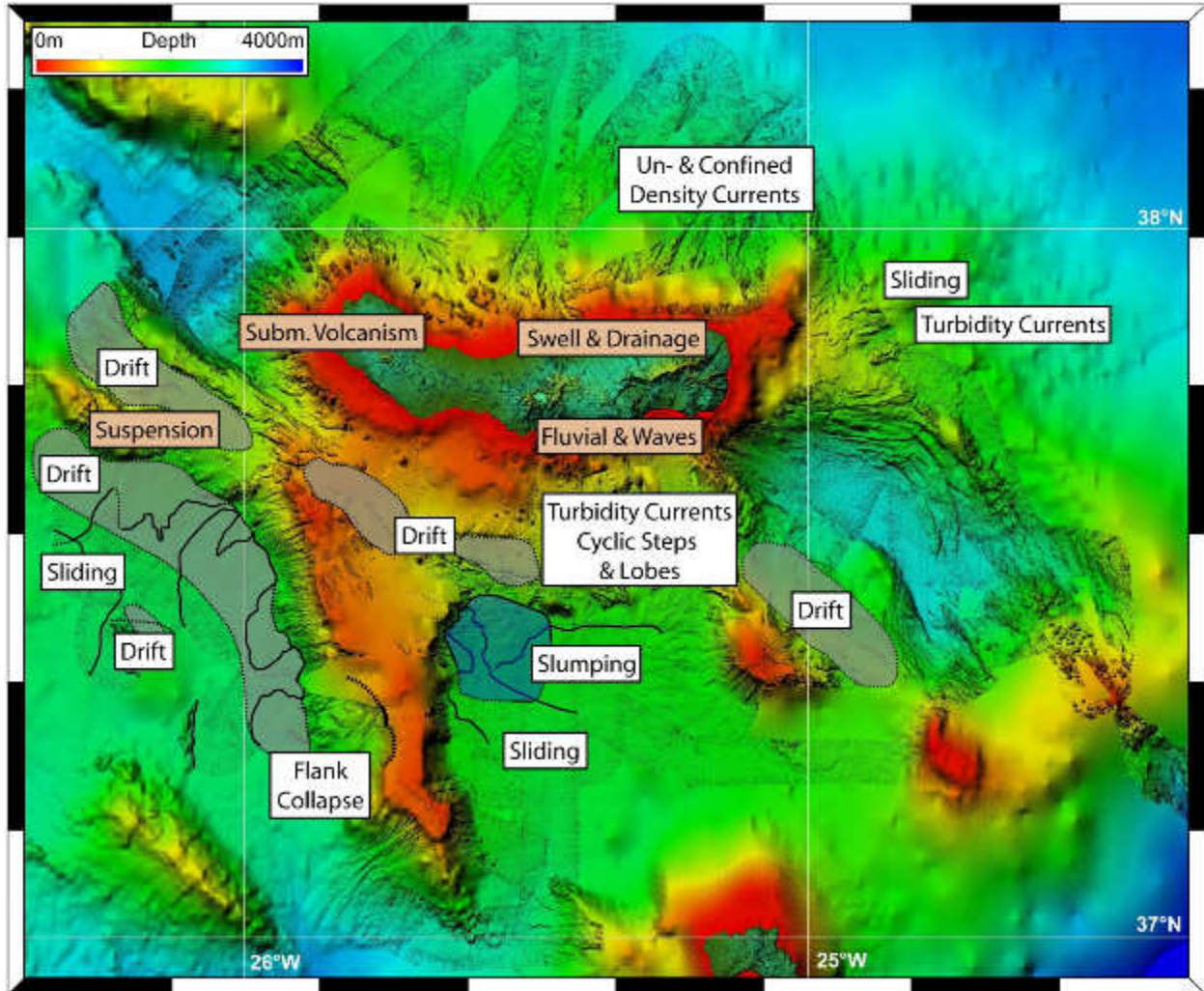


Fig. 4.11: Sediment support and sedimentation processes in the working area. Sediments originate from bottom currents, rivers, coastal erosion or are in situ generated by submarine volcanism (brown boxes). White boxes indicate the distal sedimentation settings. Black lines indicate the scarp (dashed: inferred scarps/boundaries).

4.5. Conclusion

Submarine sedimentation in the southeastern Terceira Rift is not obviously characterized by large volcanic fall deposits. Although the area east of São Miguel Island possibly represents a relevant depocenter for eolian products, sedimentation is rather dominated by the erosional products of onshore São Miguel Island and its shelf. The present-day island shelf – located in a water depth of ~140 m – is assumed to be originally formed by erosion during the Last Glacial Maximum and has been subsided by approximately ~0.6 mm/a. Shallower shelf segments presumably caused by magmatic overprint during the last post-glacial sea level rise are observable west and southeast of Sete Cidades Volcano as well as south of Fogo Volcano.

4.5. CONCLUSION

In the Sete Cidades region, the island slope below the shelf break is shaped by submarine explosive volcanism and the associated in situ generated volcanic material (see Fig. 4.11 for the different sediment sources and sedimentation settings in the southeastern Terceira Rift). In contrast, the northern slope is characterized by retrograde canyons and gullies where Fogo Volcano and the Nordeste Complex define onshore São Miguel. We concluded that the exposure to North-Atlantic storm swell – in particular during sea level lowstand – caused strong unconfined density currents along the entire shelf (line source). Associated deposits are incised by two channel systems, which merge with the canyons and gullies of the northern slope draining the terrestrial sediment load (point sources). The island slope south of Fogo Volcano and the Furnas Caldera/Povoação Depression, on the contrary, reveals cyclic steps, chutes-and-pools and turbidite lobes generated by turbidity currents caused by a uniform coastal erosion and fluvial sediment flux.

Turbidites follow morphological features like the Monaco Graben and enter the basins via structural gateways. Within the basins, bottom currents are deflected by volcanic ridges or controlled by fault scarps. Mass failures are very common phenomena in the submarine domain of the southeastern Terceira Rift. They cover the full temporal spectrum of long-time mass movements to an abrupt remobilization of sediments. Turbidites and drifts are remobilized due to differential load or tectonic events or a superposition of both effects. Caused by the same effects, the southwestern flank of Monaco Bank collapsed.

All this shows the high diversity of sedimentation processes in the southeastern Terceira Rift and the high level of mutual interaction between volcanism, tectonics, erosion, sediment transport mechanisms, oceanographic/atmospheric conditions, sediment accumulation and its remobilization.

Acknowledgements

We sincerely thank Captain Thomas Wunderlich and his outstanding crew of *RV Meteor* for their support during the M79/2 cruise. We are grateful for the financial support of the German Research Foundation (DFG, grant Hu698/19-1). The ocean numerical simulation was performed at the Deutsches Klimarechenzentrum (DKRZ), Hamburg, Germany, in the frame of DKRZ project 704. Additional acknowledgements go to the companies Halliburton-Landmark and Schlumberger for providing university grants for the seismic processing software ProMAX and seismic interpretation software Petrel, respectively, as well as to the NASA's Earth Science Data Systems program for providing the ASTER Global DEM data.

5. Conclusions and outlook

5.1. *Conclusions*

In this study I present and interpret a marine data set comprising multi-channel reflection seismic profiles and high resolution bathymetric and backscatter data. This data set is unique for the whole Azores region. Until now, bathymetric information of 1 km resolution was accessible for the southeastern Terceira Rift only. This work contributes to the low spatial resolution data available with data of a resolution of up to 10 x 10 m. Additionally, the study comprises the first multi-channel seismic data that has ever been recorded in the Azores. Results lead, first, to a significantly improved understanding of the structural evolution of the southeastern Terceira Rift with implications for the entire Azores Plateau evolution since the late Miocene. Second, by analyzing submarine volcanic cones I contribute to the ongoing discussion about deep sea explosive volcanism. Third, I show the high diversity of sedimentary processes and their interaction with volcanism, tectonics, erosion and oceanographic conditions.

Evolution and nature of the oblique ultra-slow Terceira Rift and the volcanically active Azores domain are object to many discussions since the late sixties. Recent studies suggest the Terceira Rift to be, in particular, an ultra-slow spreading axis (Vogt and Jung, 2004), an axis of a hot-spot dominated triple junction (e.g. Bourdon et al., 2005; Gente et al., 2003; Schilling 1975) or to be caused by the rigid response of the lithosphere to global plate kinematics (e.g. Neves et al., 2013). The presented study correlates the rise of volcanic systems and individual steps of the basins' evolution with distinct extension conditions, which were derived from magnetic data (Luis and Miranda et al., 2008). According to this, the Terceira Rift has not developed oblique to the extensional direction but initiated orthogonally to it. A subsequent clockwise rotation in extension to WSW-ENE at ~10 Ma indeed resulted in a present-day oblique appearance of the overall rift system, but detailed mapping of volcanic features and faults shows that the Terceira Rift adapted to the modified conditions within its inherited nature. As an example, the reader might be reminded of the rise of Monaco Bank or the stepwise evolution of the Povoação Basin. São Miguel Island, which links the laterally offset South-Hirondelle and Povoação rift basins, is interpreted to be located above a leaky transform fault referencing its unusual orientation and shape in relation to the other islands of the Azores. Extension due to the relative movement of the Eurasian and Nubian plates in the working area is focused at the southeastern Terceira Rift.

Although the existence of a hot-spot or melting anomaly is not rejected by these observations, they show the strong linkage to plate kinematic conditions and, thus, the tectonic evolution of the Terceira Rift is not primarily controlled by a MAR-hot-spot interaction. However, a hot-spot (e.g. Bourdon et al., 2005; Schilling, 1975; White and Schilling, 1978) and/or a melting anomaly in the upper mantle (Asimow et al., 2004; Bonatti et al., 1990, Métrich et al., 2014) is a feasible explanation of 1) the kind of the observed (onshore) volcanism, and 2) its existence. On the one hand, this volcanism is reflected by the subaerial exposed islands of the Azores Archipelago, whose occurrences are the “tip of the iceberg” only. On the other hand, most of the volcanic activity takes place below the sea surface. Hence, submarine volcanism is particularly accountable for the thickened crust and the corresponding elevated seafloor in the Azores region (e.g. Gente et al., 2003; Luis et al., 1998) as well as for the formation of submarine volcanic lineaments, which are partially overprinted by volcanic cones of a few hundreds of meters in height and few kilometers in diameter (e.g. Tempera et al., 2013). Detailed mapping of such cones within the southeastern Terceira Rift show that they 1) are organized by faults, 2) cluster on the submarine flank of subaerial exposed stratovolcanoes like Sete Cidades at São Miguel Island (parasitic volcanism), or 3) are significantly involved in the formation of seamounts. Morphology, reflection pattern, internal stratification and interfingering sediments of adjacent cones indicate a predominantly explosive type of volcanism – independent of and down to a water depth of 3200 m. Even though explosive volcanism in the deep sea was proven in recent years, e.g. based on the observation of associated volcanoclastic material (Hekinian et al., 2000), the general knowledge is sparse. The corresponding results of this study are therefore surprising and contribute on the ongoing discussion about deep sea related volcanism. Submarine volcanic edifices, which could present a serious volcanic risk to the population of São Miguel Island, were not observed, although explosive eruptions in a water depth of less than 300-400 m might pose a local risk at the sea surface.

Submarine and subaerial volcanism is the relevant bathymetry/topography shaping process in the Azores. Furthermore, it is the origin of the main component of the sediments, which are deposited within the southeastern Terceira Rift and the adjacent basins. Volcanic sediments are either generated in situ or originate from onshore erosional products, which are transported from e.g. São Miguel or its shelf into the deep sea by unconfined and confined density currents. Sediments are also created by coastal erosion causing the formation of the up to 14 km wide shelf of São Miguel. Based on the shelf break depth (~140 m), which is similar to those of e.g. Pico, Terceira and Faial (Quartau et al., 2015, 2014, 2012), a maximum long-term subsidence rate of ~0.6 mm/a and a relative low age of the shelf is assumed – most likely it has been formed by erosion during the last sea level minimum (18 ka after Lisiecki et al., 2005). Sedimentation within the basins occurs in strong interaction with volcanism, local tectonics, and oceanographic conditions. Volcanic and tectonic features define sediment pathways and high local sediment accumulations. Bottom currents – deflected by volcanic edifices or fault

5.2. OUTLOOK

scarps – cause erosion, non-deposition and sediment accumulation (drift bodies). Mass wasting, which initiates at the basin margins, is common in the southeastern Terceira Rift – most likely triggered by oversteepening and local seismicity, which is also responsible for the collapse of volcanic edifices as seen at the Monaco Bank.

This thesis, therefore, reveals a comprehensive study of the processes which initiated and controlled the evolution of the eastern Azores Archipelago and the southeastern Terceira Rift as well as those processes significantly shaping the sea floor in this area. All these geodynamic, volcanic and sedimentary processes are closely interlinked and cascadingly interacting - offering an incredibly exciting and challenging setting for geoscientists from different backgrounds.

5.2. Outlook

Results of this thesis have clearly improved the knowledge of the evolution and nature of the Azores Archipelago, the Terceira Rift and the westernmost part of the Eurasian-Nubian plate boundary. Nevertheless, several questions may be further evaluated or remain unanswered due to the complexity of the geological setting. Some of these questions and implications for future or ongoing work are outlined below.

Based on the orientation of volcanic lineaments, mapped offshore and reported onshore faults, it was concluded that São Miguel Island evolved above a leaky transform related to the Eurasian-Nubian plate boundary (sub-chapter 2.5.2.). For a better understanding of the lithospheric structure below São Miguel, wide-angle reflection data would be essential to verify 1) the thickness of the crust in general, 2) the thickness of the crust below São Miguel Island to derive e.g. the present-day status of isostatic compensation, and 3) the location of the elevated Moho in relation to the island to confirm the assumption of a leaky transform (should be directly below the island body) or to state an alternative e.g. simple shear graben model (should be N-S shifted in relation to the island). Such an N-S transect crossing the island was carried out by the M79/2 cruise in 2009. Analysis of the corresponding data is in process and results will be published soon.

The lack of absolute age information of submarine volcanic edifices is a serious limitation when describing the spatial evolution of the Azores. In fact, a relative chronology for the southeastern Terceira Rift was discussed in context of plate kinematic reconstructions, a single submarine and several onshore age constrains (sub-chapter 2.5.3.). However, onshore age data only reflects the upper subaerially exposed part of a volcanic island, which – considering the submarine part of the island – is a 4000-5000 m high volcanic system in total. This data may tell a lot about the subaerial evolution of such an island, but it gives no indications for its earlier

submarine stage. Thus, age information obtained by onshore drilling and a significantly higher availability of samples from submarine volcanic edifices would enormously improve our understanding of the spatial and temporal distribution of volcanism and, as a consequence, of lithospheric extension within the southeastern Terceira Rift.

The geochemical analysis of submarine samples taken from submarine cones (such as analyzed in chapter 3) may, in addition, help to better understand the driving process of submarine explosive volcanism, which is still under debate within the submarine volcanism community.

In particular the southeastern Terceira Rift still lacks available high resolution bathymetric data, which hampers a detailed mapping of the fault systems e.g. within the Hironnelle Basins or south of the Formigas Complex, where Terceira Rift and Gloria Fault merge. Therefore, little is known about the tectonics between Terceira and São Miguel as well as close to the Gloria Fault. In addition, an analysis of fault systems and relative age successions based on reflection seismic data throughout the Azores Plateau (in the best case combined with absolute age information based on geochemical analyses of samples taken from the volcanic ridges) would be of major interest to understand the temporal distribution of deformation within the whole Azores domain. This would, on the one hand, allow assigning or adapting the evolutionary model presented in this thesis to the whole Terceira Rift. On the other hand, the presence of the volcanic ridges SW of the Terceira Rift and a less pronounced rift system in prolongation to the Açor Fracture Zone and Princess Alice Bank indicate that extension is or was accumulated between the East Azores Fracture Zone and the Terceira Rift as well. Such data, therefore, could significantly contribute to the discussion, if the Eurasian-Nubian plate boundary moved northward in one or in several steps. The first assumption would imply volcanism along lithospheric fissures synchronous with the Terceira Rift evolution (sub-chapter 2.5.2. and references therein) and a possible – at least interim – independent Azores micro plate (Luis et al., 1994), whose southern boundary could be reflected by the Princess Alice Bank and the adjacent rift basins. On the contrary, a successive migration of the triple point and the plate boundary (Luis et al., 1994; Vogt and Jung, 2004) would have caused a stepwise construction of the Azores Plateau and a series of failed rifts. This would be reflected by e.g. a northeast-southwest age progression of the corresponding volcanic edifices and northeastwards thinning sediment coverage on top of the volcanic units off the islands.

Finally, large catastrophic flank collapses with associated tsunami potential are common during construction and erosion of volcanic ocean islands (e.g. Ramalho et al., 2013). However, in the working area flank collapses are not that obvious as e.g. at the Canaries (e.g. Boulesteix et al., 2013). Indeed, several flank collapses are postulated at Pico (Costa et al., 2014, 2015; Hildenbrand et al., 2012a; Mitchell et al., 2012a), Graciosa (Sibrant et al., 2014), Faial (Hildenbrand et al., 2012b), Santa Maria (Sibrant et al., 2015a) and São Miguel (Sibrant

5.2. OUTLOOK

et al., 2015b) but apart from the study at São Miguel all others are based on interpretations of the onshore morphology of the islands and, if at all, bathymetric data only. Hence, reflection seismic and additional bathymetric data could be used to verify and further determine corresponding mass waste deposits and their total volumes (as far as the seismic network is dense enough).

Bibliography

- Adam, C. et al., 2013. Mantle dynamics and characteristics of the Azores plateau. *Earth and Planetary Science Letters*, Band 362, pp. 258-271.
- Alves, T. et al., 2004. Surveying the flanks of the Mid-Atlantic Ridge: the Atlantis Basin, North Atlantic Ocean (36°N). *Marine Geology*, 209(1–4), pp. 199-222.
- Amante, C. & Eakins, B., 2009. ETOPO1 1 Arc-Minute Global Relief Model: Procedures, Data Sources and Analysis. 19 p. *Colorado: US Department of Commerce, National Oceanic and Atmospheric Administration, National Environmental Satellite, Data, and Information Service, National Geophysical Data Center, Marine Geology and Geophysics Division*.
- Argus, D. F., Gordon, R. G., DeMets, C. & Stein, S., 1989. Closure of the Africa-Eurasia-North America Plate motion circuit and tectonics of the Gloria Fault. *Journal of Geophysical Research: Solid Earth*, 94(B5), pp. 5585-5602.
- Asimow, P. D., Dixon, J. E. & Langmuir, C. H., 2004. A hydrous melting and fractionation model for mid-ocean ridge basalts: Application to the Mid-Atlantic Ridge near the Azores. *Geochemistry, Geophysics, Geosystems*, 5(1). DOI 10.1029/2003GC000568.
- Azevedo, J. & Ferreira, M. P., 2006. The volcanotectonic evolution of Flores Island, Azores (Portugal). *Journal of Volcanology and Geothermal Research*, 156(1–2), pp. 90-102.
- Baptista, M., Miranda, P., Miranda, J. & Victor, L., 1998. Constrains on the source of the 1755 Lisbon tsunami inferred from numerical modelling of historical data on the source of the 1755 Lisbon tsunami. *Journal of Geodynamics*, 25(1–2), pp. 159-174.
- Batiza, R. & White, J. D., 2000. Submarine lavas and hyaloclastite. *Encyclopedia of volcanoes*, pp. 361-381.
- Beier, C., Haase, K. M. & Abouchami, W., 2015. Geochemical and geochronological constraints on the evolution of the Azores Plateau. *Geological Society of America Special Papers*, Band 511, pp. 27-55.

- Beier, C. et al., 2008. Magma genesis by rifting of oceanic lithosphere above anomalous mantle: Terceira Rift, Azores. *Geochemistry, Geophysics, Geosystems*, 9(12). DOI 10.1029/2008GC002112.
- Beier, C., Haase, K. M. & Turner, S. P., 2012. Conditions of melting beneath the Azores. *Lithos*, 144–145(0), pp. 1-11.
- Ben-Avraham, Z., Kempler, D. & Ginzburg, A., 1988. Plate convergence in the Cyprean Arc. *Tectonophysics*, 146(1–4), pp. 231-240.
- Betzler, C. et al., 2014. Periplatform drift: The combined result of contour current and off-bank transport along carbonate platforms. *Geology*, 42(10), pp. 871-874.
- Bintanja, R., van de Wal, R. S. & Oerlemans, J., 2005. Modelled atmospheric temperatures and global sea levels over the past million years. *Nature*, 437(7055), pp. 125-128.
- Bonatti, E., 1990. Not So Hot "Hot Spots" in the Oceanic Mantle. *Science*, 250(4977), pp. 107-111.
- Booth, B., Croasdale, R. & Walker, G. P. L., 1978. A Quantitative Study of Five Thousand Years of Volcanism on Sao Miguel, Azores. *Philosophical Transactions of the Royal Society of London. Series A, Mathematical and Physical Sciences*, 288(1352), pp. 271-319.
- Borges, J. et al., 2007. The 1980, 1997 and 1998 Azores earthquakes and some seismo-tectonic implications. *Tectonophysics*, 435(1–4), pp. 37-54.
- Boulesteix, T. et al., 2013. Coeval giant landslides in the Canary Islands: Implications for global, regional and local triggers of giant flank collapses on oceanic volcanoes. *Journal of Volcanology and Geothermal Research*, Band 257, pp. 90-98.
- Bourdon, B., Turner, S. P. & Ribe, N. M., 2005. Partial melting and upwelling rates beneath the Azores from a U-series isotope perspective. *Earth and Planetary Science Letters*, 239(1–2), pp. 42-56.
- Boyer, T. et al., 2005. Objective analyses of annual, seasonal, and monthly temperature and salinity for the World Ocean on a 0.25° grid. *International Journal of Climatology*, 25(7), pp. 931-945.
- Bufo, E., Udías, A. & Colombás, M., 1988. Seismicity, source mechanisms and tectonics of the Azores-Gibraltar plate boundary. *Tectonophysics*, 152(1–2), pp. 89-118.

- Bull, S., Cartwright, J. & Huuse, M., 2009. A review of kinematic indicators from mass-transport complexes using 3D seismic data. *Marine and Petroleum Geology*, 26(7), pp. 1132-1151.
- Cannat, M. et al., 1999. Mid-Atlantic Ridge–Azores hotspot interactions: along-axis migration of a hotspot-derived event of enhanced magmatism 10 to 4 Ma ago. *Earth and Planetary Science Letters*, 173(3), pp. 257-269.
- Carmo, R., 2004. Geologia estrutural da região Povoação - Nordeste (ilha de S. Miguel, Açores). *Unpublished PhD Thesis, Universidade dos Açores*, 121p.
- Cartigny, M. J., Ventra, D., Postma, G. & van Den Berg, J. H., 2014. Morphodynamics and sedimentary structures of bedforms under supercritical-flow conditions: New insights from flume experiments. *Sedimentology*, 61(3), pp. 712-748.
- Carvalho, M., Forjaz, V. & Almeida, C., 2006. Chemical composition of deep hydrothermal fluids in the Ribeira Grande geothermal field (São Miguel, Azores). *Journal of Volcanology and Geothermal Research*, 156(1–2), pp. 116-134.
- Casalbore, D. et al., 2015. Volcanic, tectonic and mass-wasting processes offshore Terceira Island (Azores) revealed by high-resolution seafloor mapping. *Bulletin of Volcanology*, 77(3). DOI 10.1007/s00445-015-0905-3.
- Cashman, K. C. & Fiske, R. S., 1991. Fallout of Pyroclastic Debris from Submarine Volcanic Eruptions. *Science*, 253(5017), pp. 275-280.
- Chadwick, W. W. et al., 2008. Direct video and hydrophone observations of submarine explosive eruptions at NW Rota-1 volcano, Mariana arc. *Journal of Geophysical Research: Solid Earth*, 113(B8). DOI 10.1029/2007JB005215.
- Cole, P., Guest, J., Duncan, A. & Pacheco, J.-M., 2001. Capelinhos 1957–1958, Faial, Azores: deposits formed by an emergent surtseyan eruption. *Bulletin of Volcanology*, 63(2-3), pp. 204-220.
- Costa, A. et al., 2015. Catastrophic flank collapses and slumping in Pico Island during the last 130 kyr (Pico-Faial ridge, Azores Triple Junction). *Journal of Volcanology and Geothermal Research*, 302(0), pp. 33-46.
- Costa, A. et al., 2014. Large-scale catastrophic flank collapses in a steep volcanic ridge: The Pico - Faial Ridge, Azores Triple Junction. *Journal of Volcanology and Geothermal Research*, Band 272, pp. 111-125.

- Cruz, J. V. & Silva, M. O., 2000. Groundwater salinization in Pico Island (Azores, Portugal): origin and mechanisms. *Environmental Geology*, 39(10), pp. 1181-1189.
- Davis, A. & Clague, D., 2006. Volcaniclastic deposits from the North Arch volcanic field, Hawaii: explosive fragmentation of alkalic lava at abyssal depths. *Bulletin of Volcanology*, 68(3), pp. 294-307.
- Dee, D. et al., 2011. The ERA-Interim reanalysis: Configuration and performance of the data assimilation system. *Quarterly Journal of the Royal Meteorological Society*, 137(656), pp. 553-597.
- DeMets, C., Gordon, R. G. & Argus, D. F., 2010. Geologically current plate motions. *Geophysical Journal International*, 181(1), pp. 1-80.
- Deptuck, M. E., Piper, D. J. W., Savoye, B. & Gervais, A., 2008. Dimensions and architecture of late Pleistocene submarine lobes off the northern margin of East Corsica. *Sedimentology*, 55(4), pp. 869-898.
- Detrick, R. S., Needham, H. D. & Renard, V., 1995. Gravity anomalies and crustal thickness variations along the Mid-Atlantic Ridge between 33°N and 40°N. *Journal of Geophysical Research: Solid Earth*, 100(B3), pp. 3767-3787.
- Dias, N. et al., 2007. Crustal seismic velocity structure near Faial and Pico Islands (AZORES), from local earthquake tomography. *Tectonophysics*, 445(3-4), pp. 301-317.
- Dietrich, G., Kalle, K., Krauss, W. & Siedler, G., 1975. *Allgemeine Meereskunde: Eine Einführung in die Ozeanographie*. Gebr. Borntraeger. ISBN 3443010164.
- Druitt, T. H., 1985. Vent Evolution and Lag Breccia Formation during the Cape Riva Eruption of Santorini, Greece. *The Journal of Geology*, 93(4), pp. 439-454.
- Eddy, C. A., Dilek, Y., Hurst, S. & Moores, E. M., 1998. Seamount formation and associated caldera complex and hydrothermal mineralization in ancient oceanic crust, Troodos ophiolite (Cyprus). *Tectonophysics*, 292(3-4), pp. 189-210.
- Escartín, J. et al., 2001. Crustal thickness of V-shaped ridges south of the Azores: Interaction of the Mid-Atlantic Ridge (36°-39°N) and the Azores hot spot. *Journal of Geophysical Research*, 106(B10), pp. 21719-21735.
- Faccenna, C. et al., 2004. Lateral slab deformation and the origin of the western Mediterranean arcs. *Tectonics*, 23(1). DOI 10.1029/2002TC001488.

- Fan, Y., Lin, S.-J., Griffies, S. M. & Hemer, M. A., 2014. Simulated Global Swell and Wind-Sea Climate and Their Responses to Anthropogenic Climate Change at the End of the Twenty-First Century. *Journal of Climate*, 27(10), pp. 3516-3536.
- Favela, J. & Anderson, D. L., 2000. Extensional tectonics and global volcanism. *Problems in Geophysics for the New Millennium*, pp. 463-498.
- Fekete, B. M., Vorosmarty, C. J. & Grabs, W., 1999. *Global, composite runoff fields based on observed river discharge and simulated water balances, Report 22*. World Meteorological Organization–Global Runoff Data Center, Koblenz, Germany.
- Fernandes, R. et al., 2006. Defining the plate boundaries in the Azores region. *Journal of Volcanology and Geothermal Research*, 156(1–2), pp. 1-9.
- Ferreira, T., 2000. Caracterização da actividade vulcânica da ilha de S. Miguel (Açores): vulcanismo basáltico recente e zonas de desgasificação. Avaliação de riscos. *Unpublished PhD Thesis, Universidade dos Açores*.
- França, Z., 2006. Geochemistry of alkaline basalts of Corvo Island (Azores, Portugal): preliminary data. *Geogaceta*, Issue 40, pp. 87-90.
- Garcia, M. O. et al., 2006. Geology, geochemistry and earthquake history of Loihi Seamount, Hawaii's youngest volcano. *Chemie der Erde - Geochemistry*, 66(2), pp. 81-108.
- Gente, P., Dymant, J., Maia, M. & Goslin, J., 2003. Interaction between the Mid-Atlantic Ridge and the Azores hot spot during the last 85 Myr: Emplacement and rifting of the hot spot-derived plateaus. *Geochemistry, Geophysics, Geosystems*, 4(10). DOI 10.1029/2003GC000527.
- Georgen, J. E. & Sankar, R. D., 2010. Effects of ridge geometry on mantle dynamics in an oceanic triple junction region: Implications for the Azores Plateau. *Earth and Planetary Science Letters*, 298(1–2), pp. 23-34.
- Gervais, A., Savoye, B., Mulder, T. & Gonthier, E., 2006. Sandy modern turbidite lobes: A new insight from high resolution seismic data. *Marine and Petroleum Geology*, 23(4), pp. 485-502.
- Gregg, T. K. P. & Fink, J. H., 1995. Quantification of submarine lava-flow morphology through analog experiments. *Geology*, 23(1), pp. 73-76.
- Griffiths, R. W. & Fink, J. H., 1992. Solidification and morphology of submarine lavas: A dependence on extrusion rate. *Journal of Geophysical Research: Solid Earth*, 97(B13), pp. 19729-19737.

- Grimison, N. L. & Chen, W.-P., 1986. The Azores-Gibraltar Plate Boundary: Focal mechanisms, depths of earthquakes, and their tectonic implications. *Journal of Geophysical Research: Solid Earth*, 91(B2), pp. 2029-2047.
- Guest, J. et al., 1999. Volcanic geology of Furnas Volcano, São Miguel, Azores. *Journal of Volcanology and Geothermal Research*, 92(1–2), pp. 1-29.
- Gutscher, M.-A. et al., 2002. Evidence for active subduction beneath Gibraltar. *Geology*, 30(12), pp. 1071-1074.
- Haase, K. M. & Beier, C., 2003. Tectonic control of ocean island basalt sources on São Miguel, Azores?. *Geophysical Research Letters*, 30(16). DOI 10.1029/2003GL017500.
- Hekinian, R. et al., 2000. Deep sea explosive activity on the Mid-Atlantic Ridge near 34°50'N: Magma composition, vesicularity and volatile content. *Journal of Volcanology and Geothermal Research*, 98(1–4), pp. 49-77.
- Hernández-Molina, F. et al., 2014. Contourite processes associated with the Mediterranean Outflow Water after its exit from the Strait of Gibraltar: Global and conceptual implications. *Geology*, 42(3), pp. 227-230.
- Hildenbrand, A. et al., 2008. Multi-stage evolution of a sub-aerial volcanic ridge over the last 1.3 Myr: S. Jorge Island, Azores Triple Junction. *Earth and Planetary Science Letters*, 273(3–4), pp. 289-298.
- Hildenbrand, A. et al., 2012a. Large-scale active slump of the southeastern flank of Pico Island, Azores. *Geology*, 40(10), pp. 939-942.
- Hildenbrand, A. et al., 2012b. Reconstructing the architectural evolution of volcanic islands from combined K/Ar, morphologic, tectonic, and magnetic data: The Faial Island example (Azores). *Journal of Volcanology and Geothermal Research*, Band 241–242, pp. 39-48.
- Hildenbrand, A., Weis, D., Madureira, P. & Marques, F. O., 2014. Recent plate re-organization at the Azores Triple Junction: Evidence from combined geochemical and geochronological data on Faial, S. Jorge and Terceira volcanic islands. *Lithos*, 210-211(0), pp. 27-39.
- Hirn, A. et al., 1980. Aftershock sequence of the January 1st, 1980, earthquake and present-day tectonics in the Azores. *Geophysical Research Letters*, 7(7), pp. 501-504.

- Hübscher, C., 2013. Tragica - Cruise No. M79/2 - August 26 – September 21, 2009. Ponta Delgada (Azores / Portugal) – Las Palmas (Canary Islands / Spain). METEOR-Berichte, M79/2, 37 pp., DFG-Senatskommission für Ozeanographie. https://getinfo.de/app/details?id=awi:doi~10.2312%252Fcr_m79_2
- Hübscher, C. & Gohl, K., 2014. Reflection/Refraction Seismology. *Encyclopedia of Marine Geosciences*. Springer. DOI 10.1007/978-94-007-6644-0_128-1.
- Hübscher, C., Ruhnau, M. & Nomikou, P., 2015. Volcano-tectonic evolution of the polygenetic Kolumbo submarine volcano/Santorini (Aegean Sea). *Journal of Volcanology and Geothermal Research*, Band 291, pp. 101-111.
- International Seismological Centre. 2012. *On-line Bulletin*, Thatcham, United Kingdom.
- Johnson, C. L. et al., 1998. $^{40}\text{Ar}/^{39}\text{Ar}$ ages and paleomagnetism of São Miguel lavas, Azores. *Earth and Planetary Science Letters*, 160(3–4), pp. 637-649.
- Jolivet, L., Faccenna, C. & Piromallo, C., 2009. From mantle to crust: Stretching the Mediterranean. *Earth and Planetary Science Letters*, 285(1–2), pp. 198-209.
- Kokelaar, B. & Durant, G. P., 1983. The submarine eruption and erosion of Surtla (Surtsey), Iceland. *Journal of Volcanology and Geothermal Research*, 19(3–4), pp. 239-246.
- Kostic, S., 2011. Modeling of submarine cyclic steps: Controls on their formation, migration, and architecture. *Geosphere*, 7(2), pp. 294-304.
- Krause, D. C. & Watkins, N. D., 1970. North Atlantic Crustal Genesis in the Vicinity of the Azores. *Geophysical Journal International*, 19(3), pp. 261-283.
- Kueppers, U. et al., 2012. Lava balloons - peculiar products of basaltic submarine eruptions. *Bulletin of Volcanology*, 74(6), pp. 1379-1393.
- Larrea, P. et al., 2014. $^{40}\text{Ar}/^{39}\text{Ar}$ constraints on the temporal evolution of Graciosa Island, Azores (Portugal). *Bulletin of Volcanology*, 76(2). DOI 10.1007/s00445-014-0796-8.
- Laughton, A. et al., 1972. A continuous east-west fault on the Azores-Gibraltar Ridge. *Nature*, Band 237, pp. 217-220.
- Le Pichon, X. & Angelier, J., 1979. The hellenic arc and trench system: A key to the neotectonic evolution of the eastern mediterranean area. *Tectonophysics*, 60(1–2), pp. 1-42.
- Ligi, M. et al., 1999. Bouvet Triple Junction in the South Atlantic: Geology and evolution. *Journal of Geophysical Research: Solid Earth*, 104(B12), pp. 29365-29385.

- Lisiecki, L. E. & Raymo, M. E., 2005. A Pliocene-Pleistocene stack of 57 globally distributed benthic $\delta^{18}O$ records. *Paleoceanography*, 20(1). DOI 10.1029/2004PA001071.
- Løseth, T. M., 1999. Sediment instability on subaqueous slopes. *Submarine Massflow Sedimentation: Computer Modelling and Basin-Fill Stratigraphy*, pp. 15-34.
- Lourenço, N., 2007. Tectono-Magmatic Processes At The Azores Triple Junction. *PhD Thesis, Universidade do Algarve*. sapientia.ualg.pt/bitstream/10400.1/789/1/Tese_PhD_Nuno_Lourenco_format_ualg.pdf (last access: December 11th, 2012).
- Lourenço, N. et al., 1998. Morpho-tectonic analysis of the Azores Volcanic Plateau from a new bathymetric compilation of the area. *Marine Geophysical Researches*, Band 20, pp. 141-156.
- Louvat, P. & Allègre, C. J., 1998. Riverine erosion rates on Sao Miguel volcanic island, Azores archipelago. *Chemical Geology*, 148(3-4), pp. 177-200.
- Luis, J. F. et al., 1994. The Azores triple junction evolution since 10 Ma from an aeromagnetic survey of the Mid-Atlantic Ridge. *Earth and Planetary Science Letters*, 125(1-4), pp. 439-459.
- Luis, J. F. & Miranda, J. M., 2008. Reevaluation of magnetic chrons in the North Atlantic between 35°N and 47°N: Implications for the formation of the Azores Triple Junction and associated plateau. *Journal of Geophysical Research: Solid Earth*, Band 113. DOI 10.1029/2007JB005573.
- Luis, J., Miranda, J., Galdeano, A. & Patriat, P., 1998. Constraints on the structure of the Azores spreading center from gravity data. *Marine Geophysical Researches*, 20(3), pp. 157-170.
- Luis, J. & Neves, M., 2006. The isostatic compensation of the Azores Plateau: A 3D admittance and coherence analysis. *Journal of Volcanology and Geothermal Research*, Band 156, pp. 10-22.
- Magde, L. S. & Smith, D. K., 1995. Seamount volcanism at the Reykjanes Ridge: Relationship to the Iceland hot spot. *Journal of Geophysical Research: Solid Earth*, 100(B5), pp. 8449-8468.
- Marques, F. et al., 2014a. Corrigendum to "GPS and tectonic evidence for a diffuse plate boundary at the Azores Triple Junction" [Earth Planet. Sci. Lett. 381 (2013) 177-187]. *Earth and Planetary Science Letters*, 387(1:), pp. 1-3.

- Marques, F. et al., 2013. GPS and tectonic evidence for a diffuse plate boundary at the Azores Triple Junction. *Earth and Planetary Science Letters*, 381(0), pp. 177-187.
- Marques, F. et al., 2014b. The 1998 Faial earthquake, Azores: Evidence for a transform fault associated with the Nubia–Eurasia plate boundary?. *Tectonophysics*, 633, pp. 115-125.
- Marshall, J. et al., 1997. A finite-volume, incompressible Navier Stokes model for studies of the ocean on parallel computers. *Journal of Geophysical Research*, Band 102, pp. 5753-5766.
- Martínez Solares, J. & López Arroyo, A., 2004. The great historical 1755 earthquake. Effects and damage in Spain. *Journal of Seismology*, 8(2), pp. 275-294.
- Matias, L. et al., 2007. The 9th of July 1998 Faial Island (Azores, North Atlantic) seismic sequence. *Journal of Seismology*, 11(3), pp. 275-298.
- McClusky, S. et al., 2003. GPS constraints on Africa (Nubia) and Arabia plate motions. *Geophysical Journal International*, 155(1), pp. 126-138.
- McKenzie, D., 1972. Active Tectonics of the Mediterranean Region. *Geophysical Journal International*, 30(2), pp. 109-185.
- McMurtry, G. et al., 2004. Giant landslides, mega-tsunamis, and paleo-sea level in the Hawaiian Islands. *Marine Geology*, 203(3–4), pp. 219-233.
- Métrich, N. et al., 2014. Is the ‘Azores Hotspot’ a Wetspot? Insights from the Geochemistry of Fluid and Melt Inclusions in Olivine of Pico Basalts. *Journal of Petrology*, 55(2), pp. 377-393.
- Meulenkamp, J. et al., 1988. On the Hellenic subduction zone and the geodynamic evolution of Crete since the late Middle Miocene. *Tectonophysics*, 146(1–4), pp. 203-215.
- Meyer, J., Mercolli, I. & Immenhauser, A., 1996. Off-ridge alkaline magmatism and seamount volcanoes in the Masirah island ophiolite, Oman. *Tectonophysics*, 267(1–4), pp. 187-208.
- Miranda, J., Luis, J., Lourenço, N. & Goslin, J., 2014. Distributed deformation close to the Azores Triple “Point”. *Marine Geology*, 355(0), pp. 27-35.
- Miranda, J. et al., 1998. Tectonic setting of the Azores Plateau deduced from a OBS survey. *Marine Geophysical Researches*, 20(3), pp. 171-182.

- Mitchell, N. C. et al., 2008. Lava penetrating water: Submarine lava flows around the coasts of Pico Island, Azores. *Geochemistry, Geophysics, Geosystems*, 9(3). DOI 10.1029/2007GC001725.
- Mitchell, N. C., Livermore, R. A., Fabretti, P. & Carrara, G., 2000. The Bouvet triple junction, 20 to 10 Ma, and extensive transtensional deformation adjacent to the Bouvet and Conrad transforms. *Journal of Geophysical Research: Solid Earth*, 105(B4), pp. 8279-8296.
- Mitchell, N. C., Stretch, R., Tempera, F. & Ligi, M., accepted. Volcanism in the Azores: a marine geophysical perspective, In: *Volcanism in the Azores*, Beier, C., Küppers, U. (eds). Springer.
- Mitchell, N., Quartau, R. & Madeira, J., 2012a. Assessing landslide movements in volcanic islands using near-shore marine geophysical data: south Pico island, Azores. *Bulletin of Volcanology*, 74(2), pp. 483-496.
- Mitchell, N. et al., 2012b. Cone morphologies associated with shallow marine eruptions: east Pico Island, Azores. *Bulletin of Volcanology*, 74(10), pp. 2289-2301.
- Montelli, R., Nolet, G., Dahlen, F. A. & Masters, G., 2006. A catalogue of deep mantle plumes: New results from finite-frequency tomography. *Geochemistry, Geophysics, Geosystems*, 7(11). DOI 10.1029/2006GC001248.
- Montesinos, F., Camacho, A. & Vieira, R., 1999. Analysis of gravimetric anomalies in Furnas caldera (Sao Miguel, Azores). *Journal of volcanology and geothermal research*, 92(1), pp. 67-81.
- Montesinos, F. G. et al., 2003. A 3-D gravity model for a volcanic crater in Terceira Island (Azores). *Geophysical Journal International*, 154(2), pp. 393-406.
- Moore, J. G., 1985. Structure and eruptive mechanisms at Surtsey Volcano, Iceland. *Geological Magazine*, 11, Band 122, pp. 649-661.
- Moore, R., 1990. Volcanic geology and eruption frequency, São Miguel, Azores. *Bulletin of Volcanology*, Band 52, pp. 602-614.
- Moore, R. B., 1991. Geology of three late Quaternary stratovolcanoes on São Miguel, Azores. *US Geological Survey, Branch of Central Technical Reports*. No. 1900. <http://pubs.usgs.gov/bul/1900/report.pdf> (last access: July 22th, 2015)
- Moore, R. B. & Rubin, M., 1991. Radiocarbon dates for lava flows and pyroclastic deposits on São Miguel, Azores. *Radiocarbon*, Band 33(1), pp. 151-164.

- Morel, J. L. & Meghraoui, M., 1996. Goringe-Alboran-Tell tectonic zone: A transpression system along the Africa-Eurasia plate boundary. *Geology*, 24(8), pp. 755-758.
- Muecke, G. K. et al., 1974. Deep drilling in an active geothermal area in the Azores. *Nature*, Band 252, pp. 271-285.
- Mulder, T. & Cochonat, P., 1996. Classification of offshore mass movements. *Journal of Sedimentary research*, 66(1), pp. 43-57.
- Müller-Michaelis, A. & Uenzelmann-Neben, G., 2014. Development of the Western Boundary Undercurrent at Eirik Drift related to changing climate since the early Miocene. *Deep Sea Research Part I: Oceanographic Research Papers*, 93(0), pp. 21-34.
- Navarro, A., Catalao, J., Miranda, J. M. & Fernandes, R. M., 2003. Estimation of the Terceira Island (Azores) main strain rates from GPS data. *Earth, planets and space*, 55(10), pp. 637-642.
- Navarro, A. et al., 2009. Analysis of geometry of volcanoes and faults in Terceira Island (Azores): Evidence for reactivation tectonics at the EUR/AFR plate boundary in the Azores triple junction. *Tectonophysics*, 465(1-4), pp. 98-113.
- Nemeth, K., White, J. D. L., Reay, A. & Martin, U., 2003. Compositional variation during monogenetic volcano growth and its implications for magma supply to continental volcanic fields. *Journal of the Geological Society of London*, Band 160(4), pp. 523-530.
- Netzeband, G. et al., 2006. The Levantine Basin—crustal structure and origin. *Tectonophysics*, 418(3-4), pp. 167-188.
- Neves, M., Miranda, J. & Luis, J., 2013. The role of lithospheric processes on the development of linear volcanic ridges in the Azores. *Tectonophysics*, 608(0), pp. 376-388.
- Nocquet, J.-M., 2012. Present-day kinematics of the Mediterranean: A comprehensive overview of GPS results. *Tectonophysics*, Band 579, pp. 220-242.
- Nomikou, P. et al., 2012. Submarine volcanoes of the Kolumbo volcanic zone NE of Santorini Caldera, Greece. *Global and Planetary Change*, 90-91(0), pp. 135-151.
- Nomikou, P. et al., 2013. Submarine volcanoes along the Aegean volcanic arc. *Tectonophysics*, Band 597-598, pp. 123-146.
- Okubo, C. H. & Martel, S. J., 1998. Pit crater formation on Kilauea volcano, Hawaii. *Journal of Volcanology and Geothermal Research*, 86(1-4), pp. 1-18.

- Oliveira, C., Costa, A., Forjaz, V. & Nunes, J., 1990. Seismic hazard analysis in zones of time and space interdependence: An application to São Miguel Island, Azores. *Natural Hazards*, 3(1), pp. 15-29.
- Polonia, A. et al., 2011. The Calabrian Arc subduction complex in the Ionian Sea: Regional architecture, active deformation, and seismic hazard. *Tectonics*, 30(5). DOI 10.1029/2010TC002821.
- Quartau, R. et al., 2014. The morphology of insular shelves as a key for understanding the geological evolution of volcanic islands: Insights from Terceira Island (Azores). *Geochemistry, Geophysics, Geosystems*, 15(5), pp. 1801-1826.
- Quartau, R. et al., 2015. The insular shelves of the Faial-Pico Ridge (Azores archipelago): A morphological record of its evolution. *Geochemistry, Geophysics, Geosystems*, 16(5). DOI 10.1002/2015GC005733.
- Quartau, R. et al., 2012. Morphology of the Faial Island shelf (Azores): The interplay between volcanic, erosional, depositional, tectonic and mass-wasting processes. *Geochemistry, Geophysics, Geosystems*, 13(4). DOI 10.1029/2011GC003987.
- Quartau, R., Trenhaile, A., Mitchell, N. & Tempera, F., 2010. Development of volcanic insular shelves: Insights from observations and modelling of Faial Island in the Azores Archipelago. *Marine Geology*, Band 275, pp. 66-83.
- Queiroz, G., 1997. Vulcão das Sete Cidades (S. Miguel, Açores): história eruptiva e avaliação do hazard. *Unpublished PhD Thesis, Universidade dos Açores*, 226p.
- Queiroz, G. et al., 2008. The last 5000 years of activity at Sete Cidades volcano (São Miguel Island, Azores): Implications for hazard assessment. *Journal of Volcanology and Geothermal Research*, 178(3), pp. 562-573.
- Ramalho, R. S. et al., 2013. Coastal evolution on volcanic oceanic islands: A complex interplay between volcanism, erosion, sedimentation, sea-level change and biogenic production. *Earth-Science Reviews*, Band 127, pp. 140-170.
- Rebesco, M., Hernández-Molina, F. J., Rooij, D. V. & Wåhlin, A., 2014. Contourites and associated sediments controlled by deep-water circulation processes: State-of-the-art and future considerations. *Marine Geology*, 352(0), pp. 111-154.
- Reid, J. L., 1994. On the total geostrophic circulation of the North Atlantic Ocean: Flow patterns, tracers, and transports. *Progress in Oceanography*, 33(1), pp. 1-92.

- Robertson, A., 1977. Tertiary uplift history of the Troodos massif, Cyprus. *Geological Society of America Bulletin*, 88(12), pp. 1763-1772.
- Robertson, A. H., 1998. Mesozoic-Tertiary tectonic evolution of the easternmost Mediterranean area: integration of marine and land evidence.. *Proceedings of the Ocean Drilling Program, Scientific Results*, Band 160, p. Chapter 54. https://www.era.lib.ed.ac.uk/bitstream/handle/1842/559/CHAP_54.PDF?sequence=2&isAllowed=y (last access: July 7th, 2015).
- Robertson, A. H. F. & Mountrakis, D., 2006. Tectonic development of the Eastern Mediterranean region: an introduction. *Geological Society, London, Special Publications*, 260(1), pp. 1-9.
- Rubin, K. H. et al., 2012. Volcanic eruptions in the deep sea. *Oceanography*, Band 25(1), pp. 142-157.
- Sansone, F. J. & Smith, J. R., 2006. Rapid mass wasting following nearshore submarine volcanism on Kilauea volcano, Hawaii. *Journal of Volcanology and Geothermal Research*, 151(1-3), pp. 133-139.
- Schilling, J.-G., 1975. Azores mantle blob: Rare-earth evidence. *Earth and Planetary Science Letters*, 25(2), pp. 103-115.
- Schilling, J.-G., 1985. Upper mantle heterogeneities and dynamics. *Nature*, March, Band 314, pp. 62-67.
- Schilling, J.-G., Bergeron, M. B., Evans, R. & Smith, J. V., 1980. Halogens in the Mantle Beneath the North Atlantic [and Discussion]. *Philosophical Transactions of the Royal Society of London. Series A, Mathematical and Physical Sciences*, 297(1431), pp. 147-178.
- Schmincke, H.-U., 2004. *Volcanism*. Springer. ISBN 978-3-642-18952-4.
- Schmitz, W. J., 1995. On the interbasin-scale thermohaline circulation. *Reviews of Geophysics*, 33(2), pp. 151-173.
- Searle, R., 1980. Tectonic pattern of the Azores spreading centre and triple junction. *Earth and Planetary Science Letters*, 51(2), pp. 415-434.
- Searle, R. C., 1976. Lithospheric Structure of the Azores Plateau from Rayleigh-Wave Dispersion. *Geophysical Journal International*, 44(3), pp. 537-546.

- Serpelloni, E. et al., 2007. Kinematics of the Western Africa-Eurasia plate boundary from focal mechanisms and GPS data. *Geophysical Journal International*, 169(3), pp. 1180-1200.
- Serra, N. et al., 2010. On the low-frequency phase relation between the Denmark Strait and the Faroe-Bank Channel overflows. *Tellus A*, 62(4), pp. 530-550.
- Sibrant, A., Hildenbrand, A., Marques, F. & Costa, A., 2015a. Volcano-tectonic evolution of the Santa Maria Island (Azores): Implications for paleostress evolution at the western Eurasia–Nubia plate boundary. *Journal of Volcanology and Geothermal Research*, 291(0), pp. 49-62.
- Sibrant, A. et al., 2015b. Morpho-structural evolution of a volcanic island developed inside an active oceanic rift: S. Miguel Island (Terceira Rift, Azores). *Journal of Volcanology and Geothermal Research*, 301(0), pp. 90-106.
- Sibrant, A., Marques, F. & Hildenbrand, A., 2014. Construction and destruction of a volcanic island developed inside an oceanic rift: Graciosa Island, Terceira Rift, Azores. *Journal of Volcanology and Geothermal Research*, Band 284, pp. 32-45.
- Silva, P. F. et al., 2012. Palaeomagnetic study of a subaerial volcanic ridge (São Jorge Island, Azores) for the past 1.3 Myr: evidence for the Cobb Mountain Subchron, volcano flank instability and tectonomagmatic implications. *Geophysical Journal International*, 188(3), pp. 959-978.
- Silveira, G. et al., 2006. Azores hotspot signature in the upper mantle. *Journal of Volcanology and Geothermal Research*, 156(1–2), pp. 23-34.
- Silveira, G. et al., 2010. Stratification of the Earth beneath the Azores from P and S receiver functions. *Earth and Planetary Science Letters*, 299(1–2), pp. 91-103.
- Smith, D. K., 1996. Comparison of the shapes and sizes of seafloor volcanoes on Earth and “pancake” domes on Venus. *Journal of Volcanology and Geothermal Research*, 73(1–2), pp. 47-64.
- Smith, D. K. & Cann, J. R., 1999. Constructing the upper crust of the Mid-Atlantic Ridge: A reinterpretation based on the Puna Ridge, Kilauea Volcano. *Journal of Geophysical Research: Solid Earth*, 104(B11), pp. 25379-25399.
- Smith, D. K. et al., 1995a. Mid-Atlantic Ridge volcanism from deep-towed side-scan sonar images, 25°–29°N. *Journal of Volcanology and Geothermal Research*, 67(4), pp. 233-262.

- Smith, D. K., Humphris, S. E. & Bryan, W. B., 1995b. A comparison of volcanic edifices at the Reykjanes Ridge and the Mid-Atlantic Ridge at 24°–30°N. *Journal of Geophysical Research: Solid Earth*, 100(B11), pp. 22485-22498.
- Smith, T. & Batiza, R., 1989. New field and laboratory evidence for the origin of hyaloclastite flows on seamount summits. *Bulletin of Volcanology*, 51(2), pp. 96-114.
- Smith, W. H. & Sandwell, D. T., 1997. Global sea floor topography from satellite altimetry and ship depth soundings. *Science*, 277(5334), pp. 1956-1962.
- Sohn, R. A. et al., 2008. Explosive volcanism on the ultraslow-spreading Gakkel ridge, Arctic Ocean. *Nature*, Band 453, pp. 1236-1238.
- Solgevik, H., Mattsson, H. B. & Hermelin, O., 2007. Growth of an emergent tuff cone: Fragmentation and depositional processes recorded in the Capelas tuff cone, São Miguel, Azores. *Journal of Volcanology and Geothermal Research*, 159(1–3), pp. 246-266.
- Srivastava, S. et al., 1990. Motion of Iberia since the Late Jurassic: Results from detailed aeromagnetic measurements in the Newfoundland Basin. *Tectonophysics*, 184(3–4), pp. 229-260.
- Stretch, R., Mitchell, N. & Portaro, R., 2006. A morphometric analysis of the submarine volcanic ridge south-east of Pico Island, Azores. *Journal of Volcanology and Geothermal Research*, 156(1–2), pp. 35-54.
- Tempera, F. et al., 2013. Condor seamount (Azores, \{NE\} Atlantic): A morpho-tectonic interpretation. *Deep Sea Research Part II: Topical Studies in Oceanography*, 98, Part A(0), pp. 7-23.
- Thibaud, R., Gente, P. & Maia, M., 1998. A systematic analysis of the Mid-Atlantic Ridge morphology and gravity between 15°N and 40°N: Constraints of the thermal structure. *Journal of Geophysical Research: Solid Earth*, 103(B10), pp. 24223-24243.
- Udías, A., Arroyo, A. & Mezcuá, J., 1976. Seismotectonic of the Azores-Alboran region. *Tectonophysics*, 31(3–4), pp. 259-289.
- Vogt, P. & Jung, W., 2004. The Terceira Rift as hyper-slow, hotspot-dominated oblique spreading axis: A comparison with other slow-spreading plate boundaries. *Earth and Planetary Science Letters*, 218(1–2), pp. 77-90.

- Watt, S. et al., 2012. Combinations of volcanic-flank and seafloor-sediment failure offshore Montserrat, and their implications for tsunami generation. *Earth and Planetary Science Letters*, 319–320(0), pp. 228-240.
- White, J. D., Schipper, C. I. & Kano, K., 2015. Chapter 31 - Submarine Explosive Eruptions. In: H. Sigurdsson. *The Encyclopedia of Volcanoes (Second Edition)*. Second Edition. Amsterdam: Academic Press, pp. 553-569.
- White, W. M. & Schilling, J.-G., 1978. The nature and origin of geochemical variation in Mid-Atlantic Ridge basalts from the Central North Atlantic. *Geochimica et Cosmochimica Acta*, 42(10), pp. 1501-1516.
- Wood, C. A., 1980. Morphometric evolution of cinder cones. *Journal of Volcanology and Geothermal Research*, 7(3–4), pp. 387-413.
- Woolf, D. K., Challenor, P. & Cotton, P., 2002. Variability and predictability of the North Atlantic wave climate. *Journal of Geophysical Research: Oceans (1978--2012)*, 107(C10), pp. 9-1 - 9-14.
- Wortel, M. J. R. & Spakman, W., 2000. Subduction and Slab Detachment in the Mediterranean-Carpathian Region. *Science*, 290(5498), pp. 1910-1917.
- Yang, T. et al., 2006. Upper mantle structure beneath the Azores hotspot from finite-frequency seismic tomography. *Earth and Planetary Science Letters*, 250(1–2), pp. 11-26.
- Young, I., 1999. Seasonal variability of the global ocean wind and wave climate. *International Journal of Climatology*, 19(9), pp. 931-950.
- Zitellini, N. et al., 2009. The quest for the Africa–Eurasia plate boundary west of the Strait of Gibraltar. *Earth and Planetary Science Letters*, 280(1–4), pp. 13-50.
- Zitellini, N. et al., 2001. Source of 1755 Lisbon earthquake and tsunami investigated. *Eos, Transactions American Geophysical Union*, 82(26), pp. 285-291.

Acknowledgements

First acknowledgements go to my supervisor Christian Hübscher. Thank you for the freedom you gave me in science as well as for your assistance in times of uncertainty, for your continuous support throughout my occupational development, for your confidence during joint measurement campaigns and those I did on myself, for the opportunity to do such campaigns on myself at all, for all the good and fruitful discussions in matters of science as well as life. I enjoyed all the shared years during my studies and during my Diploma thesis. And, finally, I never regretted my choice to start this thesis...

I would further like to thank Sönke Reiche and Kristina Meier. Tina, many thanks for all the discussions, open ears, cigarettes, beers, for our long-term "*Empirical study about Greeks and Ouzo*", and in particular for the possibility you supported to climb Yasur Volcano and Stromboli Volcano side on side with you. Sönke, many thanks for the great time we had in our shared office, for all the helpful comprehensive discussions, for your acceptance of my taste in music (even if it finally decreased), and for the chance to accompany you on another voyage of discovery: marriage.

Thanks to Muayyad AlHseinat, Janina Kammann, Daniela Wolf and my working group for the good time I was allowed to enjoy.

I thank Sven Winter for all the time we spent together on board of ships, pontons and other swimming goods. Thanks for your guidance throughout all the technical problems and your training in maintaining air guns, streamers, sparkers, boomers, winches, compressors...and swapping foolish comments.

I want to thank all the outstanding crews of RV HEINCKE, RV ALKOR, RV MARIA S. MERIAN, RV METEOR (of whom I owe, inter alia, the dataset of this study), and RV SONNE for the great time on board of the corresponding ships.

I am grateful for the financial support of the German Research Foundation (DFG, grant Hu698/19-1).

Finally, thousandfold thanks go to Claudia Kalvelage for her continuous support, for reading all the pages I gave her, for the great time on board of RV METEOR, and for participation in the case study mentioned above – and sorry for all the thesis related minutes you had to wait.

I hereby declare, on oath, that I have written the present dissertation by my own and have not used other than the acknowledged resources and aids.

Hamburg, October 1st, 2015

Benedikt Weiß